SYNTHESIS AND CRYSTALLIZATION OF PRECISE AND RANDOM HALOGEN-CONTAINING POLYOLEFINS

By

EMINE BOZ

A DISSERTATION PRESENTED TO THE GRADUATE SCHOOL
OF THE UNIVERSITY OF FLORIDA IN PARTIAL FULFILLMENT
OF THE REQUIREMENTS FOR THE DEGREE OF
DOCTOR OF PHILOSOPHY

UNIVERSITY OF FLORIDA

2007

For Dr. Butler

ACKNOWLEDGMENTS

It is difficult to express how much my four years in graduate school have impacted my life. During this time there have been so many different experiences and challenges, which I could not have overcome without the help, guidance, and friendship of the very important people in my life.

Most of all I thank my advisor, Prof. Kenneth B. Wagener. It is because of Dr. Wagener that I came to UF to pursue graduate studies and it is because of his constant support and positive influence that I have been able to continue and complete my education here. Dr. Wagener has shown me what it means to be a person of character and a person who truly cares from his heart about the well-being of others. He is much more than an accomplished scientist and advisor, he is a source of lasting influence and inspiration.

I also thank the number of excellent scientists with whom I have had an opportunity to work. Prof. Rufina G. Alamo from Florida State University played a large role in the development of my project and taught me much to increase my knowledge and understanding. Working with Dr. Alamo has been a very valuable experience. Dr. Ion Ghivriga has also been extremely helpful in offering his expertise and time in the characterization of many of my polymer samples. Dr. Lisa Baugh, at Exxon-Mobil, has also been of great help in assisting with polymer characterization and has always been so enthusiastic and friendly.

Coworkers in the lab have also played a large role in my time here at UF. Most importantly is Alexander J. Nemeth, perhaps the most exceptional undergraduate I have ever met. Alex worked alongside me in the lab and was always eager to put in long hours in order to make sure that the experiments were done right. I will miss our teamwork and all the conversations about baseball. I also thank Dr. John C. Sworen for his guidance during the early days of my research. John was an awesome person to work with. Dr. Tim Hopkins was also a very helpful influence in

the lab. I would also like to thank the labmates and group members who made my time at UF an enjoyable and productive experience.

Thanks go also to the members of my committee. Prof. William Dolbier was not only a member of my committee; he was also my teacher, and a helpful source of great knowledge. I aspire to one day be the teacher that he is. Prof. Anthony Brennan is the coolest professor I have ever met. I enjoyed all the chances I had to interact with him. Prof. Adam Viege was also a very helpful member of my committee. Special thanks go to Prof. Ronald Castellano and Prof. Lisa McElwee-White for serving on my committee at short notice on two different occasions. Finally, I thank Prof. Merle Battiste, it was great experience to TA for him and a pleasure to discuss science with him.

I must also thank the angels of the polymer floor: Lorraine Williams, Sara Klossner, and Gena Borrero. Without their patient and kind help on a daily basis life would be so much more difficult. I will miss our conversations in the polymer office. I also thank my two closest friends on the polymer floor, Christophe Grenier and Barry Thompson.

I do not have the words to express my thanks and appreciation for my family. They have been totally supportive of me throughout my life and education. They have thought only of what will be best for me and make me happy. Their support cannot be quantified and even though they are far away, I can feel their love and support at every moment.

Finally, I need to thank the person who made my education at UF possible and that is Prof. George Butler. I am grateful that I had the opportunity to meet Dr. Butler and to get to know him, even if for just a short time. It is people like Dr. Butler that make the hopes and ambitions of others possible. It is hard to imagine the number of people that he has influenced in a positive

way through the legacy that he has established at UF. I hope that I can one day continue his legacy, which has been passed down to me through Dr. Wagener.

TABLE OF CONTENTS

page

LIST OF TABLES

LIST OF FIGURES

Abstract of Dissertation Presented to the Graduate School
of the University of Florida in Partial Fulfillment of the
Requirements for the Degree of Doctor of Philosophy

SYNTHESIS AND CRYSTALLIZATION OF PRECISE AND RANDOM HALOGEN-CONTAINING POLYOLEFINS

By

Emine Boz

August 2007

Chair: Kenneth B. Wagener
Major: Chemistry

We report the synthesis and characterization of a series of precision polyethylene (PE) structures containing a fluorine, chlorine, or bromine on each and every 9^{th}, 15^{th}, 19^{th}, and 21^{st} carbon. The use of acyclic diene metathesis (ADMET) polymerization allows unprecedented control in the synthesis of these halogen-containing PE derivatives, and results in the first bromine containing polyolefins with precisely defined primary structures. ADMET polymerization followed by hydrogenation leads to these precise structures, which have been characterized by ^{1}H NMR, ^{13}C NMR, IR, elemental analysis, TGA, DSC, and WAXD. The TGA data, coupled with elemental analysis, supply definitive proof of the structural composition through the observed thermal decomposition and release of exact masses of HX (X = F, Cl, or Br). Relative to analogous random copolymers, these precisely substituted polymers display sharper WAXD diffraction patterns, higher crystallinities and much narrower melting peaks, typical of homopolymer crystallization. This crystallization behavior is supported by solid-state NMR based on the observed equivalence in the relative distribution of halogens between crystalline and non-crystalline regions. Lattice distortions caused by the accommodation of the substituent in the lattice, render a change from orthorhombic to triclinic structures at a van der Waals atomic radius of the substituent > 1.6 Å. The observed melting and enthalpies of fusion

decrease dramatically with increasing volume of the substituent and scale proportionally to the van der Waals atomic radius in the halogenated series.

The synthesis of ethylene vinyl halide (EVH) copolymers containing fluorine, chlorine, and bromine via the ADMET copolymerization of halogen containing α-ω dienes with 1,9-decadiene is also presented. Analysis of the unsaturated prepolymers via ^{13}C NMR spectroscopy establishes the statistically random nature of the copolymers. Thermal analysis indicates a distinct difference in the crystallization behavior of these random copolymers when compared to their compositionally matched precise analogues. Here, the homopolymer crystallization is no longer observed and is replaced by a mechanism based on the selection of long crystallizable sequences. The results presented thus point to the utility of these random ADMET copolymers as suitable models for industrially relevant PE copolymers based on the perfectly linear, defect free, and statistically random copolymer composition.

CHAPTER 1
PROGRESS IN THE DEVELOPMENT OF WELL-DEFINED ETHYLENE-VINYL HALIDE POLYMERS

1.1 Introduction

Polyethylene (PE) is the largest volume polymer produced in the world today.[1] The range of applications for PE is so diverse, such that it is difficult to adequately describe. The real strength of PE is that a vast property set is available, as determined by the structural characteristics of a specific sample, which are tuned in the employed synthetic process. While variation in synthesis and processing conditions is used to target PE for given applications, the available range of properties is vastly increased through the use of polymer additives[2] or via the introduction of chemical functionality to the parent PE backbone.[3] The chemical industry has long been dominated by the additive approach, based on the simplicity and tunability of this technique. However, polymer additives do present drawbacks and fail to modify the polymer structure at its most fundamental level.[4]

Advances in polymerization techniques have now made it possible to gain an ever greater control over polymer structure at all levels, enabling the exploration of property control strictly via manipulation of macromolecular structure. Such an approach not only allows the precise tuning of properties in a single, well-defined material, but it also allows one to learn the fundamental consequences of structural modification. The strong effects of structural modification are clearly seen in the great variety of halogen containing PE analogues, in which the halogen type, content, and sequence distribution, collectively modulate the structural and physical properties of the polymer.

In this chapter, a critical survey of halogen containing polymers is presented, with the goal of illustrating what is known about the role of halogen substituents on the properties of linear PE based analogues. In order to focus on developing direct correlations between primary structure

and bulk properties, only those halogen containing polymers with just one type of halogen per sample will be considered. In the first section, industrially relevant homopolymers are described in order to establish a base point for the types of properties exhibited by these materials and the role of the halogen substituent in defining these properties. In the second section, the most common classes of chemically modified halogen containing PE analogues are examined for the structure-property relationships that can be derived from judicious structural modification.

1.2 Halogen-Containing Homopolymers

1.2.1 Poly(vinyl halides)

The simplest halogen containing iteration of PE is the family of poly(vinyl halide) (PVH) polymers shown in Figure 1-1: poly(vinyl fluoride) (PVF), poly(vinyl chloride) (PVC), poly(vinyl bromide) (PVB), and poly(vinyl iodide) (PVI). By comparing the fundamental properties of the polymers in this family, the effect of halogen type on the structural properties of these PE analogues can be understood. In all cases (as with the PE), the effect of the synthetic method cannot be ignored, as it exerts a strong influence on the polymer structure. Here, the properties presented for a given polymer will be those that result from the most common synthetic route for that specific polymer.

1.2.1.1 Poly(vinyl fluoride)

Poly(vinyl fluoride) (PVF) is represented by the repeat unit shown in Figure 1-1. Here the PE backbone has been modified only by the addition of a fluorine atom on every other carbon. While the size of fluorine is only slightly larger than that of hydrogen (van der Waals radius = 1.47 Å vs. 1.2 Å for H), the strong electronegativity difference between the C-H bond dipole and the C-F bond dipole is not negligible and plays a role in the overall structure of the polymer. The other factor that is introduced by addition of the halogen in PVF (and all of the PVH polymers) is tacticity and whether the polymer is atactic or possesses any degree of stereoregularity.

The synthesis of PVF is achieved most commonly by radical initiated suspension polymerization of vinyl fluoride,[5] although emulsion polymerization can also be used.[6] Vinyl fluoride is the most difficult vinyl halide monomer to polymerize. The result is that very high pressures are required.[7] Typically PVF contains about 88-90% head-to-tail linkages as is represented by the repeat unit, although the presence of head-to-head linkages is a consequence of the free-radical polymerization method.[8] The polymer is atactic, based on the polymerization condition used. For PVF, the molecular weight is generally reported as a viscosity average, which is approximately 60,000 in DMF at 90 °C.[9]

PVF is a semicrystalline polymer, which has a percent crystallinity (X_c) of 20-60% depending on the synthetic method used.[10] The melting temperature (T_m) for PVF is typically observed at 190 °C for commercial samples, which is ~60 °C higher than that observed for PE,[11,12,13] reflecting the stronger nature of the interactions within the crystallites in PVF. Two distinct glass transitions (T_g) are observed, which emphasize the semicrystalline nature of the polymer. The lower T_g occurs at -15 to -20 °C and corresponds to the relaxation of amorphous domains, which are free from constraint by crystallites and the upper T_g occurs at 40-50 °C and corresponds to the relaxation of amorphous domains constrained by crystallites.[14] Overall the polymer has a greater tendency to crystallize than other PVH polymers, which is due partly to the smaller size of the fluorine atom as well as to the high electronegativity of the fluorine, which induces strong dipole-dipole interactions (hydrogen bonding), enforcing a more crystalline structure. However, the significant variation in crystallinity (20-60%) is thought to be due primarily to defect structures, such as head-to-head linkages and branching but not to variations is tacticity.[10]

An orthorhombic crystal structure has been proposed for PVF, with unit cell dimensions: *a* = 8.57 Å, *b* = 4.95 Å, and *c* = 2.52 Å.[15,16] For comparison, PE is also found to crystallize with an orthorhombic structure and dimensions: *a* = 7.42 Å, *b* = 4.94 Å, and *c* = 2.55 Å.[17,18,19] The discrepancy in the unit cell dimensions, found primarily in the expansion of the lattice in the *a* dimension, reflects the larger size of the fluorine atom relative to hydrogen. Figure 1-2 illustrates the definition of the unit cell for several common unit cell types discussed in this work and pictorially shows the unit cell for PE as a representative structural example in order to visualize how polymers organize in a crystalline lattice.

PVF is more thermally stable than other vinyl halide polymers and high molecular weight PVF is reported to degrade in an inert atmosphere, with concurrent HF loss and backbone cleavage occurring at about 450 ºC.[20] In air, HF loss occurs at about 350ºC, followed by backbone cleavage around 460ºC. The excellent thermal stability is due to the large number of hydrogen bonds. This high stability is also reflected in several other physical properties of PVF, such as excellent resistance to sunlight degradation, chemical attack, water absorption, and solvent, which impart excellent outdoor durability and stain resistance.[7] This property set, coupled with a high degree of transparency to visible light, leads to the application of PVF primarily as a protective coating in a variety of outdoor and indoor settings, specifically for: buildings, trucks, trains, airplanes, greenhouses, solar cells, fuel lines, and circuit boards.[7]

1.2.1.2 Poly(vinyl chloride)

Poly(vinyl chloride) (PVC) (Figure 1-1) is the second largest volume plastic produced in industry and its relatively low cost and attractive property set lead it to be one of the most versatile and applicable polymers known.[21] PVC is synthesized via free radical suspension, emulsion, or bulk polymerization, with suspension methods accounting for 80% of the polymer produced worldwide.[22] Typical PVC has a degree of polymerization of 500-3500, corresponding

to molecular weights in the range of ~30-200 kDa.[21] Molecular weight can be tuned via reaction temperature, with higher temperatures producing lower molecular weight polymers. PVC shows a slight tendency toward a syndiotactic structure, although polymerization temperature affects the syndiotactic content, with lower temperatures leading to higher syndiotactic content. A typical sample polymerized at 50 °C (a typical industrial polymerization temperature) is 56% syndiotactic.[23] The most important structural consequence of the free radical polymerization process used is the high defect content in PVC. While the primary structure of PVC is essentially defined by head-to-tail linkages, the polymer contains many structural defects consisting of long and short chains, terminal and internal unsaturation, branching, and end group defects.[24]

In bulk samples, PVC is a semicrystalline polymer that is largely amorphous. Samples are generally less than 10% crystalline, which is primarily attributed to irregular structure, defined by random distributions of syndiotactic sequences of varied length.[25] The effect of this irregular structure is to inhibit the crystallization of the polymer based on the difficulties of like segments to find each other and pack into crystallites. The crystallites in PVC are lamellar in nature and have been assigned an orthorhombic structure with unit cell dimensions a = 10.6 Å, b = 5.4 Å, c = 5.1 Å.[26] However, the wide range of crystallite sizes and the generally imperfect nature of the crystallites leads to a broad melting temperature for PVC of ~120-260 °C.[27] The T_g of PVC is 82 °C, which leads it to be a brittle material at room temperature.[28]

The most important thermal property of PVC is related to the relative instability of PVC at elevated temperatures. Even at 100 °C PVC is known to undergo a very slow elimination of the labile chlorine atoms in the form of HCl. As the temperature is increased, the rate of HCl evolution is greatly enhanced at about 200 °C. This elimination process leads to the formation of

unsaturated sites in the polymer backbone and is characterized as the first of three steps in the thermal degredation process of PVC.[29] As double bonds are generated in the backbone, neighboring chlorine atoms become allylic chlorines, and are subsequently even more labile to further elimination. Such a process rapidly turns into a chain reaction characterized as the unzipping mechanism. Defect sites serve as initiation centers for this mechanism, as tertiary and allylic chlorines are much more easily eliminated at lower temperatures. The consequence of this first mechanistic stage of decomposition is a polyene structure, which is unstable to a variety of further reactions defining stage two of decomposition, which occurs at temperatures greater than ~350 °C. In this case, the relatively electron rich polyene structure can undergo oxidative chain scission or crosslinking reactions, such as Diels-Alder cycloadditions. The final stage of decomposition is that of char formation, in which aromatic hydrocarbons generated by extensive cross-linking and chain scission are released. However, the cross linked mass formed in step two is never fully decomposed and remains even at extremely high temperatures, above 500 °C.

The physical properties of PVC are generally widely tuned via the addition of additives and plasticizers, which can generate a range of mechanical properties in the polymer, from a rigid form to a highly flexible form. The overall good mechanical properties, coupled with a strong chemical resistance (except in the presence of low molecular weight chlorinated solvents) make PVC applicable in a diverse range of settings, which include: pipes, siding, flooring, roofing, wall covering, chemical plant construction materials, flexible wire and cable covering.[30]

1.2.1.3 Poly(vinyl bromide)

Poly(vinyl bromide) (PVB) (Figure 1-1) is significantly less well known than its analogues PVF and PVC. The main reason for the lack of application stems from the lower stability of PVB, induced by the significantly more labile C-Br bond, which renders the polymer unstable to light and heat.[31] PVB is typically synthesized by free radical methods in bulk,

solution, suspension, or emulsion, using typical peroxides or AIBN for initiation.[31] The polymer is atactic when synthesized at room temperature, but at lower polymerization temperatures tends to show increased syndiotactic character.[32] No general property set is available for a so-called "typical" sample, as with the much more commonly produced PVC, but molecular weights in the range of 20-50 kDa have been reported for PVB.[33]

The most universal property of PVB is the relative thermal instability of the polymer. Monitoring by TGA, PVB has been reported to show two distinct thermal degradation processes. The first is the loss of HBr, which reaches a maximum rate at ~100 °C (although temperatures from 100-200 °C have been reported).[34] The second stage decomposition reaches a maximum rate at ~500 °C and corresponds to the crosslinking and fragmentation of the polyene structure that is formed during the evolution of HBr. Due to the low decomposition temperature of PVB, relatively little additional thermal data is reported. The T_g of PVB has been reported to range from 50-100 °C.[28] Only a few studies have focused on the crystalline properties of PVB as measured by XRD,[35] assignment to an orthorhombic unit cell is reported[36] with dimensions a = 11.0 Å, b = 5.6 Å, c = 5.1 Å, but no percent crystallinity is given.

1.2.1.4 Poly(vinyl iodide) (PVI)

Poly(vinyl iodide) (PVI) (Figure 1-1) is even more unstable than PVB and consequently, even less literature is found concerning this polymer, which has no known applications. Reported syntheses of PVI include the gamma-ray induced radical polymerization of vinyl iodide and the AIBN initiated radical polymerization.[37,38] Sodium thiosulphate ($Na_2S_2O_3$) is an important additive to polymerizations of vinyl iodide, which acts to consume inhibitors such as iodine and hydrogen iodide, which are produced during the polymerization as the decomposition products of the vinyl iodide monomer.[39] Polymer molecular weights on the order of 4500-7500 have been

reported, but the polymer is thermally unstable and decomposes at less than 100 °C and is also unstable to light.[40]

Table 1-1 summarizes the properties of the PVH polymers discussed. It can be observed that although the orthorhombic structure of PE is maintained throughout the series, the dimensions of the unit cell increase with increasing halogen size. A concurrent decrease in T_m and percent crystallinity with increasing halogen size is also observed.

1.2.2 Poly(vinylidene halides)

Vinylidene halide polymers are the next logical iteration of halogen containing polyolefins and are represented by the repeat unit -(CH_2-CX_2)- and the common structures are shown in Figure 1-3. With two halogens on every other carbon, tacticity is not a concern in the vinylidene halide family. This homopolymer family provides a deeper insight into the effects of halogen content, when compared to the vinyl halide polymers, as well as the effects of halogen type when compared across the two full series.

1.2.2.1 Poly(vinylidene fluoride) (PVDF)

The synthesis of PVDF is achieved by radical polymerization in either emulsion or suspension of the gaseous monomer 1,1-difluoroethylene. The polymerization is generally performed in water at temperatures up to 150 °C and pressures up to 100 MPa with organic peroxides as the initiators. The degree of polymerization of industrial PVDF is usually around 1500, giving a molecular weight of 50,000 kDa (M_n, PDI =2) on average.[41] By NMR it can be observed that between 2% and 7% of head-to-head and tail-to-tail links[42] are found in typical PVDF and that the defect level increases with increasing polymerization temperature.[10] The defect linkages affect significantly the crystallization processes and the resulting morphology.[43,44]

PVDF is known to have three major crystalline forms, which find their basis in three different chain conformations, which are abbreviated as α, β, and γ. The α form is thermodynamically the most favorable because the F-F interactions are minimized by the trans-gauche conformation.[45] When PVDF is crystallized from the melt at room temperature, the α form dominates and results in polymer samples that are 50-70% crystalline.[46] The fundamental crystalline nature of such polymers is found in an orthorhombic unit cell with dimensions: *a* = 4.96 Å, *b* = 9.64 Å, *c* = 4.62 Å.[47] The T_m of the α phase is measured to be 172 °C. One of the most important consequences of the α phase is that the strong dipole moments of the CF_2 units are aligned antiparallel in adjacent chains. If the crystallization from the melt is carried out at higher temperatures (>160 °C), a new γ phase is observed. In this case a monoclinic unit cell is observed with dimensions: *a* = 4.96 Å, *b* = 9.67 Å, *c* = 9.20 Å.[48] The T_m of the γ phase is 185 °C.

A modified chain conformation relative to the α phase is observed and characterized by a trans-trans-trans-gauche conformation in which the dipole moments are now aligned in adjacent chains and do not cancel.[49] The third common form is the β phase, which is characterized by an all-trans polymer backbone, which crystallizes with an orthorhombic unit cell with dimensions: *a* = 8.58 Å, *b* = 4.91 Å, *c* = 2.56 Å. The T_m of the β phase is 178 °C.[49] In the β phase all the dipole moments are aligned parallel and thus this phase is the most interesting for electronic applications, as will be described below, based on the unusually high dielectric constant of this material.[50] Formation of the β phase is usually negligible in the melt crystallized samples, as it is not nearly as kinetically favorable as the α and γ phases. The β phase is usually derived by drawing of α phase samples at temperatures > 100 °C. The T_g of the amorphous regions of PVDF is observed at -40 - -30 °C.[51,52,53]

The thermal stability of PVDF is excellent up to 300 °C, at which point the onset of thermal degradation can be observed. At temperatures above 350 °C, a strong evolution of HF is observed.[46] The thermal stability of PVDF, coupled with the stiffness and toughness induced by the high crystalline content of the polymer, make PVDF important in applications in which toughness, impact resistance, and mechanical strength are required. PVDF is also resistant to chemicals, weathering, and light. The high dielectric constant, especially of the β phase, makes PVDF important for pyroelectric and piezoelectric applications.[41] Common uses of PVDF include coatings, laminates, tubing, piping, jacketing for wires, and piezo- and pyroelectric transducers.

1.2.2.2 Poly(vinylidene chloride) (PVDC)

While vinylidene chloride copolymers have long been well-known as among the first commercially available polymers, the homopolymer PVDC does not have sufficient thermal stability and is therefore not commercially available.[54] Nonetheless, from a structural point of view, PVDC is interesting for comparison purposes. PVDC is synthesized by a variety of free radical methods in solution, suspension, emulsion, or slurry, initiated by peroxides or azo compounds, resulting in a primarily head-to-tail polymer, which contains relatively little head-to-head defects or branching.[55] Degrees of polymerization from 100-10,000 are readily achieved in PVDC.[56] Due to the highly regular structure that is found with PVDC, a high degree of crystallinity is observed, similar to that described for PVDF above.

The physical properties of PVDC as observed by DSC, reflect the highly crystalline nature of the polymer, which shows only a very weak T_g at -19 - -11 °C in the as-polymerized samples.[57,58] Polymer melting is observed at 198-205 °C.[59,60] The unit cell as measured by XRD

of PVDC is defined by dimensions: a = 6.73 Å, b = 12.54 Å, c = 4.68 Å, and is assigned a monoclinic unit cell.[61]

The degradation behavior of PVDC is its most well-known property. At temperatures above 120 °C, PVDC begins to undergo dehydrohalogenation and a rapid evolution of HCl gas is observed just above the T_m at ~200 °C.[62] This lack of thermal stability renders PVDC commercially unviable.

1.2.2.3 Poly(vinylidene bromide) (PVDB)

Polymerization of PVDB is achieved by emulsion polymerization of vinylidene bromide.[63] As with PVB, PVDB is unstable to light and is thermally unstable. The onset of degradation for PVDB occurs at a slightly lower temperature than for PVB, but the release rate of HBr is not as rapid as for PVB.[64] Because of the relative instability of PVDB, little information exists concerning this polymer. One report does compare the observed crystal structure of PVDC and PVDB and gives unit cell dimensions for a monoclinic unit cell of PVDB of: a = 25.88 Å, b = 13.87 Å, c = 4.77 Å, and directly compared to PVDC, which was found to have unit cell dimensions: a = 22.54 Å, b = 12.53 Å, c = 4.68 Å.[65] The b and c dimensions reported here for PVDC match closely with those reported in the previous section. Notice here, that the a dimension for both PVDC and PVDB are considerably larger than the 6.73 Å reported in the previous section for PVDC and reflect a different definition of the unit cell.[61] Importantly though, the noticeable expansion in the unit cell size when going from PVDC to PVDB is a reflection of the incorporation of the larger bromine atoms into the crystalline lattice.

Table 1-2 summarizes the properties of the vinylidene halide polymers. The most important trend is observed in the unit cell dimensions of the polymers. For the three polymers in the monoclinic phase and defined by comparable unit cells, it is observed that in increasing the

size of the halogen from F to Cl to Br, the *a*, *b*, and *c* dimensions all increase steadily. This increase reflects the incorporation of the larger halogen in the crystal lattice.

1.2.3 Polytetrafluoroethylene (PTFE)

Polytetrafluoroethylene (PTFE), commonly known as Teflon, is represented by the repeat unit -(CF_2-CF_2)-. PTFE is synthesized mainly via the suspension polymerization of tetrafluoroethylene with inorganic initiators such as persulfates.[66] Molecular weights in the tens of millions (g/mol) are estimated for PTFE, although no direct solution measurements can be made, as PTFE is insoluble in all common solvents.[67] The primary structural difference of PTFE relative to all of the previously described halogen containing polyolefins is the symmetry of the repeat unit, which removes tacticity and regiochemistry (head-to-head or head-to-tail linkages) as structural factors that must be considered. Additionally, the 92-98% crystallinity observed in untreated PTFE samples reflects a predominantly unbranched chain structure.[68,69] Further, the fluorine atoms are too large to allow the polymer backbone to attain a planar zigzag conformation, and thus the chains lose the flexibility that such a conformation would allow, inducing a high degree of rigidity into the polymer backbone.[70] At low temperatures the polymer backbone displays a twist of 180 ° over 13 CF_2 groups, which actually changes to a twist of 180 ° over 15 CF_2 groups during a transition at 19 °C, as will be discussed below.[66]

Thermal analysis of PTFE shows a melt transition at 327 °C.[71] Several other important thermal transitions are observed, most notably at 19 °C, the triclinic crystal structure changes to hexagonal.[67] Whereas, below 19 °C, there is almost perfect three-dimensional order, the transition at 19 °C induces a degree of disorder during the restructuring of the crystalline packing. The cause of this reorganization at 19 °C is a slight twisting in the polymer backbone, as described above. Another transition at 30 °C further disorders the chain segments, although a hexagonal packing is retained. These two transitions are important because they occur near

ambient temperature.[67] The lattice parameters for the highly crystalline triclinic form of PTFE are: a = 9.52 Å, b = 5.59 Å, and c = 17.06 Å.[72]

PTFE has an excellent thermal stability due to the very strong C-F and C-C bonds in the polymer. Very few organic materials possess a thermal stability approaching that of PTFE, which is stable up to nearly 525 °C in air.[73] Vacuum degradation studies show an onset at 440 °C, which peaks at 540 °C. The degradation mechanism of PTFE also differs from PVF, for example, in that HF gas is not released. Instead, tetrafluoroethylene is the primary product under vacuum decomposition.[73] Importantly, due to the size of the fluorine atoms and the uniform coverage on the polymer backbone, the C-C backbone is protected from chemical attack, conferring excellent chemical stability to PTFE as well. Based on the excellent thermal and chemical stability as well as the excellent mechanical properties, PTFE finds numerous applications. The largest application area is in wiring and electronics, although a number of other applications are found in coatings and seals.[66]

A comparison of the properties of the halogen containing homopolymers leads to several definite conclusions. First, the substitution of a halogen atom for one or more of the hydrogens in the ethylene repeat unit leads to clearly defined changes in the structural properties of the polymer, which has definite consequences on the macroscopic properties and strongly influences the applicability of the polymer. Second, it is clear that in such homopolymers within a structure type (e.g. vinyl polymers), increasing the halogen size leads to an expansion of the unit cell (see Table 1-1 and Table 1-2) and a consequent change in the crystalline properties of the polymer. Finally, it is observed that increasing the number of halogens per repeating unit leads to a change in the symmetry of the unit cell, as all PVH polymers show an orthorhombic unit cell analogous to PE, but all of the PVDH polymers exhibit a monoclinic unit cell. The reduction in symmetry

with increasing halogen content reflects how the incorporation of larger atoms in place of hydrogen disturbs the packing of the PE backbone. The triclinic packing of PTFE shows a further degeneration in the symmetry of the PE lattice. In all cases such effects on the crystalline properties reflect the incorporation of the halogen into the crystal lattice in such homopolymers. Notice also that the halogen size and content affects the attainable level of crystallinity in these polymers. However, no universal correlation can be drawn based on halogen size and content alone, as such factors as tacticity and defects (e.g. head-to-head linkages) also play a strong role in the ability and extent of the polymers to crystallize. Importantly such homopolymers lead to a limited number of combinations of halogen content and distribution and thus do not allow for the derivation of a complete set of fundamental structure-property relationships. For this task, most effort has been focused on ethylene vinyl halide (EVH) copolymers, synthesized via a variety of methods as discussed in the following section.

1.3 Ethylene Vinyl Halide (EVH) Copolymers

In the previous section, we have examined halogen-containing homopolymers for the effect of halogen content, distribution, and size on the thermal and crystalline properties of the polymer. However, the range of halogen contents and distributions in such homopolymers, which are almost universally synthesized via radical polymerization from vinyl monomers, is limited. Therefore, it is interesting to examine halogen containing polyolefins synthesized via a number of other methods, which are more appropriate for generating a large range of halogen contents and distributions. In this way, a deeper understanding of the effects of halogen incorporation on the structural and morphological properties of polyolefins can be pursued. The most commonly employed techniques, to date, are halogenation of PE or analogues, dehalogenation of halogen-containing homopolymers, or copolymerization of ethylene with vinyl halide monomers. In the latter method, direct free radical copolymerization of vinyl

halides, such as vinyl chloride, and ethylene, it is difficult to control the content of the two monomer units over the full range of compositions.[74] Further, the free radical nature of the polymerization leads to poorly defined structures with high defect contents.[75,76] Direct copolymerization of vinyl chloride and ethylene using Ziegler-Natta or metallocene catalysts is also problematic based on the occurrence of side reactions with the activated chlorine atom on the monomer and the alkylaluminum cocatalyst as well as the tendency of the vinyl chloride monomer to undergo β-halo elimination after insertion into the metal-alkyl bond.[75,77] Based on these limitations, direct copolymerization has not been successfully used to investigate the compositionally dependent bulk properties of halogen containing polyolefins. Here the methods of direct polymer halogenation and dehalogenation will be examined.

1.3.1 Halogenation of Polyethylene

Direct halogenation of polyethylene has been extensively used as a technique for developing a set of structure-property relationships in halogen containing polyolefins. [78,79,80,81] Halogenation of any number of morphological forms of PE leads to "copolymers", which can exhibit a large range of halogen contents and distributions. The most relevant examples of this class of EVH copolymers are discussed below.

1.3.1.1 Fluorinated PE

The surface fluorination of PE has been the subject of numerous studies, largely focusing on how the introduction of fluorine into the surface layers will modify the surface characteristics of the polymer, such as wetability and permeability.[82] Common methods of surface fluorination are based largely on the treatment of the polymer sample with either fluorine gas or some mixture of fluorine gas in inert gaseous mixtures to yield surface fluorinated PE via a free radical fluorination process.[83,84] Plasma based fluorination schemes are also employed using agents such as CF_4 or SF_6.[85,86] In most cases the only changes in properties are confined to the surface layers

of the polymer and the bulk properties remain essentially unchanged.[87] As such, this technique has not been used to generate homogenous samples of fluorinated polymer for study of the bulk structural properties of the material.

1.3.1.2 Chlorinated PE (CPE)

The chlorination of PE is conducted using a variety of methods, such as solution, suspension, solid state, single crystal, thin film, and in the melt. The physical properties of the chlorinated polymers are strongly influenced by the structure of the polyethylene sample used as well as the specific chlorination method and conditions employed.[88] Specifically, the rate of chlorination and the polymer structure, as well as the chlorination condition (i.e.; solution, solid state, etc.) influence the chlorine content and sequence distribution in the final polymer sample.[78] This complex interplay of factors can lead to an enormous variation in polymer structure and physical properties among chlorinated PE samples.

Chlorination of PE in solution results in the most random distribution of chlorine throughout the polymer.[81] Solution chlorination specifically refers to the case where polyethylene is completely dissolved in a given solvent such that every site on the macromolecules are able to react with chlorine. When the chlorine content is less than 50% by weight, the probability of chlorine substitution on a CHCl unit or neighboring unit is very small based on the bulky Cl atom, resulting in a random spatial distribution of Cl atoms along the backbone. At greater than 50% by weight, however, geminal chlorination and vicinal chloroination becomes more commonplace,[89,90] with vicinal being favored.[91] The most commonly used solvents are chlorohydrocarbons, such as tetrachloroethane, tetrachloromethane, dichloromethane, or chlorobenzene. Chlorination is effected in a variety of ways, commonly using irradiation, thermal initiation, or radical initiating species in the presence of chlorine gas. The consequence of this completely random chlorination process is the regular variation in

physical properties of a series of CPE samples prepared from a specific PE sample, where the percentage of chlorine introduced into the backbone is the primary factor influencing physical properties. Variation in the properties of the initially used PE sample will however introduce a further level of complexity in comparing CPE samples prepared from different PE samples.

The variation in thermal properties of solution chlorinated PE reflects the random nature of the chlorination process. Increasing the chlorine content results in a decrease in the flexibility of the polymer backbone, which is reflected by the regular increase in glass transition temperature with increasing Cl content. This regular increase also points to the random distribution of Cl atoms in the polymer. The consequence is that CPEs possessing intermediate degrees of chlorination (~15% by weight) show elastic properties, while those samples with high degrees of chlorination (>50% by weight) are rigid.[81,90,92] The overall crystallinity and melting point of CPE samples decreases with increasing chlorine content and above 37 wt% chlorine, crystallinity is totally inhibited.[90] The gradual disappearance of crystallinity with increasing Cl content is explained by the increasing incorporation of Cl into the crystalline phase at higher chlorine contents in the random polymers. The incorporation of the Cl atoms into the crystalline phase as defects results in the observed lower melting temperatures, smaller crystallite size, reduced crystallinity, and decreased degree of crystalline perfection.[93] The distribution of Cl atoms in CPE has been studied by DSC and WAXD. Diffraction data show that the *a* and *b* dimensions of the unit cell gradually expand with increasing chlorine content, which is attributed to the accommodation of the chlorine atoms into the crystalline lattice. While the PE starting material shows an orthorhombic crystal structure, the samples of CPE with the higher chlorine contents show distorted orthorhombic or pseudohexagonal in the extreme of degree of chlorination.[93]

Closely related to solution chlorination is another solution based technique; suspension chlorination. The main difference between solution and suspension chlorination is that under suspension conditions, the PE is not fully dissolved and thus all sites on the polymer backbone are not equally susceptible to attack by chlorine. The consequence is a distinct property set reflecting the non-random and often blocky chlorinated structure.[93] Suspension chlorination of PE is generally carried out using a water suspension method[94] or using high concentrations of PE in organic solvent at temperatures below the melting point of the polymer.[79] In either case, chlorine gas is introduced into the system and initiation is commonly affected thermally or by irradiation. Chlorination occurs primarily in the amorphous regions[80] of the polymer or at the edge of the crystalline domain.[93] With higher chlorine contents, diffusion of chlorine gas into the crystalline region results in chlorination of the crystalline phase as well. The chlorination of the crystalline phase occurs from the outside edge of the crystal inward and results in the simultaneous conversion of the crystalline to amorphous regions.[93] This two-step process is responsible for the blocky nature of the resulting CPE polymers and also leads to the significantly higher chlorine contents in the amorphous regions of the polymer, which display much higher contents of geminal dichloro species relative to the solution chlorinated PE of the same chlorine content.

The thermal behavior of suspension chlorinated PE reflects the non-random substitution pattern. The as-prepared samples show melting temperatures and thermogram shapes equivalent to that of the parent PE sample on the first scan, but with proportionally decreasing enthalpies of melting (ΔH_f) relative to the increasing chlorine contents. Subsequent scans show that melting temperatures have shifted to slightly lower temperatures and have become broader with measured enthalpies proportionally smaller than those measured before the initial melt. This

behavior is indicative of the behavior of a block copolymer in which the chlorine rich segments remain amorphous and the ethylene segments are the only ones capable of melting and recrystallizing. Thus the important factors are the degree of chlorination, which determines how much of the initially crystalline PE domains remain non-chlorinated and the thickness of the original crystalline domains. These conclusions are supported by WAXD, which shows that the unit cell dimensions, *a* and *b*, for the suspension chlorinated PE does not change with increasing chlorine contents, indicating that chlorine is essentially excluded from the crystallites. This is in stark contrast to the case of the solution chlorinated PE as described above. Regardless of the chlorine content, samples of suspension chlorinated PE retain the orthorhombic crystal structure of the parent PE, but with decreasing diffraction peak intensity with increasing chlorine content. Based on these results and in comparison with the results from solution chlorination, it is clear that chlorine content and distribution are critical factors affecting the overall degree of crystallinity and the crystalline structure of CPE samples.

An extension of suspension chlorination is the chlorination of PE single crystals in suspension. Here large single crystalline PE samples are prepared via careful purification and crystallization, which gives uniform single-layer crystals.[95] In this case, chlorination is performed in a suspension of the PE single crystals where the chlorine gas is introduced in the presence of an initiator. Here, chlorination proceeds via a two-step mechanism in which rapid chlorination occurs first at the chain folds and then is followed by a slower chlorination and subsequent dissolution of chain segments on the edge. The polymer then chlorinates inwards from the edges generating a bimodal polymer composition with a highly soluble chlorinated fraction and an insoluble crystalline fraction with a very low chlorine content. The same is true

for the chlorination of PE single crystals in the solid state with either initiation via irradiation or in the absence of irradiation.[96,97]

Like suspension chlorination, solid state chlorination is a process in which PE samples are exposed to chlorinating conditions where differential reactivity exists between different portions of the polymer. Chlorination in the solid state can be performed on PE powders or films in addition to single crystals as mentioned above. For samples in the solid state chlorine gas is generally passed over the PE sample and initiation is either thermal or radiation based. The characteristics of the chlorination reaction for powdered samples reacted below the melting temperature of the PE sample are very similar to those for suspension polymerization, showing high degrees of chlorination in the amorphous regions and chlorination to a lesser extent in the crystalline regions.[78] No change in the unit cell dimensions are observed in the powdery samples, indicating that chlorine is not incorporated to a large extent in the crystalline portions of the polymer samples and relatively little change in the a dimension is observed even in the melt crystallized samples, also indicating that even upon recrystallization little chlorine is incorporated into the PE crystal lattice. This behavior is typical for blocky polymers and is similar to the behavior observed in suspension chlorinated PE.[98]

The results for thin film samples are also quite similar[99,100] and point to the fundamental consequence of using a heterogeneous chlorination system as opposed to the homogeneous system used in solution chlorination. In the solution case, all sites on the polymer chain are equally likely to be chlorinated at early reaction times and at higher chlorination contents, a spatially distributed chlorine pattern is favored, further randomizing the CPE structure. However in the case of heterogeneous chlorination as observed in suspension or in the solid state, differential reactivity exists not only between the amorphous and crystalline regions, but between

the different surfaces of the crystal and between the exterior and interior of the crystalline domains. The consequence for all of the heterogeneous chlorinations is a blocky primary structure as reflected by thermal and structural characterization.

1.3.1.3 Brominated PE

The most common method for the bromination of PE is via suspension bromination in the presence of elemental bromine and light.[101] This technique is used for the free-radical bromination of either semicrystalline PE or single crystal PE. Common solvents for suspension bromination are bromobenzene, tetrachloroethylene, or carbon tetrachloride. The amount of bromine introduced into the PE sample is a function of the sample type (single crystal or semicrystalline) and the reaction time. Evaluation of the resulting thermal and crystalline properties provides information on the effect of bromine content, with respect to the distribution.

Suspension bromination of semicrystalline high density polyethylene (HDPE)[102] results in the generation of a blocky rather than a random distribution of bromine atoms along the PE backbone. It is observed that bromination occurs only in the amorphous regions of the polymer. Further, the greater the extent the bromination, the greater the decrease in the overall crystallinity of the polymer in melt recrystallized polymer samples. Such behavior leads to the conclusion that the bromine atoms are behaving as a defect, limiting the ability of the polymer to crystallize. Long crystallizable methylene sequences are retained in the polymer after bromination, but their ability to crystallize via a mechanism based on the selection of such long sequences is inhibited as the bromine content of the polymer increases. The melting point of such blocky brominated polymers after melt-recrystallization is gradually depressed from the 130 °C observed for the pure HDPE to a value of ~124 °C in all samples with at least 6% bromine by weight. This leveling off effect is a characteristic of blocky copolymers and specifically characteristic of such samples in which additional bromination beyond 6 wt% does not increase the number of non-

crystallizable sequences, but simply increases the density of bromine atoms within such sequences, which are formed in the amorphous region of the initial polymer sample.

Suspension bromination of single crystal PE produces quite different results.[103] In this case, bromination occurs almost exclusively at the fold surface of the crystals. Examination of the orthorhombic unit cell parameters show almost no change for the as-brominated samples, as would be expected for the case when bromine atoms are only added at the fold surface and not within the bulk crystal. Upon melt-annealing, both the *a* and *b* dimensions (the *c* dimension – the chain direction - shows no change) of the unit cell increase steadily with increasing bromine content up to 6.7% bromine by weight. Beyond 6.7% bromine and up to 19.1% (the highest value measured), the *a* and *b* dimensions stay relatively constant. This phenomenon can be explained by the fact that bromination of the single crystal starting material only occurs at the fold surface. After the as-brominated sample is melted and it is cooled, the chains reorganize themselves during the recrystallization process, and the incorporation of bromine defects into the crystal is consistent with the increasing *a* and *b* dimensions of the unit cell. A steady increase in the *a* and *b* dimensions up to about 6.7% bromine is consistent with the presence of an increasing number of defect sites that are available for incorporation into the crystal. Beyond this bromine content, essentially all of the original fold surfaces contain at least one bromine atom and start to be subject to multiple brominations. As such, beyond 6.7% bromine, the *a* and *b* dimensions stay essentially constant, as the number of defect sites has leveled off.

The changes in ΔH_f with increasing bromine content can also be explained. For the as-brominated samples, the ΔH_f is essentially constant for all samples. A slight decrease of less than 4% in the ΔH_f value is observed with 19.1% bromine by weight. In this case an average of >4 bromine atoms are present per fold. As a result, with such a high concentration of bromine

present at the fold surfaces, a significant amount of strain is expected to be induced in the crystalline region adjacent to the fold surface, resulting in a decrease in ΔH_f. For the melt-recrystallized samples, a steady decrease in ΔH_f is observed with increasing bromine content. This steady and large decrease (a 58% decrease is observed for the sample with 19.1% bromine) is consistent with the incorporation of defects into the crystal lattice. Beyond 6.7 wt% of bromine, the continual decrease in ΔH_f reflects the incorporation of larger defects (multiply brominated fold-surface segements) rather than the incorporation of additional defect sites.

Further, based on this model and the results of the XRD and changes in ΔH_f discussed above, the changes in T_m with increasing bromine content can also be explained. For the as-brominated samples, the T_m onsets are essentially constant across the entire range of bromination. However, for the melt-recrystallized samples, the T_m onset shows a steady decrease up to the point where one bromine atom per fold surface had been introduced; i.e., up until the point where the number of defect sites remains constant. The incorporation of such defects into the crystal reduces the level of perfection and simultaneously reduces the T_m. Beyond this level of bromination, larger decreases in the T_m onset reflect the incorporation of larger defects into the crystal, which further distort the structure and decreases the T_m.

1.3.2 Dehalogenated Homopolymers

Another method that has been successfully employed for the synthesis of EVH copolymers is the reductive dehalogenation of halogen containing homopolymers. This method has been employed for the reductive dehalogenation of PVC[104,105,106] and PVB.[107] However, the only extensive structural characterizations of the resulting EVH copolymers have focused on EVC generated from PVC. The common synthetic method employed in this case is the reductive dechlorination by reaction with tri-*n*-butyltin hydride.[108] Specifically, PVC is dissolved in THF

and in the presence of a catalytic amount of AIBN, a 20% excess of tri-*n*-butyltin hydride, relative to the desired level of dechlorination, is reacted with PVC, as seen in Figure 1-4. As a consequence of the homogeneous reaction conditions, a random-like distribution of vinyl chloride and ethylene comonomer units is achieved. In this way, a family of copolymers with equivalent chain lengths and polydispersities is achieved by using a single batch of PVC to generate such a family.[108] Also, a family of EVC copolymers with varying comonomer compositions can be achieved, that would not be possible via direct copolymerization of ethylene and vinyl chloride. The random-like distribution allows one to study the effect of halogen content and sequence distribution without the limitations of the previously described halogenation methods, which generally selectively halogenated only certain portions of the polymers.

In the most complete study of a family of EVC copolymers generated via the reductive dehalogenation of PVC, samples with varying chlorine contents ranging from pure PE (fully reduced PVC) to a sample with 37.3 mol% vinyl chloride were used.[108] Analysis by WAXD showed that as the chlorine content of the samples increased a progressive change in the crystalline properties of the polymers was observed. First, an expansion of the orthorhombic unit cell of PE was observed, mainly in an increase in the *a* dimension from 7.48 Å in pure PE to 8.95 Å in the EVC sample with 37.3 mol% vinyl chloride (VC). This corresponds to a 20% expansion in the *a* dimension of the unit cell. Concurrent with the increasing dimension of the unit cell is a gradual change in the crystalline lattice from orthorhombic to pseudohexagonal. Between 13.6 and 21.2 mol% VC units, the change from orthorhombic to pseudohexagonal is observed. Both of these results indicate that chlorine is incorporated into the crystal lattice as a defect. At low concentrations of chlorine, the defect is easily incorporated into the crystal lattice with little

disruption of the overall crystalline structure. However, with increasing chlorine content, the presence of a larger amount of defect not only decreases the ordering within the crystal lattice, but also decreases the overall crystallinity on the sample as the defect inhibits crystallization.[74] Therefore, the percent crystallinity of the samples decreases from more than 60% with pure PE to essentially 0% when 40 mol% VC units are present. The thermal properties of these random EVC copolymers also supports the incorporation of VC units into the crystal lattice as a defect. Here, DSC indicates that the T_m of the samples decreases from 128 °C with PE to 20 °C with the 37.3 mol% VC sample.

1.3.3 Synthesis of EVH Copolymers via Ring Opening Metathesis Polymerization (ROMP) Followed by Hydrogenation

Another method for synthesizing random EVH copolymers has been recently described. In this case ring opening metathesis polymerization (ROMP)[109] has been employed to achieve random EVC copolymers via the copolymerization of cyclooctene and 5-chlorocyclooctene, followed by hydrogenation as seen in Figure 1-4. By varying the comonomer ratios, vinyl chloride contents from 0-50% were achieved. Analysis via DSC and WAXD was used to examine the crystalline properties of these polymers. As the VC content increased from zero to 13.5 mol%, the orthorhombic unit cell was observed to expand and the reflections in the XRD became broader, both of which indicate that the chlorine atoms are entering the orthorhombic crystal lattice. In fact at 13.5 mol% VC, the unit cell is actually transformed to a distorted orthorhombic or pseudohaxagonal unit cell. With higher VC contents (16, 20.8, and 25 mol%), a true hexagonal unit cell is observed. The crossover in behavior after 13.5 mol% VC is also observed via DSC. For zero to 13.5 mol% VC, the T_m gradually decreases, the melting peak becomes broader, and the overall crystallinity decreases with increasing VC content. These three features are consistent with the incorporation of chlorine, as a defect, into the crystal. For the

samples with 16, 20.8, and 25 mol% VC, the T_m shows only the slightest changes between samples and shows an increasing sharpness with increasing chlorine content. The authors postulate that the unusual melting behavior at high VC contents may be a result of regular chlorine placement along the chain. The authors also suggest that such regular placement of chlorine atoms along the polymer chain would nicely explain the observed hexagonal crystal structure at high VC contents, as the hexagonal form is generally not encountered in ethylene copolymers with high comonomer content and the hexagonal form could be expected to accommodate the chlorine atoms more easily than the orthorhombic form.

1.4 Acyclic Diene Metathesis (ADMET) Polymerization as a Route for Deriving Structure-Property Relationships in EVH Polymers

Considering the above methods for attaining EVH polymers, it is clear that control over halogen content can be achieved in each of these methods, but control over sequence distribution cannot be attained. Therefore, even though the properties of EVH polymers with different halogen contents are known to vary, deriving exact relationships between primary structure and physical properties is unattainable because a precise distribution of comonomer units between crystalline and amorphous domains has yet to be determined.[110]

Despite the lack of a precise model for understanding the variation in the properties of EVH polymers, there is great practical interest in these materials.[110] Specifically, the introduction of ethylene units into a PVC chain will serve the role of an internal plasticizer, which can give many advantages over the introduction of an external plasticizer and lead to a new range of materials properties from a single component material.[111] From a more fundamental standpoint, this class of polymers is also of great interest for developing a precise understanding of the relationship between molecular structure and physical properties in semicrystalline polymers in general, where EVH polymers could serve as an all-purpose model for this class of polymers. As

described above however, no specific catalyst system has been developed to effectively copolymerize ethylene and vinyl halides, leading to the necessity to look toward model EVH polymers to establish the fundamental significance of this class of polymer. Such a focus on model polymers will not only help to derive structure property relationships, but will shift focus to the development of effective catalysts for the synthesis of EVH copolymers.[109] It is difficult however to find suitable model systems that will allow the development of precise structure property relationships[112] and will not be limited by the quality of the synthetic or preparative method.

Ayclic diene metathesis polymerization (ADMET)[113] has been used to achieve an EVC polymer with both precisely controlled chlorine content and sequence distribution,[114] here such a level of control allows one to derive precise relationships between polymer primary structure and physical properties in EVC polymers. Further, ADMET allows the investigation of a much greater range of polymers with precisely distributed chlorine atoms, as the linear α-ω dienes used in ADMET are free of the structural constraints required for monomers used in ROMP. Presented here is the full characterization of new expanded family of precise and random EVH polymers (Figure 1-4) in which a range of precise halogen contents and precise and random sequence distributions are examined in order to generate structure-property relationships useful for developing a deeper understanding of the importance of primary structure control in EVH polymers.

Table 1-1. Properties of poly(vinyl halide) polymers.

Polymer	T_m (°C)	X_c (%)	Unit cell type	Unit cell dimensions (Å)	Decomposition temperature (°C)
PE (HDPE)	125-134	62-80	Orthorhombic	*a* = 7.42 *b* = 4.94 *c* = 2.55	348
PVF	190	20-60	Orthorhombic	*a* = 8.57 *b* = 4.95 *c* = 2.52	450
PVC	120-260	<10	Orthorhombic	*a* = 10.6 *b* = 5.4 *c* = 5.1	200
PVB	----------	----------	Orthorhombic	*a* = 11.0 *b* = 5.6 *c* = 5.1	<100
PVI	----------	----------	----------	----------	<100

Table 1-2. Properties of poly(vinylidene halide) polymers.

Polymer	T_m (°C)	X_c (%)	Unit cell type	Unit cell dimensions (Å)	Decomposition temperature (°C)
PVDF	172 (α)	50-70 (α)	Orthorhombic (α)	*a* = 4.96 (α) *b* = 9.64 *c* = 4.62	350
	178 (β)		Orthorhomnic (β)	*a* = 8.58 (β) *b* = 4.91 *c* = 2.56	
	185 (γ)		Monoclinic (γ)	*a* = 4.96 (γ) *b* = 9.67 *c* = 9.20	
PVDC	198-205	----------	Monoclinic	*a* = 6.73 *b* = 12.54 *c* = 4.68	200
			Monoclinic	*a* = 22.54 *b* = 12.53 *c* = 4.68	
PVDB	----------	----------	Monoclinic	*a* = 25.88 *b* = 13.87 *c* = 4.77	<100

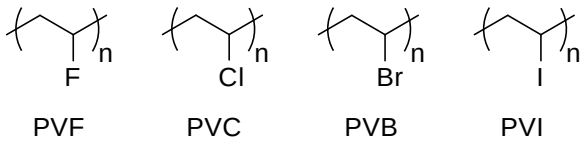

Figure 1-1. Structure of poly(vinyl halide) polymers.

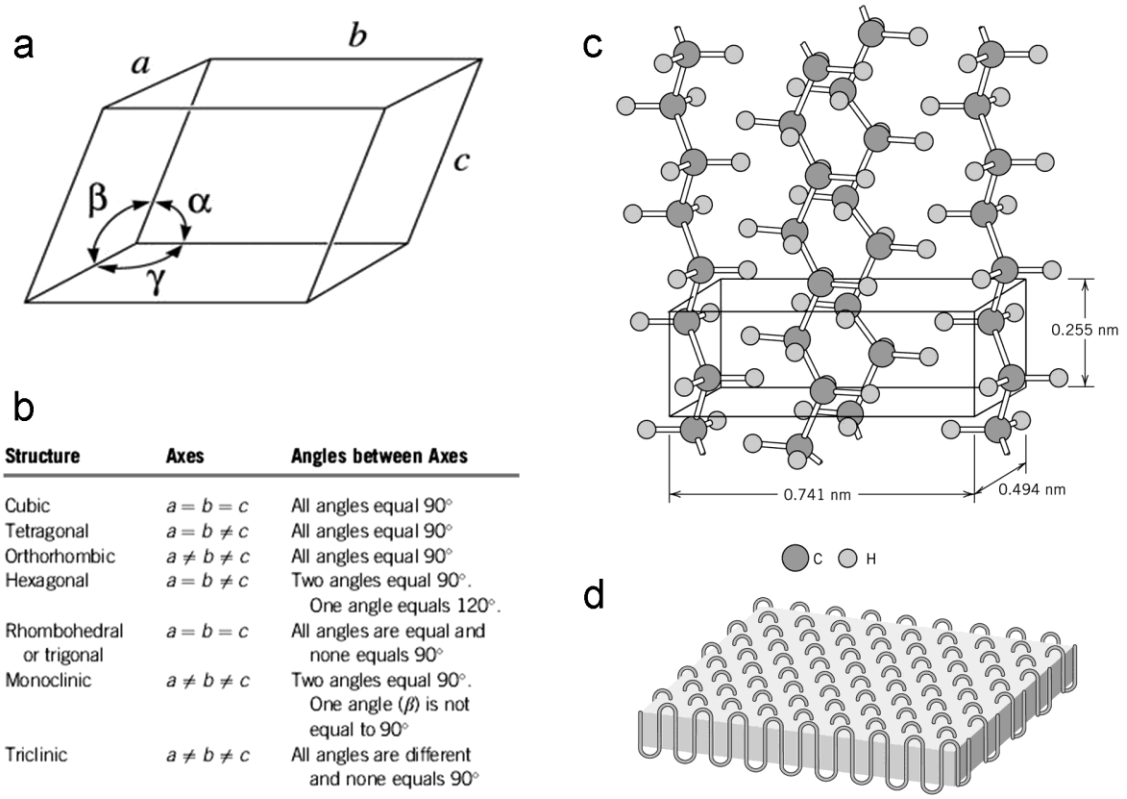

Figure 1-2. Unit cell parameters. (a) Generalized unit cell showing axes (*a*, *b*, *c*) and angles (α, β, γ). (b) Parameters for specific unit cell types. (c) Orthorhombic unit cell for polyethylene showing unit cell dimensions and superimposed polyethylene chains. (d) Single crystal of polyethylene illustrating the chain-folded lamellar structure.

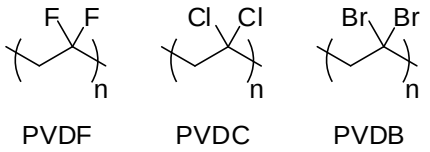

Figure 1-3. Structures of poly(vinylidene halide) polymers.

Chlorination of PE

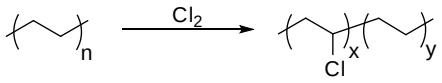

Reductive Dehalogenation of PVC

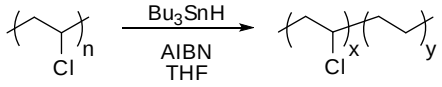

Random EVC Copolymers via ROMP

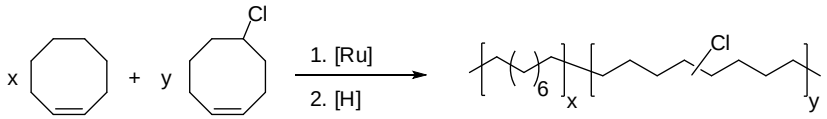

Precise EVC Polymers via ADMET

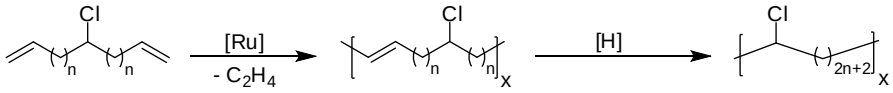

Random EVC Copolymers via ADMET

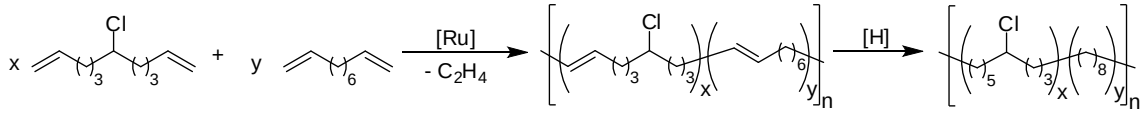

Figure 1-4. Routes to EVC polymers.

CHAPTER 2
SYNTHESIS AND CRYSTALLIZATION OF PRECISION ADMET POLYOLEFINS CONTAINING HALOGENS

2.1 Introduction

Polyolefins are among the most important large volume polymers produced today.[1] Polyethylene (PE) has found use in such diverse areas as packaging, biomaterials, microelectronics, and protective coatings,[115] all of which depend on the tunable semicrystalline morphology of the polymer.[116] Modification of the parent structure through halogen incorporation, as in the case of poly(vinyl chloride) (PVC) or poly(tetrafluorethylene) (PTFE), [117] further extends the range of applications as a result of changes in polymer structure at all levels.[118,119] [120]

Ethylene-vinyl halide (EVH) copolymers also are of interest. Ethylene-vinyl chloride (EVC) copolymers offer improved thermal stability relative to PVC.[121] Similarly, ethylene vinyl fluoride (EVF) polymers are of value, such as poly(vinyl fluoride) (PVF), poly(vinylidene fluoride) (PVF_2), and poly(ethylene-*alt*-tetrafluorethylene).[122] Ethylene vinyl bromide copolymers[123] and partially brominated polyethylene[102] are less well known.

Synthesizing copolymer variants of common halogenated polyolefins can be challenging due to reactivity ratio issues present during copolymerization[124, 125] and due to the ineffectiveness of post polymerization attempts to produce well-defined structures.[125,126] Of the various techniques that have been used to synthesize EVH copolymers, the simplest approach is halogenation of PE, a procedure which gives an irregular distribution of halogens along the polymer backbone. Further, the properties of the resulting polymer are highly dependent on the structure of the PE used and the conditions employed for the halogenation.[125, 126] Another typical

post-polymerization method is reductive dehalogenation,[125] where chemical reducing agents such as tributlytin hydride are used to replace halogens with hydrogens, yielding materials that experience the same structural irregularities problematic in all post polymerization strategies. The direct free radical copolymerization of ethylene and vinyl-halide comonomers yields copolymers containing numerous structural defects and consequent instability.[121] Regardless of monomer ratios, the copolymers contain inordinately high vinyl contents as a result of reactivity ratio imbalances, a phenomenon that can only be slightly improved by use of γ-ray induced polymerization.[74]

Olefin metathesis chemistry offers an alternative synthetic route to such polymers, based on the development of well-defined late transition metal catalysts.[127] Ruthenium catalyzed ring opening metathesis polymerization (ROMP) can yield EVC copolymers possessing well-defined structures.[121] Acyclic diene metathesis polymerization (ADMET) [128, 129] has also been used for the synthesis of a precisely defined EVC polymer.[114] With ADMET, variation in the monomer structure gives access to a broad range of precisely defined polymers, allowing direct correlation of structure-property relationships.[113] The ability of ADMET to produce PE structures with precisely placed pendant groups is generating a wealth of structure/property data at the moment.

As has been known for decades now, the random incorporation of relatively small amounts (<10 mol%) of a structural irregularity in polyethylene (PE) generates copolymers possessing thermal properties that adhere to thermodynamic principles of phase transitions in two-component systems.[130, 131, 132] The vast quantity of experimental data that exists unequivocally demonstrates that side groups such as ethyl, propyl, vinyl acetate, styrene and others are not incorporated into the copolymer crystal lattice.[133] Their solid-liquid transition follows the basis of Flory's equilibrium theory derived on the assumption of formation of a pure crystalline

phase.[134] On the other hand, smaller side groups such as methyl, chlorine and oxygen can be partially incorporated into the crystalline lattice.[131, 132] A different partitioning of the side group has an important impact on the thermodynamic and physical properties of these copolymers. Thus, melting temperatures of random copolymers with Cl pendant groups and CH_3 branches are significantly higher than those of copolymers with matched compositions of side groups excluded from the crystal.[131] The differences reflect the fraction of longer continuous crystallizable sequences present in the former type.

The analysis of the thermodynamic behavior of random ethylene copolymers with > ~10 mol% branch points in the main chain is more complex. At this branching level, melting temperatures and degree of crystallinity usually deviate upward from the linear trends observed at the lower branching contents,[130, 135, 136] and divergences are accentuated for copolymers with side groups that can be accommodated in the crystal.[109,137] In reference to thermodynamic principles, concerns are raised about the actual branching distribution in highly branched systems and how closely the crystallization behavior follows models based on selection of crystallizable sequences. On one hand, at large branching contents the usual temperature rising elution fractionation (TREF), crystallization fractionation (CRYSTAF) or NMR methods used to probe branching distributions either fail or become overwhelming in complexity.[138, 139] On the other hand, the decreased length of continuous methylene sequences may induce a different crystallization mode, as occasionally speculated[109] and in line with observations of a change in crystallographic packing with increasing comonomer content.[109, 137, 140, 141] Understanding the details of the crystallization behavior for these highly branched systems can only be accomplished via model polymers with well-defined microstructures. ADMET polymerization

leads to polymers with precisely defined microstructures and, hence, to excellent models to study the crystallization behavior of highly branched ethylene copolymers.

ADMET polymerization followed by hydrogenation produces either the linear polymer chain or ethylene copolymer–type branched molecules that lack any branching composition distribution. [114,128] This "clean polycondensation" chemistry is used here to produce a branched architecture characterized by the precise branch placement every "n" fixed methylene runs according to the repeated structural unit $-[(CH_2)_n-CHX]_y-$.

The unique characteristics of these systems permit the study of ideal models of functionalized polyethylenes with precisely placed substituents in which *n* and *X* can be varied independently. They are models for polyethylenes with controlled hydrogen substitution.

We now report the ADMET synthesis and crystallization of a series of precision polyethylene structures containing fluorine, chlorine, and bromine located on each and every 19th carbon (n = 18) along the polymer backbone. Included in this study is the synthesis of the first bromine containing polyolefin with a precisely defined primary structure, demonstrating that the weaker carbon-bromine bond survives both the metathesis and hydrogenation chemistry employed. Not included is the comparative polymer containing iodine, as this precision polyolefin has eluded our efforts to create it. We continue to investigate synthetic routes to the iodine analogue copolymer, for it will become important in the final analysis of these halogenated polyolefins. For now, the synthesis and primary structure characterization of the fluorine, chlorine, and bromine containing polyolefins presented here delineates the opportunity for a detailed understanding of the effects of halogen incorporation in polyolefins.

The effect of the substituent on the crystallographic packing is extracted using IR spectroscopy and wide angle X-ray diffraction (WAXD), while the partitioning of the substituent

between crystalline and non-crystalline regions is inferred from solid-state NMR spectroscopy and from the polymer's thermal behavior. Since small atoms, such as oxygen and fluorine are expected to be accommodated in the all trans polyethylene lattice, the systematic increase of van der Waals radius of the substituents in the series allows quantitative data of the degree to which the orthorhombic polyethylene lattice can tolerate atomic hydrogen substitution. The thermodynamic properties of these model systems will be directly correlated to substituent radius and bond lengths and will establish fundamental grounds for strategies to modify structural and thermal behavior of polyethylenes.

2.2 Results and Discussion

2.2.1 Synthesis

The synthesis of fluorine, chlorine, and bromine substituted EVH polymers with a halogen on each and every 19th carbon required the preparation of α–ω diene monomers, followed by ADMET polymerization and subsequent exhaustive hydrogenation as shown in Figure 2-1. All three halogen-containing monomers were derived from a common ketone precursor **1**,[142] which was reduced to the alcohol **2**,[143] prior to halogenation. The fluorine monomer (3) was synthesized in good yield from **2** using diethylaminosulfurtrifluoride (DAST). Chlorination was achieved by tosylation of **2** followed by nucleophilic displacement with LiCl, while the bromine monomer (5) was synthesized directly by action of CBr_4 /PPh_3 on the alcohol **2**. Monomers **4**[114] and **5** were then subjected to ADMET polymerization in the bulk using first generation Grubbs' catalyst.[127] The fluorine monomer **3**, was polymerized in solution (methylene chloride) as this monomer is a solid as opposed to **4** and **5**, which are oils. In a similar manner, the ketone starting monomer (1) was polymerized in toluene using first generation Grubbs' catalyst.

These unsaturated ADMET-EVH polymers were subjected to exhaustive hydrogenation to generate precision halogenated polyolefins. The nomenclature acronym used herein is UPE19X,

where U indicates unsaturation and PE19X indicates a polyethylene backbone with a halogen substituent (X) on every 19th carbon. In the case of UPE19F and UPE19Cl, diimide reduction[144] gave clean conversion of the unsaturated polymer to the fully saturated polymer as evidenced by IR and NMR. Diimide reduction proved ineffective for UPE19Br. In this case it is likely that the presence of nucleophilic species in the hydrogenation mixture resulted in the displacement of the bromine, a mechanistic event facilitated both by the weaker carbon bromine bond and the better leaving character of the bromine relative to chlorine and fluorine. Successful hydrogenation was achieved for UPE19Br as well as UPE19O (the polymer product of monomer 1) using Wilkinson's catalyst.[145] Polymer molecular weights were found to range from a M_w of 11,300-12,000 g/mol for PE19F and PE19O respectively (GPC vs. PE) to 38,000-49,500 g/mol for PE19Br and PE19Cl respectively (GPC vs. PS) as listed in Table 2-1.

2.2.2 Primary Structure Characterization.

The primary structure for these well-defined halogenated polyolefins was established using a combination of ^{1}H NMR, ^{13}C NMR, TGA (thermogravimetric analysis), IR spectroscopy, and elemental analysis. The precise structure of the polymers is supported by NMR, while TGA results prove the composition of the polymer through the clearly observed thermal decomposition and release of exact masses of HX (calculated HF = 7.0% and HBr = 23.5%, found HF = 7.3 % and HBr = 22.7%), followed by catastrophic decomposition; as illustrated for PE19F and PE19Br in Figure 2-2 and previously observed for PE19Cl.[114] The mass loss in all cases is in accord with the theoretically calculated value.

Figure 2-3 shows the IR spectra for thin films of the three halogenated polymers, data which also serve to support the expected primary structure. Here the absence of a peak at 967-969 cm^{-1}, corresponding to the out-of-plane C-H wag (γ_w) of an alkene,[145,146] indicates complete

hydrogenation of the polymer backbone. Further, the IR spectra support the presence of each of the expected halogens on the polymer backbone. For PE19F, the sharp peak at 1068 cm^{-1} protruding from a broader underlying peak is characteristic of the C-F stretch.[147] The peaks observed at 611, 660, and 802 cm^{-1} in PE19Cl are characteristic of C-Cl stretching vibrations,[126, 148] while for PE19Br, the peak at 612 cm^{-1} is assigned to the vibrations of the C-Br bond.[102]

These IR data also provide an insight into the crystalline structure of these precisely halogenated polymers. In this regard, the significant peaks are those found at ~720 and ~1470 cm^{-1} which correspond to the vibrational modes of the CH_2 sequences in PE analogues.[126] For PE19F, the doublets observed at 721-730 and 1463-1472 cm^{-1} are the same as observed in crystalline PE. The band at ~720 cm^{-1} corresponds to long trans CH_2 sequences and the band at 730 cm^{-1}, is associated with the rocking vibrations of CH_2 sequences of five or more carbons.[126, 149] The IR spectra for PE19Cl and PE19Br are clearly different from those for the fluorinated analogue PE19F and pure PE, suggesting a distinct difference in the crystalline packing of these polymers. The Cl and Br precision polymers show a single peak rather than doublets at ~720 and ~1470 cm^{-1} suggesting that these polymers possess similar crystalline features, yet differ from the fluorine and pure polyethylene counterparts. Both WAXD and solid-state ^{13}C NMR studies of the crystalline structure, presented in the following sections support these results.

2.2.3 Wide Angle X-Ray Diffraction (WAXD)

X-ray diffractograms of halogen containing ADMET samples cooled from the melt at 1°C/min are shown in Figure 2-4 together with the patterns of a matched PE19O (with a C=O group on each and every 19th carbon) and of a linear polyethylene narrow fraction in the same molecular weight range. It is at first evident that all samples display very sharp diffraction peaks, except for the broader pattern of the brominated material. In contrast, random ethylene

copolymers with the same type of branching and with similar, and lower, branching levels are known to display much broader WAXD patterns.[108,109,145] Hence, the sharp diffractograms of Figure 2-4 point to a homopolymer rather than copolymer-like crystallization behavior of these polyolefins. It is also evident that while substitution of the hydrogen for O or F every 19th carbon does not alter the orthorhombic unit cell packing of the linear chain, substitution with a bulkier atom promotes formation of a different crystallographic phase.

Diffraction peaks found at ~19° and ~22° for Cl and Br containing samples were also found in similar precisely placed methyl branched polymers and indexed as (010) and (100) diffractographic planes of a triclinic cell.[150] Therefore, in reference to this pattern, the diffractograms of PE19Cl and PE19Br are assigned to triclinic structures. Compared to the orthorhombic packing displayed by PE and polymers with F and O substitutions, the triclinic pattern is a degeneration in the scale of symmetry supporting previous speculation[150] that a reduced order is needed to facilitate minimum spatial requirements to accommodate the bulky Cl, Br, or CH_3 groups between adjacent molecules in the crystal. The triclinic pattern differs substantially from a single diffraction pattern observed for methyl branched polyethylenes or for ethylene vinyl chlorides with the same content of side groups but randomly distributed.[108, 109, 140, 141, 145,] In these systems single WAXD peaks were associated with defective orthorhombic or pseudohexagonal structures. Therefore, the progression of WAXD patterns of Figure 2-4 clearly evidence that both, *type and distribution* of the substituent, impact the chain ordering of branched or substituted polyethylenes at the most fundamental level.

The 2θ values of the diffraction peaks, together with other characterization data, are listed in Table 2-1 for the PE and ADMET precisely substituted polymers. Also listed are X van der Waals radii and C-X bond lengths. Inspection of these data allows evaluation of lattice

expansions in reference to geometric constraints imposed by the solute X in the adjoining matrix. Compared to the unsubstituted polyethylene chain, the shift of 2θ (110) and 2θ (200) in the PE19F and PE19O patterns to lower angular values, reflects the expansion of the orthorhombic lattice due to an increase in both, van der Waals radius and bond length of C-F and C=O respectively. Similarly, the increase in the spacing of the triclinic (010) plane from 2θ = 22.47º (3.96 Å) for PE19Cl to 2θ = 21.95º (4.05 Å) for PE19Br is also explained by the increased radius and bond length of the Br atom. Therefore, the angular shifts follow expectations from the significant incorporation of side groups in the crystalline structure. In addition, sharp diffraction peaks in most patterns point to a high correlation of diffractographic planes and, hence, to highly organized crystalline structures. Given the atactic character of the substitution,[114] it appears that for the samples analyzed here, the orientation of the substituent with respect to the backbone chain has a negligible effect on the correlation between crystallographic planes. Calculated unit cell dimensions and densities of the orthorhombic lattices are listed in Table 2-2. Pertinent data for dimensions of the triclinic lattices could not be obtained since they would require observation of at least five independent WAXD reflections.[150]

The diffractograms of Figure 2-4 also indicate that there is a significant amorphous region in these systems that increase with the bulkiness of the substituent. To estimate the degree of crystallinity from the diffractograms, the WAXD patterns obtained at 150 °C were scaled and subtracted from the room temperature patterns. Crystallinity levels obtained are listed in Table 2-2-1 and range from 83% for PE to ~ 40% for PE19Br. In comparison, random ethylene copolymers with the same level of methyl branching or chlorine pendant groups (~5.3 mol%), display much lower levels (~25%) and less organized crystallinities.[74,109,128] One can then conclude that the initial selection of long methylene sequences, present in the random system,

over sequences containing for example Cl or Br substituents, imposes additional constraints in the topology of the remaining melt for gathering additional sequences with the required length to propagate crystallization. More specifically, in the random systems, the crystallization is primarily driven by the selection of continuous crystallizable sequences longer than a critical value, while shorter sequences remain uncrystallized. Clearly, the lack of branching distribution in ADMET polyethylenes with side groups on every 19th carbon, invokes a homopolymer-like crystallization with a driving force led by the accommodation of the side group in an all *trans* backbone packing conformation. This crystallization mode explains the sharp diffractograms. Thus, while the melting behavior of the random samples is invariably broad, precisely substituted polymers melt sharply as clearly indicated by the melting thermograms of PE21CH_3 and the randomly distributed counterpart (with matched methyl content) in Figure 8 of reference 145. The change in crystallographic packing of random vs. precisely placed methyl branched ADMET systems is also clear evidence of their different crystallization behavior.[145]

The fact that precisely substituted ADMET polymers display relatively high levels of crystallinity suggest a crystalline state built on the basis of substitutional solid solutions.[151] In packing backbone sequences in all *trans* conformation, substitution of a H for O, F, Cl or Br on each and every 19th carbon, creates lattice distortions on levels proportional to the solute's van der Waals radius. As seen in Table 2-1, the orthorhombic lattice is preserved in this series up to a radius of ~ 1.6 Å while bulkier atoms cause large lattice distortions to the point that correlated symmetry between crystallographic planes is only found within a different phase with significantly larger dimensions.[152] In reference to the hydrogen, the discontinuity of isomorphic structures in this series occurs at a difference in van der Waals radius of ~ 30%. This is larger than the ~ 15% or lower difference usually quoted for formation of isomorphic metallic solid

solutions,[151] but not unexpected, taking into account the chain connectivity of polymer molecules and the weaker covalent bonding.

2.2.4 Melting and Crystallization Behavior

A further insight into the unique crystallization mode of this family of precisely substituted polyethylenes is given by their crystallization and melting behaviors as measured by differential scanning calorimetry (DSC) shown in Figure 2-5. The sharpness of the crystallization and melting traces are typical of the behavior of low molecular mass homopolymers, and they contrast with much broader endotherms displayed by random ethylene copolymers of similar branching composition.[74, 131, 145] Thus, thermodynamic features also point to a mechanism for ordering the precisely branched ADMET polymers that differs from a partitioning of sequences along the crystallization process, which is typical of the random behavior.[132, 135] In the latter, a richer melt in substituents is inevitable due to the chain's non-crystallizable short sequences; this feature leads to an inequality in partitioning of the substituent between the crystalline and non-crystalline regions. As a consequence, the composition of the melt coexisting with crystallites changes continuously during melting, leading to the broad endotherms usually observed in the random systems.[130, 135, 153]

The peak melting temperatures decrease dramatically and proportionally to the van der Waals radius in the series of halogenated polymers, as seen in Figure 2-6, projecting a value of ~ 30 ºC for the melting temperature of the iodine polymer with the same substituent pattern. We observe that for similar van der Waals radii, shorter bond lengths increase the melting temperature as evidenced by the ~ 7 degrees higher melting of PE19O compared to PE19F. Similarly, the melting temperature of PE19CH_3[128] is higher than predicted from van der Waals radii arguments; due to a much shorter C-C bond length. The high heat of fusion of PE19F

(Table 2-1) is associated with a high electronegativity of the F atom and its likelihood of increasing intermolecular secondary bonding compared to the other members of the series.

Clearly, the variation in crystallization and melting temperatures in this series is indicative of the degree to which each substitution perturbs the symmetry of the neighboring carbons in the lattice. Accommodation of the larger atoms must, by necessity, distort the all *trans* ordering of vicinal intra and intermolecular carbons resulting in a more defective structure and, as a consequence, in significantly altered thermodynamic data.

2.2.5 Solid-state NMR

Crystallographic and thermal properties of the series of precision substituted polyethylenes, such as the change and expansion of the unit cell and over 75 ºC decrease in melting temperature with increasing van der Waals radius, were interpreted as the result from the need to pack in crystalline arrays continuous molecular segments that include the side groups. In this section, the inclusion of halogens in the crystalline regions is probed by direct solid-state NMR analysis of resonances belonging to or associated with the side group in ordered and disordered environments. Of the ADMET polymers investigated, PE19F is the best-suited candidate to reveal differences between crystalline and non-crystalline side groups. In this sample, direct polarization solid-state ^{19}F NMR provides information on all fluorine atoms at high sensitivity while information via ^{13}C NMR of the solid samples relies only on ~1% natural abundance of the ^{13}C isotope.

The directly polarized ^{19}F spectrum of PE19F obtained under high power ^{1}H decoupling (DD) and magic angle spinning (MAS) of 14,000 Hz is given in Figure 2-7a. The spectrum was obtained with a recycle time of 20 s to ensure complete F magnetization recovery. Paralleling the expected incorporation of a large fraction of F atoms in the crystalline regions, two distinctive resonances are observed associated with fluorine atoms in crystalline (-179.4 ppm) and non-

crystalline (-181.9) environments. The integrated intensity associated with each resonance was extracted from a fit of the total intensity with two Lorenztian peaks, which led to a crystallinity of 56% in very good agreement with the 57% value obtained by WAXD for the same sample. Such a good correspondence is expected if PE19F crystallizes as a homopolymer with no discrimination in the partition of the F side groups between the different phases of the crystalline structure. Contrasting with a clear difference in chemical shift between ordered and disordered F, the spin-lattice relaxation times (T_1^F) associated with both regions are very similar, 3.85 s and 3.36 s respectively, denoting the lack of specific orientation of the F with respect to the backbone chain and the defective nature of this atom in the crystalline lattice.

Although the solid-state ^{19}F NMR spectrum of Figure 2-7a evidences clearly the presence of F atoms in two different conformational environments, it does not provide direct quantitative information on the content of F in each region. This information is feasible via solid state ^{13}C NMR by the correlation between CH and CH_2 carbons pertaining to crystalline and non-crystalline environments. Moreover, the ^{13}C DD/MAS spectrum of PE19F was not recorded as the lower sensitivity of ^{13}C observation added to our inability to decouple both ^{1}H and ^{19}F simultaneously will undoubtedly result in a broad featureless CH resonance.

Solid-state DD/MAS ^{13}C NMR spectra were obtained for the other two halogen substituted polyethylenes of the series and are given in Figures 2-7b and 2-7c for PE19Cl and PE19Br respectively. Prior to acquisition of fully relaxed spectra, carbon spin-lattice relaxation times for CH, α CH_2 and crystalline CH_2 groups in both polymers were estimated as 1.5 s, 2 s and 25 s respectively. Accordingly, fully relaxed single pulse spectra of >2600 transients were collected at room temperature under MAS and high power ^{1}H decoupling using recycle times of 120 s. Small peaks observed at 15.3 ppm are associated with spinning side bands. The main resonance

centered at 34.1 ppm corresponds to crystalline CH_2 in the all *trans* conformation and is shifted 1.3 ppm downfield in reference to the crystalline orthorhombic CH_2 resonance of linear polyethylene, which is centered at 32.8 ppm under the same field and experimental conditions. This shift points to a crystallization pattern for PE19Cl and PE19Br that differs from the orthorhombic symmetry as previously observed by WAXD. A correspondence with similar downfield shifts observed in solid n-alkanes that pack in a triclinic phase as compared to the n-alkane orthorhombic symmetry,[154] serves as additional indirect evidence of the triclinic packing of these polymers. By analogy to the spectrum of solid PE, the resonance at 31.5 ppm is assigned to non-crystalline CH_2 carbons and by comparison to the spectrum recorded in solution, peaks centered at 41.2 and 41.4 ppm and at 67 and 62.5 ppm are assigned to α CH_2 and CH carbons of PE19Cl and PE19Br, respectively. The chemical shift for β CH_2 is mostly hidden beneath the 31.5 ppm resonance of the amorphous CH_2 carbons.

As previously indicated, the peak corresponding to the CHX carbon is ideal for monitoring the partitioning of Cl and Br atoms between crystalline and non-crystalline regions. For this purpose the information from the CHX resonance is useful when both phases contain a sufficiently large number of CHX groups to overcome the low sensitivity nature of ^{13}C detection, and when crystalline and non-crystalline phases display a resolved difference in their CHX chemical shift. An additional constraint to acquire spectra with high signal/noise ratio in our samples was the small quantities of ADMET polymers available for these experiments (~35mg). The spectral region associated with the CHX resonance is expanded in the inset of figures 7b and 7c. Both consist of two largely overlapping resonances centered at 66.9 and ~64 ppm for PE19Cl and at 62 and 59 ppm for PE19Br. In consonance with the resonances observed in PE19F in Figure 2-7a, the CHX observed resonances indicate that at least two populations of

methine carbons with significantly different conformations are present in crystalline PE19X polymers. Small protrusions in the downfield wings of the crystalline CHX resonance are attributed to a high noise level from the small quantities sampled. The contribution from the interface will be buried within the crystalline and non-crystalline CHX resonances. Owing to the fact that the difference in chemical shift and the ratio of peak heights of these two resonances are very similar to the values of crystalline (34.1 ppm) and non-crystalline (31.5 ppm) CH_2 peaks, both CHX resonances are assigned to crystalline methine (66.9 ppm, 62 ppm) and non-crystalline methine (64 ppm, 59 ppm) carbons. The observed chemical shifts for crystalline and non-crystalline CHCl in Figure 2-7b are identical to the values reported by Tonelli *et al.* in a study of the structure of ethylene-vinyl chloride copolymers using CP/MAS techniques.[108]

From the integrated intensities of the combined (crystalline and non-crystalline) CHX resonances and the intensity of α CH_2 resonance (~41.0 ppm) relative to the CH_2 resonances (34.1 and 31.5), contents of chlorine and bromine of 5.4 ± 0.3 mol% and 5.3 ± 0.2 mol% are calculated, respectively. These values match the content of halogen in the molecule from the primary structure (5.3 mol%) and evidence the quantitative nature of the DD/MAS spectrum. In other words, all types of carbons of PE19Cl and PE19Br were relaxed after the 120s delay. Since both CH_2 and CHX carbons have very similar distributions in amorphous and crystalline environments, from the equivalence in the corresponding intensity ratios, we conclude that chlorine and bromine groups must be uniformly distributed between the phases. Upon crystallization there is no discrimination for the partitions of CHX units between crystalline and non-crystalline regions. In contrast, the DD/MAS spectrum of a randomly distributed ethylene-vinyl chloride with similar chlorine content displayed much broader resonances and no

distinction between crystalline and amorphous CHCl carbons.[108] In the random copolymer at least 20% of the chlorines were estimated to be included in the crystal.

The distribution of side groups among the different phases of the semicrystalline structure was also probed by additional cross-polarized (CP) under MAS NMR experiments that isolate the spectra of the crystalline regions.[155, 156] Resonances in the crystalline spectra that are associated with the methine carbon or carbons adjacent to the methine group allow direct quantitative data on the content of these groups in the crystalline regions and, hence, on the partitioning of the side groups. As mentioned in the experimental part, the CP method used here for isolating the crystal spectra is based on differences in $T_{1\rho}^{H}$ of crystalline and non-crystalline regions. These values were estimated for the more intense ~34 ppm peak and are listed in Table 2-3 for the linear and three halogenated polymers. All the samples display a fast relaxing component, 2 ms < $T_{1\rho}^{H}$ < 4 ms, and a slower one ($T_{1\rho}^{H}$ > 6 ms), associated with the non-crystalline and more rigid crystalline phases respectively. Owing to a modest contrast in crystalline and non-crystalline proton mobility for PE19Cl and PE19Br in the frequency level at which $T_{1\rho}^{H}$ is active, a 5 ms ^{1}H spin locking filter was applied for these two polymers prior to CP, and a longer one (7 ms) was used to filter most of the non-crystalline regions of PE19F. Consequently, crystalline spectra would be more strongly weighted after the filter. In addition to this filter, to further null or decrease the contribution of the non-crystalline carbons, a fraction of the unfiltered CP spectra (shown in Figure 2-8a) is subtracted from the spectrum generated with spin locking.[155, 156] The scaling factor for subtraction is chosen as the largest number that leaves no regions with negative intensities in the spectral region between 10 and 120 ppm. The resulting crystalline spectra are shown in Figure 2-8b and the corresponding observed chemical shifts for crystalline carbons in the halogenated series are listed in Table 2-4.

Unfiltered CP MAS spectra, shown in Figure 2-8a reveal an increase of the intensity of the amorphous CH_2 resonance (~31 ppm) with the size of the substituent, thus reflecting a decrease of crystallinity from PE19F to PE19Br in the series, in consonance with the WAXD data. Also of interest is the chemical shift corresponding to crystalline CH_2 of PE19F, observed at 33.1 ppm, a value that is very close to the all trans orthorhombic linear polyethylene. This correspondence in chemical shifts confirms that PE19F maintains the orthorhombic packing of the PE chain.

Resonances of carbons associated with the substituents are still observed in the filtered crystal spectra (Figure 2-8b) even after subtraction of most of the amorphous components. These include the methine, the α CH_2 (~ 40 ppm) and the β CH_2 (observed at 28.6 ppm for PE19F, at ~31.0 ppm for PE19Cl and buried within the main CH_2 resonance in the spectrum of PE19Br). Observation of these resonances confirms that all the types of halogen side groups are incorporated in the crystalline regions of these systems. This assertion is at variance with recent predictions from molecular dynamics (MD) simulations of the crystallization process of precisely placed methyl and chlorine side groups,[157] yet agrees with more abundant qualitative data, estimated from WAXD and DSC, for the random systems[103, 158, 159, 160] and precisely placed methyl branched polymers[150] which indicated that all types of side groups of interest here are incorporated in the crystal lattice.

The resolved character of relatively sharp α CH_2 resonances and the resonance associated with the CHX in the crystalline spectra allow us to integrate these lines against the integrals of the main peaks and, thus, deduce the concentration of F, Cl, and Br groups in the crystal. These data are also listed in Table 2-4. Accounting for the larger experimental error associated with integration of broad CHX resonances, the values obtained for the concentration of halogen in the crystal from any of the resonances associated with the side groups are very similar to the

concentration of halogen in the chain (5.3 mol%). Therefore, analyses of CP MAS spectra confirm the results obtained from the DD/MAS spectrum of PE19F, PE19Cl and PE19Br. They also confirm the uniform distribution of the halogen in the semicrystalline structure and thus, the homopolymer crystallization behavior of these systems.

2.3 Conclusions

The synthesis and unique crystallization behavior of a series of precisely substituted polyolefins, with halogens (F, Cl, Br) or ketone groups on each and every 19th carbon, has been described, with synthesis of the precise, bromine-containing polymer (PE19Br) proving to be most challenging. Difficulties in isolating PE19Br were overcome via use of mild hydrogenation conditions using Wilkinson's catalyst. The very sharp diffraction patterns observed by WAXD and the narrow melting and crystallization peaks found by DSC for these polymers conform with a homopolymer-like crystallization. These observations contrast with much broader diffraction and melting peaks observed in ethylene copolymers with matched concentrations of randomly distributed side groups. In reference to the random copolymers, precisely substituted ADMET polymers display relatively high levels of crystallinity, as measured by WAXD, and a crystalline state built on the basis of substitutional solid solutions. The accommodation of O, F, Cl or Br groups in the crystal creates lattice distortions on levels proportional to the solute's van der Waals' radius. The magnitude of the distortions are such that the PE orthorhombic lattice is only preserved up to a radius of ~1.6 Å (F, O substituents). Accommodation of bulkier substituents (Cl, Br) degenerates the correlated symmetry to a triclinic lattice with significantly larger dimensions. Direct solid-state ^{19}F and ^{13}C NMR investigations of the crystalline and non-crystalline regions evidence a uniform partitioning of all of these substituents between the different phases. While crystallization of the random type is led by the selection of long crystallizable sequences, in these precision polyolefins it is governed by the accommodation of

the side groups into the crystal. As such, both *type and distribution* of the substituent impact the chain ordering of branched and substituted polyethylenes at the most fundamental level.

2.4 Experimental Section

Chemicals. Chemicals were purchased from the Aldrich Chemical company and used as received unless noted. Grubbs' first generation ruthenium catalyst, bis(tricyclohexylphosphine)-benzylidine ruthenium (IV)dichloride, was purchased from Strem Chemical and stored in an Argon filled dry box prior to use. Wilkinson's catalyst $RhCl(PPh_3)_3$ was purchased from Strem. Methylene chloride and *o*-xylene were distilled over CaH_2. PE (M_n = 13.1 kg/mol, PDI = 1.26) was obtained from the Societe Nationale des Petroles d' Aquitaine (SNPA).

Instrumentation. Solution ^1H NMR (300 MHz) and ^{13}C NMR (75 MHz) spectra were recorded on a Varian Associates Gemini 300, VXR 300 or Mercury 300 spectrometer. All chemical shifts for ^1H and ^{13}C NMR were referenced to residual signals from $CDCl_3$ (^1H = 7.27 ppm and ^{13}C = 77.23 ppm) with an internal reference TMS 0.03% v/v. High-resolution mass spectral (HRMS) data were obtained on a Finnegan 4500 gas chromatograph/mass spectrometer using the electron ionization (EI) mode. Elemental analyses were carried out by Atlantic Microlabs Inc., Norcross, GA.

The GPC measurements for samples in THF were taken on a Waters GPCV 2K instrument. Samples were run with HPLC grade THF at 40 ^{0}C on Water StyragelHR 5E columns relative to polystyrene standards. Polymer molecular weights reported versus polyethylene standards were measured using a Waters Associates 150C high temperature gel permeation chromatograph equipped with three Polymer Laboratories mixed bed Type B columns and an internal DRI detector. The mobile phase was BHT-inhibited 1,2,4-trichlorobenzene (135 °C, flow rate 1.0 mL / minute, typical sample concentration 2 mg / mL).

IR data was obtained using a Perkin-Elmer Spectrum One FTIR outfitted with a $LiTaO_3$ detector. Measurements were automatically corrected for water and carbon dioxide. Thermogravimetric analysis (TGA) data was obtained with a Perkin-Elmer 7 series thermal analysis system. The TGA samples (2-5 mg) were heated from -10 ºC to 800 ºC at 10 ºC/min. Melting and crystallizations were obtained at 10 °C/min in a Perkin Elmer differential scanning calorimeter DSC-7 with Pyris software under nitrogen flow and calibrated with indium.

WAXD diffractograms were collected at room temperature on samples crystallized from the melt at ~ 1 °C/min using a slit collimated Siemens D-500 diffractometer in a 2θ range between 5º and 40º with a step size of 0.02º. The instrument was calibrated for d spacing with a standard polished piece of polycrystalline quartz, and the film thickness was offset using shims. The diffractogram of molten polyethylene, used to estimate the degree of crystallinity, was collected at 150°C on a Siemens D500 with an attached Anton Paar HTK high temperature head.

DD/MAS solid-state ^{19}F NMR spectra were obtained in a Bruker DRX 600 MHz spectrometer operating at 600.13 and 564.68 MHz for ^{1}H and ^{19}F, respectively, under MAS frequency of 14,000 Hz and a decoupling power for ^{1}H of 71 KHz. Spin lattice relaxation times were obtained via inversion recovery using ^{19}F 90 and 180 degree pulse length of 2 and 4 μs, respectively. Chemical shifts were quoted with respect to the ^{19}F isotropic signal of flufenamic acid ($COOH–C_6H_4–NH–C_6H_4–CF_3$) at -61.5 ppm as external reference.

^{13}C NMR spectra of the solid polymers were obtained in a Bruker DMX300 spectrometer operating at 75.5 MHz for ^{13}C and at 300.2 MHz for ^{1}H. The experiments for both types of solid-state NMR were conducted at room temperature using a Bruker solid-state probe for 4 mm rotors under a MAS frequency of 4000 Hz. The small quantities (< 100 mg) available for these polymers were placed in the center of the zirconium rotors and the empty spaces filled with fine

paper tissue or teflon tape. The nutation frequencies associated with the ^{13}C and ^{1}H radio frequency fields in the CP experiments were 62 kHz for both isotopes. The ^{1}H nutation frequency applied for decoupling was 83 kHz. Two different types of ^{13}C NMR spectra were collected under high power ^{1}H decoupling, single pulse spectra with recycle delays sufficiently long to fully recover the magnetization of carbons in amorphous and crystalline environments and $^{1}H - ^{13}C$ cross polarization combined with MAS (CP MAS) spectra. Contact times for cross-polarization were 0.5 – 0.7 ms. Fixing the CP time and varying a proton spin locking pulse length, prior to cross polarization, enables estimation of rotating-frame relaxation times, $T_{1\rho}^{H}$, for the protons. Values of $T_{1\rho}^{H}$ for crystalline and amorphous regions, usually very different, can be used to filter the amorphous phase prior cross polarization. The procedures have been detailed in previous works.[155, 156] Chemical shifts were measured with respect to tetramethylsilane at 0 ppm and using glycine's carbonyl carbon at 173 ppm as external reference. All peak fit analyses were carried out using the software GRAMS from Galactic Corp.

Synthesis. Heneicosa-1,20-dien-11-one (1). was synthesized using a published procedure.[142] The ketone (1) was then reduced to heneicosa-1,20-dien-11-ol (2) using a method similar to that reported.[143] The ^{1}H NMR and ^{13}C NMR were in agreement with spectra found previously and the purity of the compounds was supported by elemental analysis.

11-Fluoro-heneicosa-1,20-diene (3). A solution of 5 g (0.031 mol) diethylaminosulfur trifluoride (DAST) in 25 mL CH_2Cl_2 was cooled to -78 ^{o}C and a solution of 5 g (0.016) 2 in 25 mL CH_2Cl_2 and dry pyridine (2.5mL) were added dropwise. The mixture was stirred at this temperature for 2 hr and then warmed to room temperature and stirred overnight. At this time water was added and the organic phase was extracted with CH_2Cl_2 and then dried with Na_2SO_4 and then the solvent was removed to give a white solid which was purified by chromatography

using 97:3 hexanes:ethyl acetate to give 2.85 g (57%) of the product. ^{1}H NMR (300 MHz $CDCl_3$) δ 5.82 (m, 2H), 4.97 (m, 4H), 4.54-4.38 (dp, 1H), 2.05 (q, 4H), 1.7-1.2 (bm, 28H). ^{13}C NMR (75 MHz, $CDCl_3$) δ 139.44, 114.35, 64.61, 38.74, 34.03, 29.68, 29.63, 29.39, 29.32, 29.14, 26.71. HRMS calcd for $C_{21}H_{39}F$ (M^+), 310.3036; found 310.3041. Anal. Calcd for $C_{21}H_{39}F$: C, 81.22; H 12.66; F, 6.12. Found: C, 81.21; H, 12.76; F, 6.03.

11-Chloro-heneicosa-1,20-diene (4). To 25 mL of dry pyridine at 0 ^{o}C was added 4.5g ($2.4x10^{-2}$ mol) of tosyl chloride and 6.2 g ($2.0x10^{-2}$ mol) of heneicosa-1,20-dien-11-ol under argon. The mixture was stirred overnight. After filtration, 200 mL ether was added into the mixture. The mixture was washed with 1M HCl (50 mL x3), washed with water (50 mL x3), dried over $MgSO_4$, and the solvent was removed under vacuum to yield a crude yellow oil. Purification by chromatography on silica with ether-hexane (15:85) as eluent gave the tosylate which was carried on to the next step. To 150 mL of dry acetone was added 6.8 g (0.16 mol) of LiCl and 5.0 g (0.016 mol) of the 11-tosyl-heptadeca-1,20-diene under argon. After refluxing for 5 days, the mixture was cooled to room temperature. At this time water was added and the solution was extracted with ether (x3). The organic layer was then washed saturated $NaHCO_3$ followed by brine and then dried with $MgSO_4$. After filtration the solvent was removed under vacuum to yield clear oil. The clear oil was purified by flash column chromatography using hexane to yield the desired product as a clear oil (3.7 g, 57%). ^{1}H NMR (300 MHz $CDCl_3$) δ 5.79 (m, 2H), 4.79 (m, 4H), 3.86 (m, 1H), 2.02 (q, 4H), 1.69 (m, 4H), 1.50-1.27 (br, 24H). ^{13}C NMR (75 MHz, $CDCl_3$) 139.13, 114.12, 64.29, 38.50, 33.80, 29.45, 29.40, 29.16, 29.09, 28.90, 26.48. Anal. Calcd for $C_{21}H_{39}Cl$: C, 77.14; H 12.02; Cl, 10.84. Found: C, 77.15; H, 12.11; Cl, 10.57.

11-Bromo-heneicosa-1,20-diene (5). A solution of heneicosa-1,20-dien-11-ol (2) (5 g, $1.6x10^{-2}$ mol) and CBr_4 (6.3g, $1.9x10^{-2}$ mol) in CH_2Cl_2 (25 mL) was prepared in a 500 mL flask and cooled to 0 ^oC. Triphenyl phosphine (6.2g, $2.4x10^{-2}$ mol) was added slowly with stirring. Upon addition of the phosphine, the colorless solution turned a pale brown color and was stirred for an additional 4 h at room temperature. The crude product was concentrated under reduced pressure and phosphine oxide was recrystallized from diethyl ether at -20 ºC. The solution was filtered and the product was purified by flash chromatography using hexane as the eluent to give 5.2 g (88%) of the product as an oil. ^1H NMR (300 MHz $CDCl_3$) δ 5.80 (m, 2H), 4.95 (m, 4H), 4.01 (m, 1H), 2.05 (q, 4H), 1.78 (m, 4H), 1.50-1.27 (br, 24H). ^{13}C NMR (75 MHz, $CDCl_3$) δ 139.14, 114.11, 58.87, 39.16, 33.77, 29.41, 29.38, 29.07, 29.03, 28.89, 27.55. HRMS calcd for $C_{21}H_{39}Br$ (M^+), 370.2235; found, 370.2229. Anal. Calcd for $C_{21}H_{39}Br$: C, 67.90; H 10.58; Br, 21.51. Found: C, 68.01; H, 10.57; Br, 21.21.

General procedure for bulk polymerization. Monomer and Grubbs' first generation catalyst were combined in a ratio of 500:1 under argon atmosphere. The polymerization was conducted at 35-40 ºC under vacuum with stirring for 5 days. The reaction was then stopped and 5 mL of toluene was added to dissolve the polymer with stirring. The reaction was allowed to cool to room temperature. The polymers were then precipitated by dripping the toluene solution into cold acidic methanol. They were then isolated by filtration and dried.

General procedure for solution polymerization. Monomer and Grubbs' first generation catalyst (500:1 ratio) were dissolved in CH_2Cl_2 for polymerization of PE19F and in toluene for PE19O under argon and stirred at 35-40 ^oC for 5 days. The same procedure as described above was used to isolate the polymer.

Polymerization of 11-Fluoro-heneicosa-1,20-diene (UPE19F). Synthesized by the solution method as above using 1.0 g ($3.2x10^{-3}$mol) 3, $5.3x10^{-3}$g ($6.4x10^{-6}$mol) of Grubbs' first generation catalyst. Analytical yield. ^{1}H NMR (300 MHz $CDCl_3$) δ 5.80 (b, 0.28H), 5.38 (m, 2H), 4.95 (b, 0.70 H), 4.55-4.35 (dp, 1H), 1.95 (m, 4H), 1.65-1.15 (b, 30 H). ^{13}C NMR (75 MHz, $CDCl_3$) δ 130.64, 130.17, 95.87, 93.65, 35.64, 35.36, 32.85, 29.94, 29.81, 29.80, 29.70, 29.42, 27.51, 25.46, 25.40.

Polymerization of 11-Chloro-heneicosa-1,20-diene (UPE19Cl). Synthesized by the bulk method as above using 1.0 g ($3.1x10^{-3}$mol) 4, $5.0x10^{-3}$g ($6.1x10^{-6}$mol) of Grubbs' first generation catalyst. Analytical yield. ^{1}H NMR (300 MHz $CDCl_3$) δ 5.80 (b, 0.02H), 5.35 (m, 2H), 4.95 (b, 0.08 H), 3.85 (p, 1H), 1.95 (m, 4H), 1.65 (m, 4H), 1.55-1.15 (b, 24 H). ^{13}C NMR (75 MHz, $CDCl_3$) δ 130.57, 130.10, 64.56, 38.77, 32.81, 29.96, 29.87, 29.72, 29.66, 29.50, 29.43, 29.36, 27.44, 26.74.

Polymerization of 11-Bromo-heneicosa-1,20-diene (UPE19Br). Synthesized by the bulk method as above using 1.0 g ($2.7x10^{-3}$mol) 5, $4.4x10^{-3}$g ($5.4x10^{-6}$mol) of Grubbs' first generation catalyst. Analytical yield. ^{1}H NMR (300 MHz $CDCl_3$) δ 5.80 (b, 0.05H), 5.35 (m, 2H), 4.95 (b, 0.14 H), 4.02 (p, 1H), 1.95 (m, 4H), 1.75 (m, 4H), 1.6-1.2 (b, 24 H). ^{13}C NMR (75 MHz, $CDCl_3$) δ 130.75, 130.29, 59.41, 39.62, 33.01, 30.16, 30.05, 29.89, 29.85, 29.69, 29.55, 29.49, 28.01, 27.63.

General Procedure for hydrogenation. The polymers containing F or Cl halogens (UPE19F and UPE19Cl) were then hydrogenated using a modified version of the method described by Hahn[144] by dissolving in dry *o*-xylene under argon and adding 3.3 equivalents of *p*-toluenesulfonyl hydrazide (TSH) and 4 equivalents of tri-*n*-propyl amine (TPA). The solutions were refluxed for 9 hours and then cooled to room temperature. The hydrogenated polymer was

precipitated into ice-cold methanol and isolated by filtration. The dried polymer was then redissolved in toluene and re-precipitated by dipping into ice-cold acidic methanol. A white solid was collected by filtration and the polymers were isolated in quantitative yield.

The polymers containing Br halogen (UPE19Br) and ketone (UPE19O) were hydrogenated using a 150 mL Parr high-pressure reaction vessel equipped with a glass liner and Teflon stirbar. Unsaturated polymer (1.0g) and Wilkinson's catalyst (0.02g) were added to the glass liner under nitrogen blanket. Finally, 20 mL of toluene were added. The vessel was sealed and attached to a grade 5 hydrogen tank and purged with hydrogen several times. The bomb was charged with 500 psi of H_2 and stirred for 5 days at 80 ºC. The hydrogenated polymer was dissolved in toluene, and precipitated into methanol. The polymer was then filtered and dried under reduced pressure.

PE19F. Hydrogenation was performed as above. ^{1}H NMR (300 MHz, toluene-d_8) δ 4.43-4.27 (dm, 1H), 1.7-1.2 (bm, 36H). ^{13}C NMR (75 MHz, toluene-d_8) δ 95.21, 92.96, 36.08, 35.79, 30.30, 30.26, 30.19, 30.16, 25.81, 25.75. M_w (GPC vs. PE) = 11,300 g/mol. PDI = (M_w/M_n) = 1.52. Anal. Found: C, 77.62; H, 14.16; F, 5.77.

PE19Cl. Hydrogenation was performed as above. ^{1}H NMR (300 MHz, $CDCl_3$) δ 3.86 (p, 1H), 1.68 (m, 4H), 1.55-1.15 (b,32H). ^{13}C NMR (75 MHz, $CDCl_3$) δ 64.56, 38.75, 29.92, 29.88, 29.82, 29.75, 29.43, 26.73. M_w (GPC vs. PS) = 49,500 g/mol. PDI = (M_w/M_n) = 2.22. Anal. Found: C, 74.98; H, 13.87; Cl, 10.66. A lower molecular weight sample used in the DD/MAS solid-state ^{13}C NMR: M_n (^{1}H NMR) = 12,000 g/mol.

PE19Br. Hydrogenation was performed as above.^{1}H NMR (300 MHz $CDCl_3$) δ 4.03 (p, 1H), 1.79 (m, 4H), 1.6-1.2 (bm, 32H). ^{13}C NMR (75 MHz,$CDCl_3$) δ 59.26, 39.42, 29.93, 29.88, 29.82, 29.74, 29.32, 27.82. M_w (GPC vs. PS) = 38,100 g/mol. PDI = (M_w/M_n) = 1.72. Anal. Found: C, 60.58; H, 11.43; Br, 19.54.

PE19O. Hydrogenation was performed as described above and the analytical characterization was consistent with that previously reported in the literature.[161]

Table 2-1. Crystalline data of precision ADMET polyolefins (PE19X) with general structure – $[(CH_2)_{18}\text{-}CHX]_y$- Melting and crystallization temperatures and heat of fusions correspond to samples crystallized and melted at 10 °C/min.

Sample	Atom[(a)] (X)	Mn[(b)] 10^{-3} (g/mol)	*Mw/Mn*	Packing cell	2θ (degrees)				Tm (°C)	Tc (°C)	ΔH (J/g)	Xc[(c)] (%)	vdW[(d)] (Å)	C-X[(e)] (Å)
					110	200	100	010						
PE	H	13.1	1.26	Orthorh	21.64	24.02			133.0	115	238	83	1.2	1.09
PE19O	O	3.4[*]	3.55	Orthorh	21.43	23.28			134.7	120	106	60	1.52	1.2
PE19F	F	7.5[*]	1.52	Orthorh	21.23	23.60			127.5	113	207	57	1.47	1.35
PE19Cl	Cl	22.3[#]	2.22	Triclinic			19.10	22.47	72.7	63	105	50	1.75	1.78
PE19Br	Br	22.2[#]	1.72	Triclinic			19.20	21.95	61.5	43	55	40	1.85	1.95
$PE19CH_3$[145]	CH_3	11.3	1.90	Triclinic			18.75[(f)]	21.75[(f)]	57	51	96	nd	2.0	1.54

(a) Every 19th carbon. (b) Measured by [*] GPC vs. PE and [#] GPC vs. PS.(c) Crystallinity from WAXS. Samples crystallized at 1 ºC/min.(d) Van der Waals radii.(e) C – X bond length.(f) $–CH_3$ group on and every 21st carbon[150]

Table 2-2. Lattice parameters from WAXD for orthorhombic PE19X (X = H, O, F) crystals.

	PackingCell	a (Å)	b (Å)	c (Å)	V ($Å^3$)	Density (g/cm^3)
PE	Orthorh	7.410	4.934	2.547	93.131	0.9983
PE19O	Orthorh	7.643	4.937	2.547	96.098	0.9748
PE19F	Orthorh	7.540	5.032	2.547	96.639	0.9802

Table 2-3. $T_{1\rho}{}^H$ estimations from two-component fits for PE19X (X = H, F, Cl, Br). Values in ms.

Sample	Fast	Slow
PE	2	25
PE19F	1.8	24
PE19Cl	3.8	6
PE19Br	2.2	8

Table 2-4. ^{13}C NMR chemical shifts for crystalline carbons of PE19X precision ADMET polyolefins (X = F, Cl, Br) and concentration of X groups in the crystal.

	Chemical Shift (ppm)				Concentration of X in Crystal (mol %)[(a)]		
Sample	CH2 (PE-like)	α CH2	β CH2	CHX	From α CH2 intensity	From β CH2 intensity	From CHX intensity
PE	32.8						
PE19F	33.1	38.1	28.6	97[(b)]	5.0	5.8	4.5
PE19Cl	34.1	41.0	~31	67	5.2	5.8	5.5
PE19Br	34.1	41.5	N O[(c)]	62.5	5.0		4.7

(a) Calculated from ratio of integrated intensities in the crystalline spectra (Figure 2-8). (b) Broad resonance. (c) Not Observed

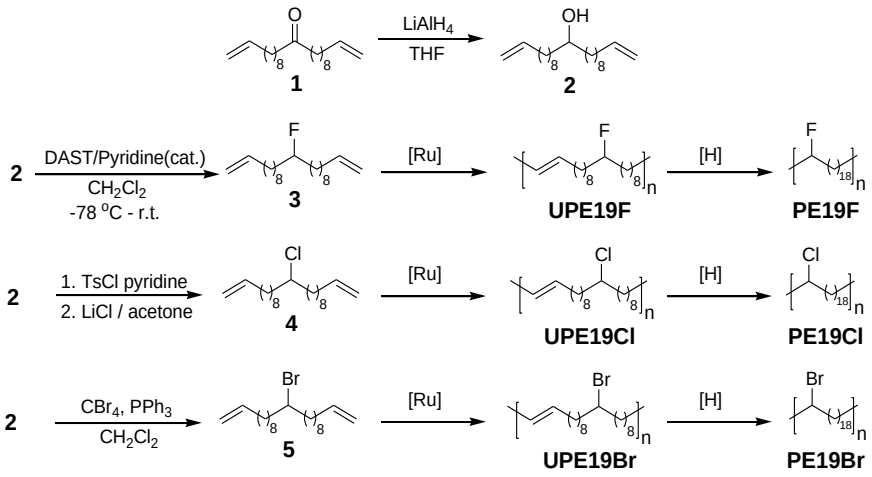

Figure 2-1. Monomer and Polymer Synthesis.

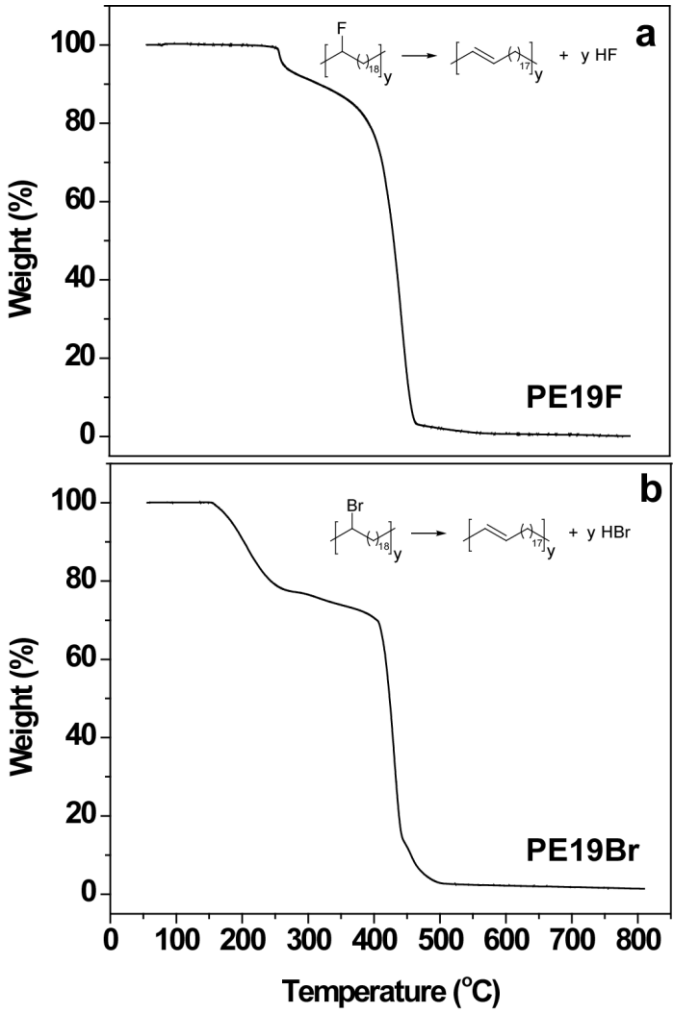

Figure 2-2. TGA for PE19F (a) and PE19Br (b) showing the loss of HF and HBr respectively, followed by catastrophic decomposition.

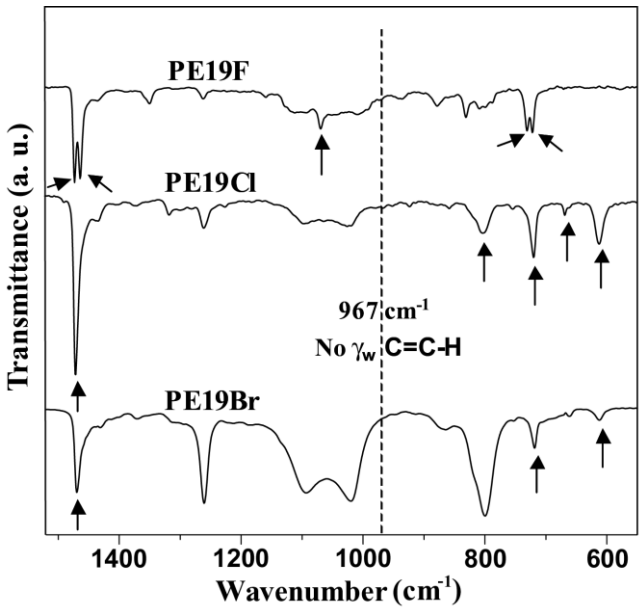

Figure 2-3. IR spectra for thin films of PE19F, PE19Cl, and PE19Br cast on KBr disks.

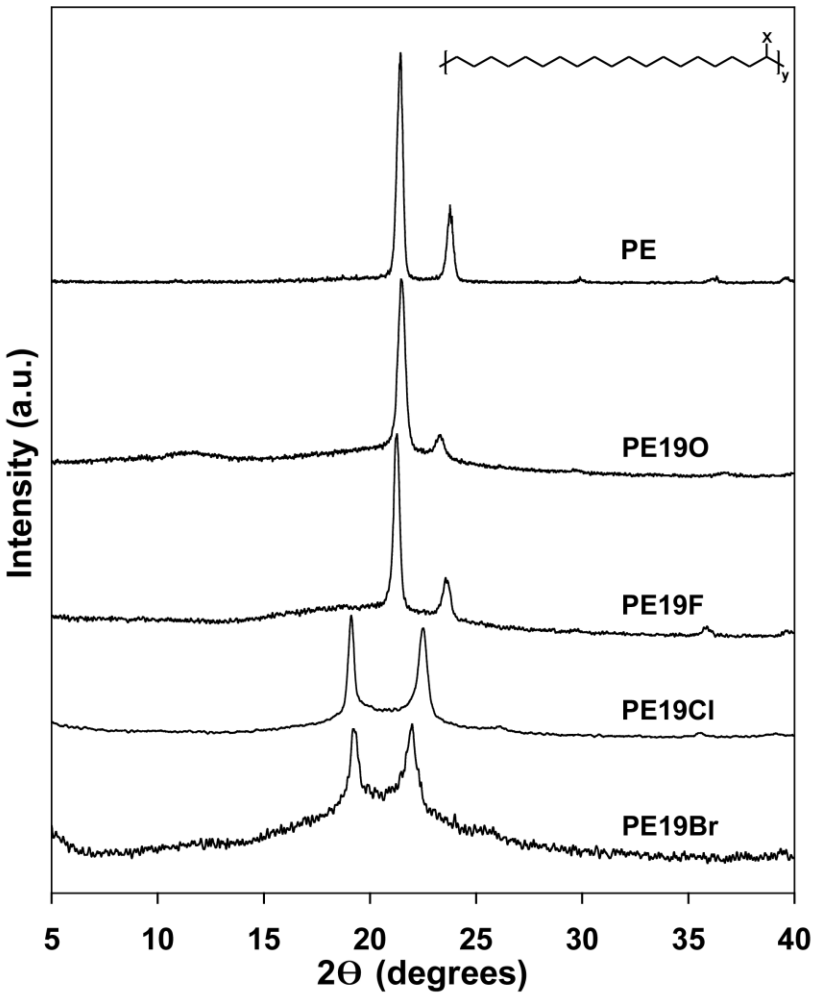

Figure 2-4. WAXD diffractograms of linear PE and ADMET precisely substituted polyethylenes slowly cooled from the melt at ~1°/min. The pendant group (X = H, O, F, Cl, Br) is indicated in each pattern.

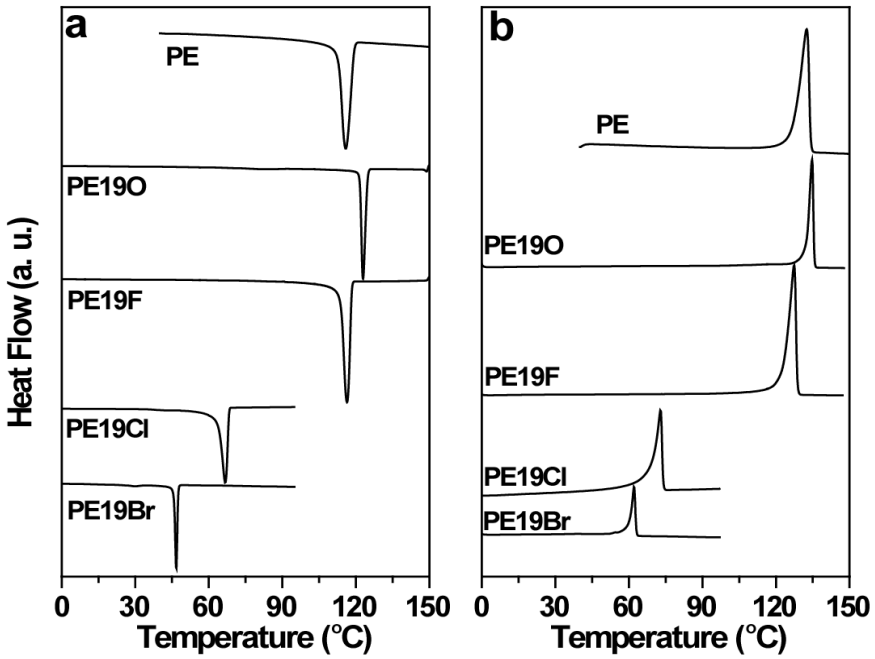

Figure 2-5. DSC exotherms (a) and endotherms (b) of linear PE and precisely substituted polyethylenes cooled from the melt at 10 ºC/min and further heated at 10 ºC/min.

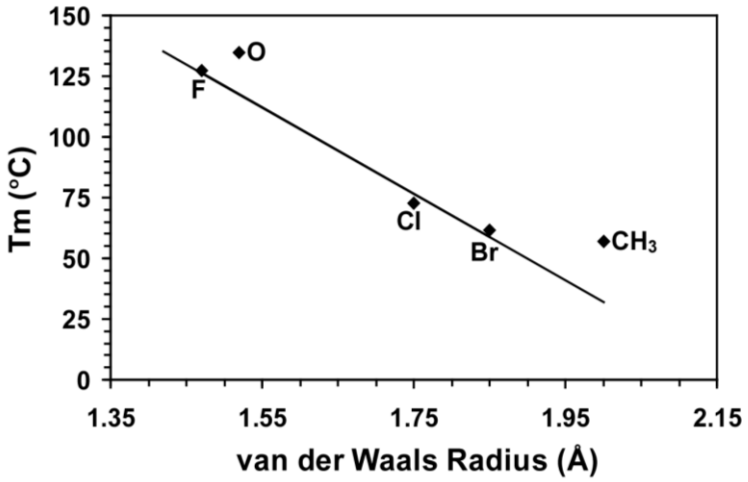

Figure 2-6. Peak melting temperatures of precisely substituted polyethylenes (PE19X) versus van der Waals radius of substituent (X). The linear regression was applied to halogenated samples.

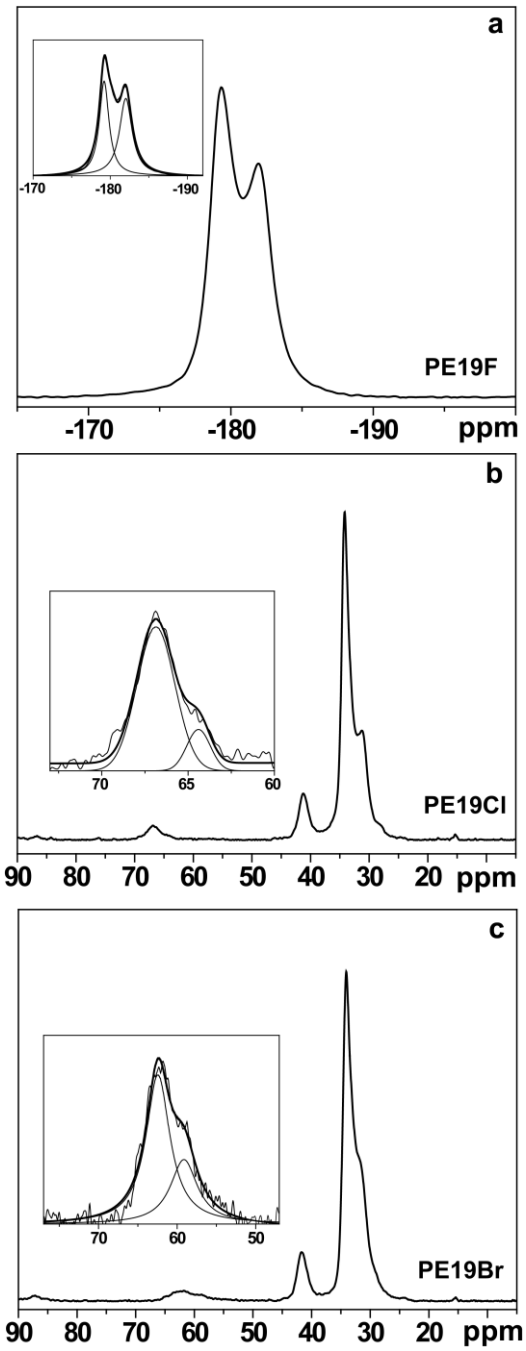

Figure 2-7. Fully relaxed ^{19}F (a) and ^{13}C NMR (b, c) DD/MAS spectra of PE19F, PE19Cl and PE19Br respectively. The Fit of the ^{19}F NMR spectral intensity with two Lorentzian components, corresponding to crystalline and non-crystalline F environments is shown in the inset. Also shown are expansions of the 50 to 80 ppm regions of the ^{13}C NMR spectra fitted with two components for better distinction of CHCl and CHBr crystalline and non-crystalline resonances. $[-(CH_2)_{16}-CH_2(\beta)-CH_2(\alpha)-CHX-]_y$

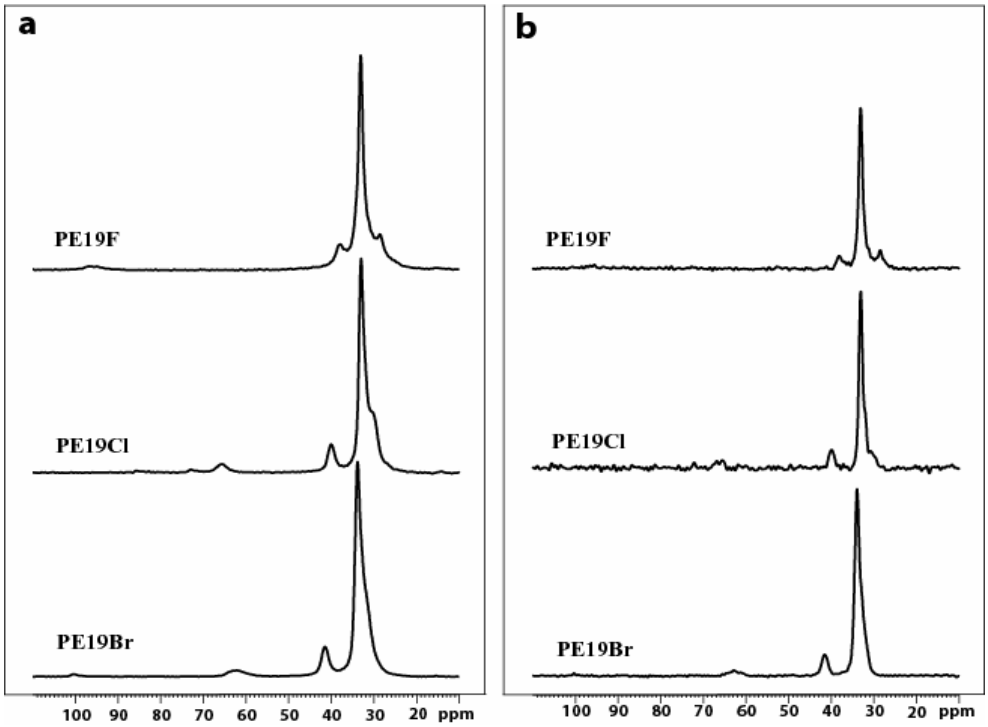

Figure 2-8. Solid state ^{13}C NMR. (a) Unfiltered ^{13}C NMR CP MAS spectra and (b) ^{1}H spin locking filtered (crystalline) spectra of precision PE19X (X = F, Cl, Br) polyolefins.

CHAPTER 3
PRECISION ETHYLENE / VINYL CHLORIDE POLYMERS VIA CONDENSATION POLYMERIZATION

3.1 Introduction

As the second largest volume plastic produced in industry,[162] poly(vinyl chloride) (PVC) continues to find a growing range of applications and is projected to have an increasing demand in the near future.[163] Common applications of PVC include pipes, siding, molding, windows, and flooring.[30] For many applications, the properties of PVC must be modified in order to increase performance and stability. While the addition of additives is the most common way to modify the characteristics of PVC for a specific application, the physical properties and stability are greatly affected by the primary structure of the PVC itself.[22] For example, the amount of syndiotactic segments in PVC has a strong effect on the melting point and overall crystallinity of the polymer and the content of defects, such as branching, head-to-head linkages, and unsaturated sites plays a major role in determining the stability of PVC to the "zipper" mechanism responsible for its degradation at elevated temperatures. The occurrence of defects and the lack of control over primary structure is the consequence of the free-radical initiated methods, which are used in the synthesis of nearly all PVC produced.[24] Based on this and the ubiquitous use of additives to modify properties in PVC, detailed information about the effect of primary structure on materials properties is often not pursued. However, vinyl-chloride copolymers are used as a means to access a variety of new property sets and to combine the attractive properties of PVC with other polymers, while minimizing the weaknesses of PVC.[164]

Ethylene-vinyl chloride (EVC) copolymers are an attractive class of polymers, which are pursued as a means of capitalizing on the strengths of PVC and polyethylene (PE). Here, judicious compositional control is a route to developing a series of polymers with accurately controlled properties as determined by the composition of the polymer itself. However, based on

the methods by which these EVC polymers are usually synthesized, little primary structure control is achieved and the more-or-less random structures give little information about how chlorine content and sequence distribution directly affect the materials properties of the polymers. There are three common methods for the preparation of EVC polymers: copolymerization of ethylene and vinyl chloride using free radical[165,166,167] or Ziegler-Natta techniques,[75,77] reductive dechlorination of PVC,[104,105,106] and chlorination of polyethylene.[78,79,80,81] In the direct free radical copolymerization of vinyl chloride and ethylene, it is difficult to control the content of the two monomer units over the full range of compositions.[74] Further, the free radical nature of the polymerization leads to poorly defined structures with high defect contents. Direct copolymerization of vinyl chloride and ethylene using Ziegler-Natta or metallocene catalysts is also problematic based on the occurrence of side reactions with the activated chlorine atom on the monomer and the alkylaluminum cocatalyst as well as the tendency of the vinyl chloride monomer to undergo β-halo elimination after insertion into the metal-alkyl bond.[75,77] In the case of the reductive dechlorination of PVC, while the ability to generate a family of EVC polymers with varying Cl contents and with identical chain lengths from a single PVC sample is a strong point for a model,[108] this class still suffers from defects present in the parent PVC.[107]

The most common method used for synthesizing EVC polymers is the chlorination of PE either under homogenous or heterogeneous conditions. In homogeneous, or solution based techniques, chlorine is distributed randomly throughout the polymer.[81] At low chlorine contents, the probability of chlorine substitution on a CHCl unit or neighboring unit is very small based on the bulky Cl atom, resulting in a random spatial distribution of Cl atoms along the backbone. At higher chlorine contents however, geminal chlorination and vicinal chlorination becomes more

commonplace.[89,90,91] In heterogeneous methods such as suspension, or solid state, the main drawback here is the blocky nature of the formed polymers based on the tendency for chlorination to occur in the amorphous regions of the polymer and at the edge of the crystalline domains.[80,93] Considering the above methods for attaining EVC polymers, it is clear that control over chorine content can be achieved in each of these methods, but control over sequence distribution cannot be attained. Therefore, even though the properties of EVC polymers with different chlorine contents are known to vary, deriving exact relationships between primary structure and physical properties is unattainable because a precise distribution of comonomer units between crystalline and amorphous domains has yet to be determined.[110]

Despite the lack of a precise model for understanding the variation in the properties of EVC polymers, there is great practical interest in these materials.[110] Specifically, the introduction of ethylene units into a PVC chain will serve the role of an internal plasticizer, which can give many advantages over the introduction of an external plasticizer and lead to a new range of materials properties from a single component material.[74,111] From a more fundamental standpoint, this class of polymers is also of great interest for developing a precise understanding of the relationship between molecular structure and physical properties in semicrystalline polymers in general, where EVC polymers could serve as an all-purpose model for this class of polymers.[110] As described above however, no specific catalyst system has been developed to effectively copolymerize ethylene and vinyl chloride, leading to the necessity to look toward model EVC polymers to establish the fundamental significance of this class of polymer. Such a focus on model polymers will not only help to derive structure property relationships, but will shift focus to the development of effective catalysts for the synthesis of EVC copolymers.[109] It is difficult however to find suitable model systems that will allow the development of precise

structure property relationships[112] and will not be limited by the quality of the synthetic or preparative method.

Recently, olefin metathesis chemistry combined with post-polymerization hydrogenation has emerged as an attractive route for synthesizing polyolefins bearing a variety of substituents.[113] For EVC polymers, ring opening metathesis polymerization (ROMP) has been employed to make a series of polymers with varying chlorine contents.[121] The absence of defects in polymers produced by ROMP leads to materials with well-defined primary structures and chlorine contents that are tuned by controlling the ratio between chlorinated and non-chlorinated monomers. The sequence distribution is nonetheless still random. Alternatively, acyclic diene metathesis polymerization (ADMET) has been used to achieve an EVC polymer with both precisely controlled chlorine content and sequence distribution,[168] here such a level of control allows one to derive precise relationships between polymer primary structure and physical properties in EVC polymers. Further, ADMET allows the investigation of a much greater range of polymers with precisely distributed chlorine atoms, as the linear α-ω dienes used in ADMET are free of the structural constraints required for monomers used in ROMP. We present here the full characterization of a new expanded family of precise EVC polymers in which a range of precise chlorine contents and sequence distributions are examined in order to generate structure-property relationships useful for developing a deeper understanding of the importance of primary structure control in EVC polymers.

3.2 Results and Discussion

3.2.1 Monomer and Polymer Synthesis

Synthesis of the necessary chlorinated α-ω diene monomers is illustrated in Figure 3-1. The alcohol precursors (**4-6**) were prepared as described earlier.[169] Conversion of the alcohols to

the corresponding chlorine monomers (**7**-**9**) by reaction with carbon tetrachloride and triphenylphosphine preceded bulk polymerization with Grubbs' first generation ruthenium catalyst to yield the unsaturated ADMET polymer UPEXCl. The nomenclature acronym used herein is UPEXCl, where U indicates unsaturation and PEXCl indicates a polyethylene backbone with a chlorine substituent on every X^{th} carbon, where X = 9, 15, 21. Exhaustive hydrogenation by diimide reduction[144] gave clean conversion to the fully saturated polymers **PE9Cl**, **PE15Cl**, and **PE21Cl**. Polymer molecular weights are shown in Table 3-1 and vary between 31,000 and 51,000 g/mol.

3.2.2 Primary Structure Characterization

The primary structure of these well-defined UPEXCl and PEXCl polymers was established using a combination of ^{1}H NMR, ^{13}C NMR, TGA (thermogravimetric analysis), IR spectroscopy, and elemental analysis. Figure 3-2 shows the ^{1}H NMR and ^{13}C NMR spectra for a typical conversion of a symmetrical chlorine containing alpha-omega diene monomer **7**, 6-chloroundeca-1,10-diene, to its unsaturated ADMET polymer **UPE9Cl**, and then to its precisely substituted saturated polymer analogue with a chlorine atom on each and every 9^{th} carbon **PE9Cl**.

Figure 3-2a and d illustrate the ^{1}H NMR and ^{13}C NMR spectra for the monomer **7** showing the assigned protons and carbons 1 through 6 in (5.0, 5.8, 2.1, 1.5, 1.7, 3.9 ppm) ^{1}H NMR and in (115.1, 138.6, 33.4, 25.9, 38.1, 64.0 ppm) the ^{13}C NMR respectively. Figure 3-2b and e illustrate the ^{1}H NMR and ^{13}C NMR spectra for the unsaturated ADMET polymer **UPE9Cl**. In the proton spectrum (Figure 3-2b) two triplets are observed in the region 5.34-5.40, corresponding to the *cis* and *trans* configurations of the double bond. The ^{13}C satellite of the major peak is a doublet of triplets, with a coupling constant of 17.5 Hz, therefore the major peak was assigned to *trans*. The *trans*: *cis* ratio determined from the carbon spectrum (Figure 3-2e), is 4 : 1. The peaks for the

terminal vinyl moiety appeared at 4.99 (*CH_2 trans*), 4.93 (*CH_2 cis*) and 5.81 (*CH*). The degree of polymerization (DP) was determined by integration of these signals against the two triplets in the region 5.34-5.40 and the values are shown in Table 3-2. The proton signals for **UPE9Cl** were assigned from the DQCOSY spectrum. The protons in positions 1 and 2 displayed different chemical shifts in the *trans* and *cis* moieties, being 0.03 ppm upfield and 0.03 ppm downfield in *cis* as compared to *trans*, in positions 1 and 2, correspondingly. The GHMBC spectrum revealed both the one-bond and the two- or three-bond couplings between protons and carbons, for both the *cis* and the *trans* moieties. The proton and carbon chemical shifts have been assigned based on these cross-peaks and are presented in Table 3-2, together with the *trans* : *cis* ratio.

The differences between the chemical shifts of a carbon atom in the *trans* and *cis* moieties, $\Delta\delta_{trans\text{-}cis} = \delta_{trans} - \delta_{cis}$, have been measured in a ^{13}C spectrum acquired with a digital resolution of 0.9 ppb and are given, in ppb in Table 3-2. $\Delta\delta_{trans\text{-}cis}$ are noticeable for carbons up to four bonds away from the double bond, and for an alkyl moiety free of the influence of other groups (double bonds or chlorine atoms must be some 7-10 bonds away) typical values in the order of distance, starting with the carbon of the double bond, are: 465, 5339, -110, -137, -37 ppb.

Further, in Figure 3-2c the ^1H NMR for **PE9Cl** shows a methine proton (α=5) at 3.9 ppm, and methylene protons (β=4) at 1.7 ppm and (1-3) at 1.2-1.6 ppm. The ^{13}C NMR data exhibited in Figure 3-2f reveal that five sp^3 carbon signals are present in this polymer, which contains a methine carbon (α=5, 64.6 ppm), and methylene carbons (β=4, 38.8 ppm), (δ=2, 29.6 ppm), (ε=1, 29.4), (γ=3, 26.7). The chemical shift range observed for polymer **PE9Cl** are in very good agreement with the values in the literature for the random ethylene/vinyl chloride copolymers.[104, 121,125, 170] In the random case, several different methine and other methylene chemical shifts are observed due to the random nature of the polymer structure. Obtaining only five different

carbons for ~49,000 molecular weight polymers unequivocally confirms the precise structure of these polymers. These spectral data not only support the primary structure of the repeat unit but also suggest that no side reactions are detectable within the limitations of the NMR instrument. Elemental analysis results also show good agreement between theoretical and experimental values (see experimental section).

The olefin region in these NMR spectra also illustrates the conversion of monomer to unsaturated polymer with the disappearance of the terminal olefin at 5.0 and 5.8 ppm in the monomer and the subsequent growth of internal olefin resonance at 5.4 ppm in the unsaturated polymer **UPE9Cl**, a result consistent with the GPC results given in Table 3-1. Upon exhaustive hydrogenation, these olefin resonances completely disappear. The ^{13}C NMR spectra support exhaustive hydrogenation as well; note that the sp^2 resonances in the unsaturated polymer (*trans*, 130.2 ppm, *cis*, 129.7 ppm) completely disappear after hydrogenation giving **PE9Cl** (confirmed by IR). These spectra are typical for all the ADMET polyethylenes synthesized in the series, and they illustrate the degree of structure control that is possible. These conclusions are valid for the **UPE15Cl**, **UPE21Cl** polymers as well; the chemical shift values are given in Table 3-2 and in the experimental section. This detailed NMR study confirms the precise nature of the examined polymers and the degree of absolute control over primary structure afforded by ADMET polymerization followed by exhaustive hydrogenation.

The IR spectra in Figure 3-3 display characteristic information regarding the primary structure of the polymers, where the absence of a peak at 967 cm^{-1} for all three EVC polymers indicates complete hydrogenation, based on the disappearance of the out-of plane olefin C-H wagging vibrational mode. The first spectral segment with characteristic information is the C-C1 stretching region between 600 and 700 cm^{-1}. For PVC, three broad bands are observed centered

at 615, 636, and 693 cm^{-1},[148] where the "broadness" results from the contributions from a number of different conformations and configurations. For the EVC polymers, the resonances in the 600-700 cm^{-1} region are significantly narrowed relative to PVC as the number of chlorines is reduced and number of CH_2 sequences increased. The spectra then consist of two single narrow bands at 660-661 and 609-611 cm^{-1}, which have been assigned to isolated gauche, and trans C-C1 stretching respectively.[126] Going from **PE9Cl** to the **PE21Cl**, decreases the gauche to trans ratio as the number of CH_2 units between Cl atoms increases. This observation is significant because it shows a distortion of the all trans-trans zigzag conformation of the backbone at higher chlorine contents. Another region of particular interest is the 700-850 cm^{-1} region where methylene rocking motions are observed. The resonance at 758 cm^{-1} has been assigned to the methylene rocking motion in PVC, specifically the rocking mode of a CH_2 unit between two CHCl units. As the concentration of CH_2 units increases going from PVC through the EVC series, the peak at 758 cm^{-1} decreases in intensity and the peak at 723-718 cm^{-1} increases in intensity, which is characteristic of CH_2 rocking modes for longer methylene sequences. In the case of PE a doublet is observed at 730 and 719 cm^{-1}, which has been assigned to rocking vibrations of long methylene sequences. This doublet in PE, which is specifically associated with the orthorhombic crystal structure, is not observed for any of the EVC polymers suggesting that a different crystalline structure exist for these materials.[148]

Bands between 1400 and 900 cm^{-1} are difficult to assign to individual vibrational components, since most resonances overlap with other resonances. The numerous resonances in this region are rapidly reduced in intensity as the number of chlorines is decreased. Exceptions are the 1332 and 963 cm^{-1} bands which are dominated by C-C stretching and CH_2 wagging motions of short sequences. In the case of EVC polymers, the peak at 1332 cm^{-1} decreases with

decreasing chlorine content and the peak at 963 cm^{-1} fully disappears for all of the EVC polymers. Additionally, all the peaks in the area of the 1254 cm^{-1} multiplet arise from methine bending modes and are sensitive to sequence length and/or environment. The decrease in the intensity of the 1254 cm^{-1} peak with decreasing chlorine content is indicative of the smaller chlorine contents and the changing environment caused by the presence of longer methylene sequences.[148]

The C-H bending modes at 1435/1426 cm^{-1} for PVC broaden into a singlet as the number of chlorines is decreased. Concomitant with the 1435/1426 cm^{-1} loss is the growth of the 1467-1471 cm^{-1} resonance which eventually becomes the 1472/1462 cm^{-1} doublet assigned to the methylene bending modes in PE.[148] The shoulders observed in the EVC samples at 1457 and 1434 cm^{-1} correspond to the bending modes for the β and α methylenes. It can be observed that the intensity of the peaks at 1457 and 1434 cm^{-1} increases with increasing chlorine content in the EVC polymers. The above IR study clearly illustrates the evolution of the PVC structure through a series of precise EVC polymers with decreasing chlorine content to the pure PE backbone.

3.2.3 Thermal Analysis – TGA

While NMR and IR support the proposed primary structure, TGA results directly support the precise composition of the polymers. Figure 3-4a displays the thermal decomposition curves of all three polymers as shown relative to PE and PVC. All three EVC polymers exhibit a two-stage decomposition, where the first stage corresponds to the loss of HCl and the second stage marks the catastrophic decomposition of the polymer. Analogous to our previous work on ethylene vinyl halide polymers and the reported decomposition of PVC, the mass loss in the first stage quantitatively reflects the halogen content of the polymer. The observed values for mass

loss in the first stage are found to be in agreement with the calculated HCl content for each of the EVC polymers at 23%, 15%, and 11% for **PE9Cl**, **PE15Cl**, and **PE21Cl** respectively. Figure 3-4a also shows that the onset of decomposition for the first stage loss of HCl increases with decreasing chlorine content (see Table 3-1). The EVC samples become more stable with increasing content of ethylene units as the labile chlorine content decreases, since the chain reaction (zipper mechanism) resulting in HCl loss is restricted by more ethylene units compared to PVC. This effect is called inner stabilization.[105] The stabilization of the EVC samples can also be partially attributed to the lack of tertiary or allylic chlorines, which are generally found in PVC. However in the second stage of decomposition, the onset for PVC is higher than that for the EVC polymers and this difference can be attributed to a high concentration of conjugated carbon-carbon double bonds that begin to crosslink and are converted into char.[171] Even at temperatures above 500 ºC, after the EVC polymers have completely decomposed, residual char is observed in PVC and a non-zero mass is observed in PE, which is attributed to catalyst residue.

Figure 3-4b compares the stability of the EVC polymers to that of PVC under isothermal decomposition at 180 °C. Here, a temperature of 180 °C is chosen as it is below the onset of decomposition for any of the polymers, ensuring that any mass loss may be attributed to HCl loss. The percentage HCl loss is normalized to the overall HCl content in each of the polymers to reflect the relative amount of a given polymer's HCl loss over a given time interval. All samples undergo a rapid loss of 3.5-6.8% of the total HCl content of the polymer during the first hour. However, after the first hour, the degradation rate of the EVC polymers levels off leading to a total HCl loss of only ~6% even after four hours at 180 °C, while the PVC sample continues to degrade at nearly a constant rate, leading to the loss of ~40% of the HCl content after four

hours. Structural precision and the absence of defects make the difference. Precise EVC polymers are more stable to the applied isothermal decomposition than PVC, a result which can be attributed to the suppression of the zipper mechanism found in PVC and induced by the extended spacing between chlorine atoms (referred to as inner stabilization as described above) in the precise polymers.

3.2.4 DSC

The DSC data for the precision polymers is shown relative to that for PE and PVC in Figure 3-5 for both the crystallization (Figure 3-5a) and melting (Figure 3-5b) behavior, and the results are summarized in Table 3-1. Increasing the chlorine atom content results in a decrease of T_m, and ΔH_m. This behavior indicates an increase in the degree of disorder in the crystal owing to the introduction of the chlorine atom into the crystal lattice. When we compare these results with our previous work on precision ethylene/vinyl bromide polymers,[169] it becomes clear that Br atoms lower the melting point and ΔH_m more than the chlorine atoms for polymers with the same halogen content. Assuming a similar distribution of the halogen (Cl or Br) between crystalline and non-crystalline regions,[168] the difference in thermal behavior correlates with larger lattice strains in the precision vinyl bromide series.

The sharp crystalline and melting traces seen in Figure 3-5 are typical of homopolymers and are in stark contrast to the broad traces observed in random EVC polymers of similar chlorine content.[74] This suggests a difference in the crystallization process for ADMET EVC polymers relative to random EVC polymers, which is not based on the selection of long crystallizable sequences. It is likely that the crystallization of precisely substituted Cl samples evolves by incorporating in the crystallite long chain segments without chlorine discrimination.[168] **PE9Cl** displays a sharp crystallization peak and a dual melting transition, the

latter caused by a melting-recrystallization process enabled by the presence of relatively high Cl contents in the crystal (Figure 3-6). The lower melting peak corresponds to the initial crystallites, while crystals formed during the heating scan melt at a higher temperature. Recrystallization is suppressed at the heating rate of 40 ^{o}C/min. Reducing the Cl content in the series, and hence in the crystal, leads to less defected, thicker crystallites not subject to melt-recrystallization as indicated in Figure 3-5 by sharp single meltings of **PE15Cl** and **PE21Cl.** The dramatic decrease of heat of fusion for **PE9Cl** relative to **PE15Cl** and **PE21Cl** suggests a lower degree of crystallinity, indicating that the increased content of bulky atoms along the chain inhibits the ability of the polymer to crystallize to a greater extent. The greater amorphous content of **PE9Cl** is evidenced by a more visible T_g relative to the other precise polymers. Interestingly we observe a linear correlation between the T_g of PVC at 80 °C, the T_g of PE at -120 °C,[172] and the value for **PE9Cl** at -33 °C with mass fraction of Cl in the polymer. The glass transition temperature of **PE9Cl** decreases with decreasing chlorine content relative to PVC due to the high mobility of the ethylene units.

Figure 3-7 shows the linear relationship between T_m and the number of CH_2 groups in the repeating unit. In accord with the behavior of trans-poly(alkenamers), the melting temperature increases with increasing number of carbon atoms in the repeating unit for materials that crystallize with the same crystal structure, as is expected in this case.

3.3 Conclusion and Outlook

Herein we have described the synthesis of a family of precise ethylene/vinyl chloride polymers that contain a chlorine atom on each and every 9th, 15th, and 21st carbon respectively. The precise primary structure has been confirmed by ^{1}H NMR and ^{13}C NMR spectroscopy, which allow for the assignment of each chemical shift observed to one unique methylene or methine group within the repeat unit. The presence of only those shifts corresponding to a

precision polymer reinforces the ability of ADMET to generate precise and defect free polymers. The thermal characterization of the polymers via DSC suggests a crystallization process typical of homopolymers as evidenced by the sharp melting and crystallization transitions. The homopolymer behavior is indicative of a precise structure that crystallizes in such a fashion to incorporate the chlorine atoms into the crystal lattice, in sharp contrast to random EVC polymers. Melting and crystallization temperatures scale proportionally to the number of CH_2 groups in the repeating unit. The heat of fusion decreases drastically with increasing Cl content in the series, with values of < 30 J/g for **PE9Cl** suggesting that beyond a certain critical chlorine content in these precise polymers, the bulky chlorine atoms begin to inhibit the crystallization process. Further work aimed to provide direct evidence of the crystal structure via WAXD, crystal composition via solid state NMR and lamellar morphology is currently underway.

3.4 Experimental

Chemicals. Chemicals were purchased from the Aldrich Chemical Company and used as received unless noted. Grubbs' first generation ruthenium catalyst, bis(tricyclohexylphosphine)-benzylidine ruthenium (IV)dichloride, was purchased from Strem Chemical and stored in an Argon filled dry box prior to use. Methylene chloride and *o*-xylene were distilled over CaH_2. The same ADMET PE sample published[145] by our group was used for comparison. PVC was purchased from the Aldrich Chemical Company, Product Number 389293.

Instrumentation. Solution ^{1}H NMR (300 MHz) and ^{13}C NMR (75 MHz) spectra were recorded on a Varian Gemini 300, VXR 300 or Mercury 300 spectrometer. All chemical shifts for ^{1}H and ^{13}C NMR spectroscopy were referenced to residual signals from $CDCl_3$ (^{1}H = 7.27 ppm and ^{13}C = 77.23 ppm) with an internal reference TMS 0.03% v/v to internal TMS standard for 0. The **UPEXCl** polymers were also characterized by standard 2D NMR experiments run on

a Varian Inova 500 instrument (500 MHz for ^{1}H and 125 MHz for ^{13}C). In all the NMR work the solvent was chloroform-*d* and the temperature was 25 ºC.

High-resolution mass spectral (HRMS) data were obtained on a Finnegan 4500 gas chromatograph/mass spectrometer using the electron ionization (EI) mode. Elemental analyses were carried out by Atlantic Microlabs Inc., Norcross, GA. The GPC measurements for samples in THF were taken on a Waters GPCV 2K instrument. Samples were run with HPLC grade THF at 40 °C on Waters Styrage1HR 5E columns monitored with an internal differential refractive index detector (DRI) relative to polystyrene standards. Polymer molecular weights reported vs polyethylene standards were measured using a Waters Associates 150C high-temperature gel permeation chromatograph equipped with three Polymer Laboratories mixed bed Type B columns and an internal DRI detector. The mobile phase was BHT-inhibited 1,2,4-trichlorobenzene (135 °C, flow rate 1.0 mL/minute, typical sample concentration 2 mg/mL). IR data was obtained using a Perkin-Elmer Spectrum One FTIR outfitted with a $LiTaO_3$ detector. Measurements were automatically corrected for water and carbon dioxide. Thermogravimetric analysis (TGA) data was obtained with a Perkin-Elmer 7 series thermal analysis system. The TGA samples (2-5 mg) were heated from 50 ºC to 700 ºC at 10 ºC/min under nitrogen. Melting and crystallizations were obtained at 10 °C/min in a differential scanning calorimeter TA Instrument DSC-Q1000 V9.6 Build 290 under nitrogen flow and calibrated with indium.

Synthesis: General procedure for Grignard reaction. Synthesis of 5-bromopent-1-ene (**1**), 8-bromooct-1-ene (**2**), 11-bromoundec-1-ene (**3**) undeca-1,10-dien-6-ol (**4**), heptadeca-1,16-dien-9-ol (**5**), and tricosa-1,22-dien-12-ol (**6**) was described previously.[169]

General procedure for chlorination reaction. The precursor alcohol **4**, **5**, or **6** (1 equiv.) and Ph_3P (1.5 equiv.) were dissolved in CCl_4 under argon. The reaction was stirred overnight at

80 ºC. The solution was concentrated, and pentane was added. The mixture was filtered, and the filtrate was concentrated under vacuum to yield chlorinated ADMET monomers 6-chloroundeca-1,10-diene (**7**), 9-chloroheptadeca-1,16-diene (**8**), and 12-chlorotricosa-1,22-diene (**9**). The chlorinated ADMET monomers were purified with column chromatography on silica gel eluted by hexane (yield 70-80%).

6-chloroundeca-1,10-diene (7). ^{1}H NMR (300 MHz $CDCl_3$) δ 5.81 (m, 2H), 5.00 (m, 4H), 3.91 (p, 1H), 2.09 (m, 4H), 1.81-1.42 (br, 8H). ^{13}C NMR (75 MHz, $CDCl_3$) δ 138.55, 115.09, 64.00, 38.08, 33.40, 25.90. HRMS calcd. for $C_{11}H_{19}Cl$ $(M+Cl)^-$, 221.0858; found, 221.0866. Anal. Calcd. for $C_{11}H_{19}Cl$: C, 70.76; H, 10.26; Cl, 18.99. Found: C, 70.93; H, 10.25; Cl, 18.74.

9-chloroheptadeca-1,16-diene (8). ^{1}H NMR (300 MHz $CDCl_3$) δ 5.81 (m, 2H), 4.97 (m, 4H), 3.90 (p, 1H), 2.05 (m, 4H), 1.70 (m, 4H), 1.60-1.20 (br, 16H). ^{13}C NMR (75 MHz, $CDCl_3$) δ 139.31, 114.44, 64.52, 38.71, 33.96, 29.24, 29.19, 29.04, 26.66. HRMS calcd. for $C_{17}H_{31}Cl$ (M^+), 270.2114; found, 270.2112. Anal. Calcd. for $C_{17}H_{31}Cl$: C, 75.38; H, 11.54; Cl, 13.09. Found: C, 75.53; H, 11.52; Cl, 13.00.

12-chlorotricosa-1,22-diene (9). ^{1}H NMR (300 MHz $CDCl_3$) δ 5.81 (m, 2H), 4.97 (m, 4H), 3.89 (p, 1H), 2.04 (m, 4H), 1.71 (m, 4H), 1.60-1.20 (br, 28H). ^{13}C NMR (75 MHz, $CDCl_3$) δ 139.45, 114.33, 64.61, 38.75, 34.03, 29.73, 29.72, 29.68, 29.41, 29.35, 29.16, 26.72. HRMS calcd. for $C_{23}H_{43}Cl$ (M^+), 354.3053; found, 354.3066. Anal. Calcd. for $C_{23}H_{43}Cl$: C, 77.81; H, 12.21; Cl, 9.99. Found: C, 77.88; H, 12.22; Cl, 10.00.

General procedure for bulk polymerization. Monomer and Grubbs' first generation catalyst were combined in a ratio of 500:1 under argon atmosphere. The polymerization was conducted at 35-40 ºC under vacuum with stirring for 5 days. The reaction was then stopped and 5 mL of toluene was added to dissolve the polymer with stirring. The reaction was allowed to

cool to room temperature. The polymers were then precipitated by dripping the toluene solution into cold acidic methanol. They were then isolated by filtration and dried. Polymers were then redissolved in 50 mL of toluene and treated with THP (tris(hydroxymethyl)phosphine)) in order to remove any residual catalyst.[173] The polymers were then reprecipitated into acidic methanol, filtered and dried.

Polymerization of 6-chloroundeca-1,10-diene (UPE9Cl). M_w (GPC vs. PS) = 37,100 g/mol. PDI = (M_w/M_n) = 1.84. For ^{1}H NMR and ^{13}C NMR data see Table 3-2.

Polymerization of 9-chloroheptadeca-1,16-diene (UPE15Cl). M_w (GPC vs. PS) = 39,800 g/mol. PDI = (M_w/M_n) = 1.81. For ^{1}H NMR and ^{13}C NMR data see Table 3-2.

Polymerization of 12-chlorotricosa-1,22-diene (UPE21Cl). M_w (GPC vs. PS) = 67,100 g/mol. PDI = (M_w/M_n) = 1.84. For ^{1}H NMR and ^{13}C NMR data see Table 3-2.

General Procedure for hydrogenation. The chlorine containing polymers (**UPE9Cl**), (**UPE15Cl**), and (**UPE21Cl**) were then hydrogenated using a modified version of the method described by Hahn[144] by dissolving in dry *o*-xylene under argon and adding 3.3 equivalents of *p*-toluenesulfonyl hydrazide (TSH) and 4 equivalents of tri-*n*-propyl amine (TPA). The solutions were refluxed for 9 hours and then cooled to room temperature. The hydrogenated polymer was precipitated into ice-cold methanol and isolated by filtration. The dried polymer was then redissolved in toluene and re-precipitated by dipping into ice-cold acidic methanol. A white solid was collected by filtration and the polymers were isolated in quantitative yield.

PE9Cl. ^{1}H NMR (300 MHz $CDCl_3$) δ 3.89 (p, 1H), 1.71 (m, 4H), 1.62-1.0 (bm, 12H). ^{13}C NMR (75 MHz, $CDCl_3$) δ 64.58, 38.75, 29.64, 29.37, 26.71. Anal. Calcd.: C, 67.27; H, 10.66; Cl, 22.06. Found: C, 67.25; H, 10.65; Cl, 20.92. M_w (GPC vs. PS) = 48,700 g/mol. PDI = (M_w/M_n) = 1.78.

PE15Cl. ^{1}H NMR (300 MHz $CDCl_3$) δ 3.90 (p, 1H), 1.71 (m, 4H), 1.6-1.2 (bm, 24H). ^{13}C NMR (75 MHz, $CDCl_3$) δ 64.63, 38.76, 29.90, 29.87, 29.82, 29.76, 29.43, 26.74. Anal. Calcd.: C, 73.58; H, 11.94; Cl, 14.48. Found: C, 73.66; H, 12.00; Cl, 14.26. M_w (GPC vs. PS) = 51,400 g/mol. PDI = (M_w/M_n) = 1.75.

PE21Cl. ^{1}H NMR (300 MHz $CDCl_3$) δ 3.90 (p, 1H), 1.74 (m, 4H), 1.6-1.2 (bm, 36H), 0.9 (t, 0.15H). ^{13}C NMR (75 MHz, $CDCl_3$) δ 64.62, 38.76, 29.94, 29.88, 29.82, 29.76, 29.44, 26.74. Anal. Calcd.: C, 76.66; H, 12.56; Cl, 10.78. Found: C, 76.64; H, 12.61; Cl, 10.57. M_w (GPC vs. PE) = 31,100 g/mol. PDI = (M_w/M_n) = 4.43.

Table 3-1. Molecular weight and thermal data for unsaturated (UPEXCl) and saturated (PEXCl) polymers.

Sample	M_w x10^3	$M_w \backslash M_n$	T_g(ºC)	T_m(ºC)	T_c(ºC)	ΔH_m(J/g)	First stage onset of decomposition[e](ºC)	Second stage onset of decomposition[f](ºC)
UPE9Cl	37[a]	1.84	-63	-	-	-	292	385
UPE15Cl	40[a]	1.81	-57	24	-6	27	320	413
UPE21Cl	67[a]	1.84	-37	46	32	67	332	415
PVC	43	1.95	80	-	-	-	274	450
PE9Cl	49[a]	1.78	-33	41	15	26.7	295	418
PE15Cl	51[a]	1.75	-	63	54	87.4	301	420
PE21Cl	31[b]	4.43	-	81	70	111.3	327	407
PE	16[c]	1.60	-120[d]	129	118	185.0	348	384

a.) GPC vs. PS in THF; b.) GPC vs. PE in DCB; c.) ref[145]; d.) ref [174]; e.) Recorded at first stage 10% total mass loss under nitrogen gas, 10 °C/min.; f.) Recorded at second stage 10% total mass loss under nitrogen gas, 10 °C/min.

Table 3-2. Proton and carbon chemical shifts (in ppm) and $\Delta\delta_{trans\text{-}cis}$ (in ppb) for polymers UPE9Cl, UPE15Cl, and UPE21Cl.

compound	trans:cis / DP	position	1	2	3	4	5	6	7	8	9	10	11
UPE9Cl	5.0	δC	130.20	32.00	26.40	37.90	64.00						
		$\Delta\delta_{trans\text{-}cis}$	514	5334	-148	-86	31						
	100	δH	5.40	1.99, 1.99	1.59, 1.46	1.70, 1.70	3.89						
UPE15Cl	4.4	δC	130.30	32.50	29.50	29.00	29.10	26.50	38.50	64.30			
		$\Delta\delta_{trans\text{-}cis}$	475	5387	-115	-136	-41	0	0	14			
	72	δH	5.38	1.97, 1.97	1.34, 1.34	1.27, 1.27	1.33, 1.30	1.51, 1.39	1.69, 1.69	3.88			
UPE21Cl	4.1	δC	130.30	32.60	29.70	29.20	29.49	29.56	29.52	29.20	26.50	38.50	64.30
		$\Delta\delta_{trans\text{-}cis}$	465	5399	-110	-137	-37	0	0	0	0	0	0
	148	δH	5.38	1.96, 1.96	1.33, 1.33	1.27, 1.27	1.27, 1.27	1.27, 1.27	1.27, 1.27	1.27, 1.27	1.51, 1.39	1.69, 1.69	3.88

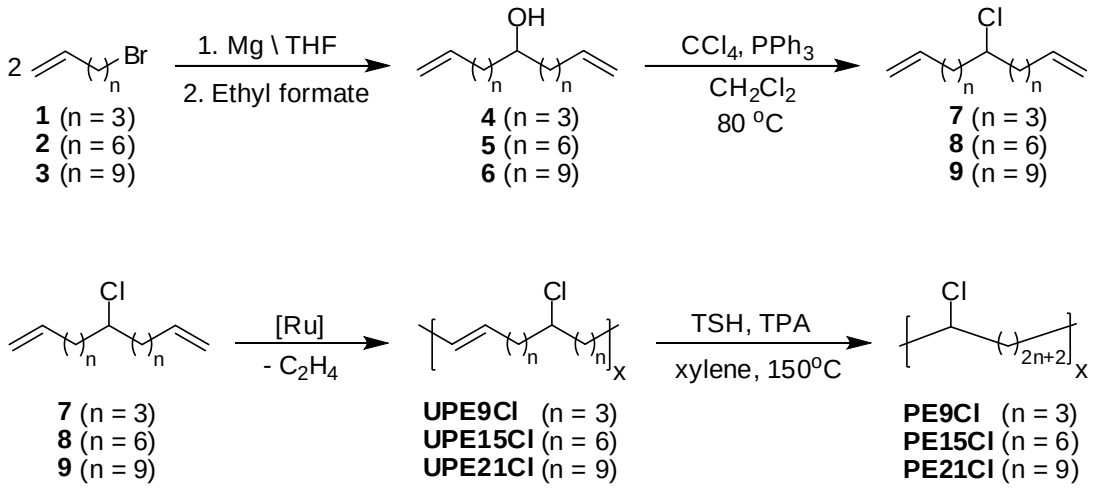

Figure 3-1. Synthesis of PEXCl polymers.

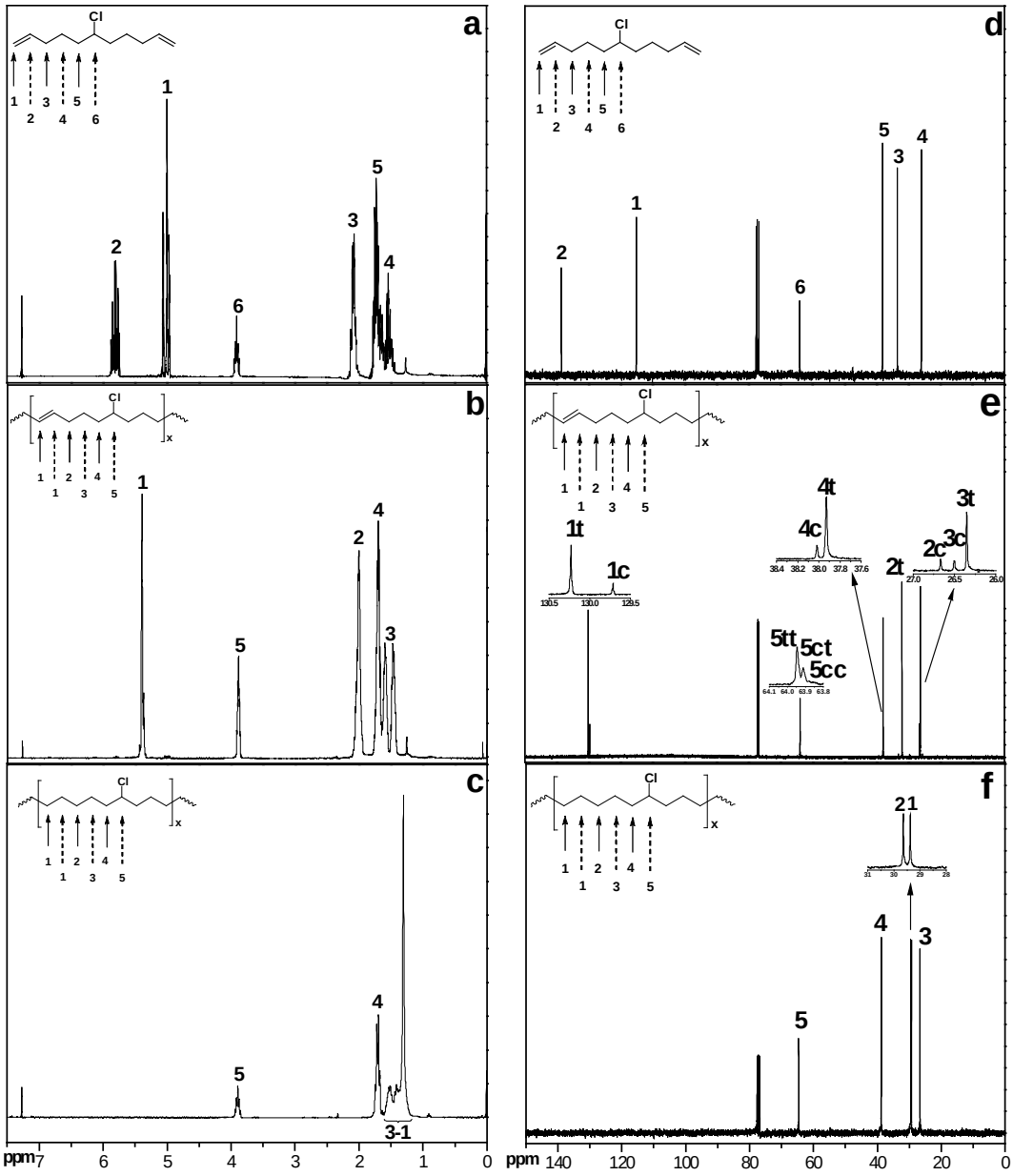

Figure 3-2. ^{1}H NMR spectra for monomer 7 (a), UPE9Cl (b), PE9Cl (c) and ^{13}C NMR spectra for monomer 7 (a), UPE9Cl (b), PE9Cl (c).

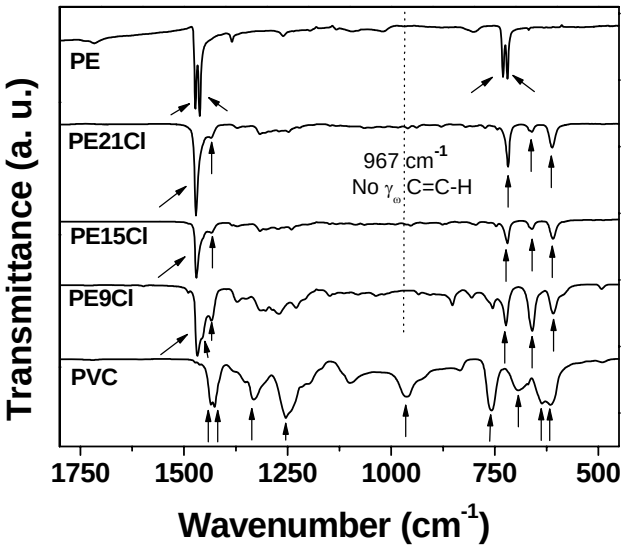

Figure 3-3. IR of PE, PE21Cl, PE15Cl, PE9Cl, and PVC.

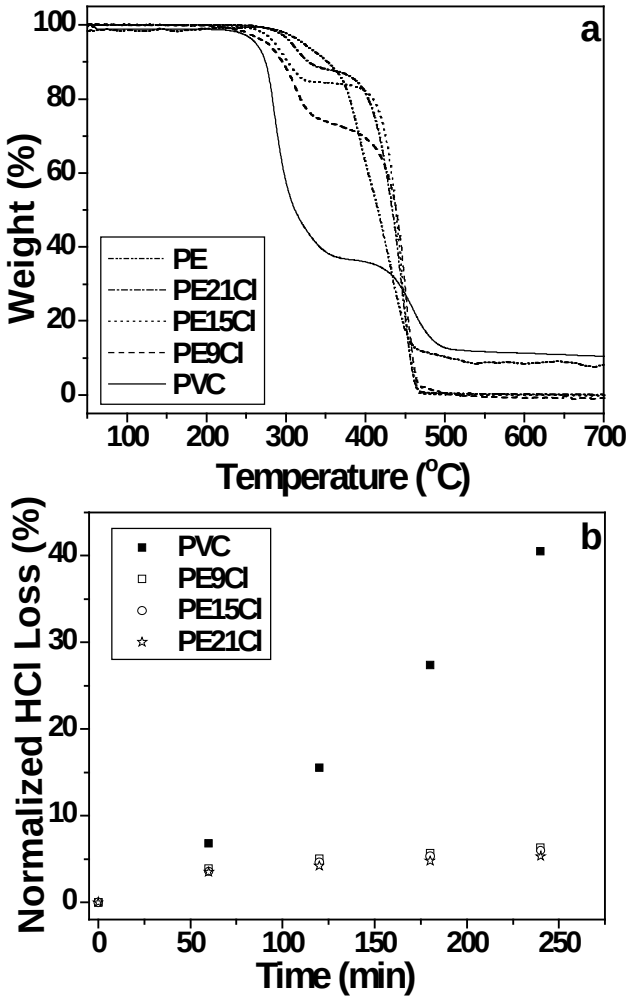

Figure 3-4. TGA results for PE, PE21Cl, PE15Cl, PE9Cl, and PVC. (a) TGA results for PE, PE21Cl, PE15Cl, PE9Cl, and PVC. (b) Normalized HCl loss data for PVC, PE9Cl, PE15Cl, PE21Cl under isothermal (180 °C) degradation measured under nitrogen atmosphere.

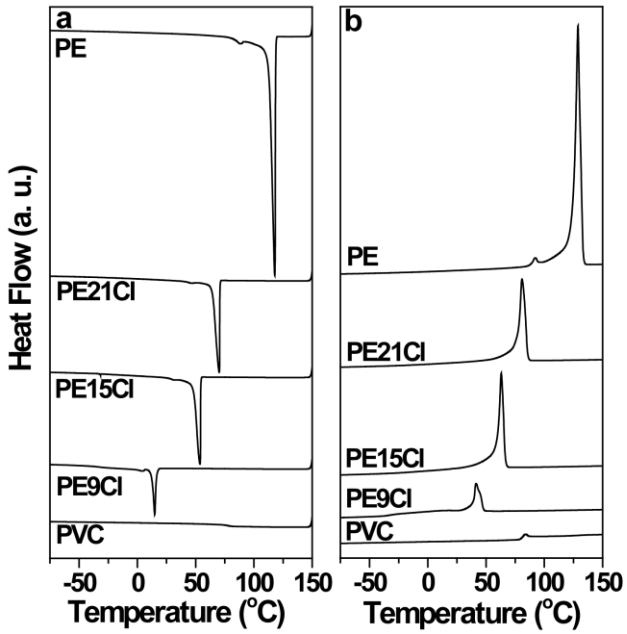

Figure 3-5. DCS exotherms (a) and endotherms (b) of PE9Cl, PE15Cl, PE21Cl, relative to PE and PVC.

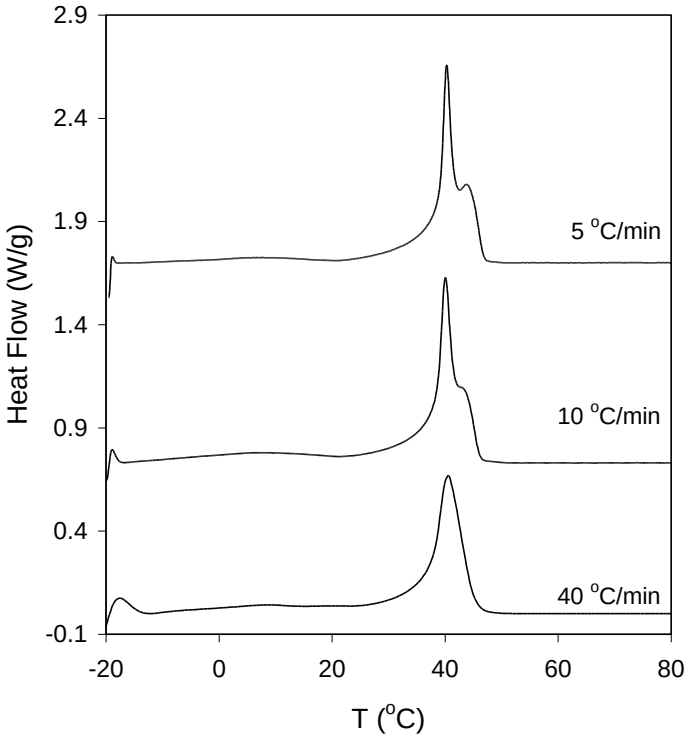

Figure 3-6. DSC endotherms for PE9Cl at heating rates of 5, 10, and 40 °C/min.

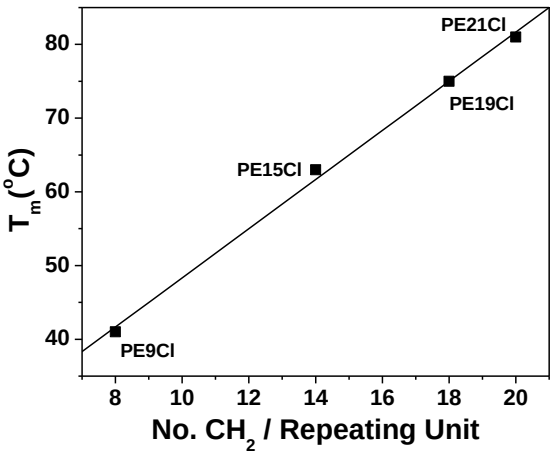

Figure 3-7. Trends for the variation in T_m vs. the number of CH_2 per repeat unit.

CHAPTER 4
PRECISION ETHYLENE/VINYL BROMIDE POLYMERS

4.1 Introduction

The importance of polyolefins in industry is reflected by the enormous volumes of these polymers that are produced on an annual basis.[116] While polyethylene (PE) is the most abundant of these polymers, polyethylenes modified with halogens such as poly(vinyl chloride), are extensively employed as a result of the tailored sets of properties they possess.[118,175] Ethylene/vinyl bromide (EV/B) polymers have received significantly less attention than their ethylene/vinyl fluoride (EVF) or ethylene/vinyl chloride (EVC) counterparts because they are difficult to synthesize, especially those having a well-defined structure.[123]

No direct synthetic copolymerization methods exist that combine vinyl bromide and comonomers;[107] instead a variety of postpolymerization bromination strategies have been employed. The most common techniques employ either bromination of a suspension of PE, or solution bromination.[102] Similarly, solution hydrobromination of polyoctenamer has been used.[176] Additionally, surface bromination of thin PE films with bromine vapor has been described.[177] Another somewhat different approach to these polymers involves reductive debromination of poly(vinyl bromide).[107]

Deficiencies in the above techniques can be attributed to the incorporation of structural defects in the polymer precursor (e.g. branching, cyclic defects caused by backbiting) as well as the uncontrolled chemical events that accompany postpolymerization bromination.[107] Further, the uncontrolled incorporation of bromine, which is assured when using these techniques, leads to polymers with a non-uniform distribution of bromine or even a blocky primary structure.[102] Consequently, the pursuit of optimized routes to well-defined EV/B copolymers remains relevant. For example, EV/B copolymers could serve as the precursor to a variety of modified

polyolefins via substitution of the bromine atom[178,179] or, they could prove useful in selective crosslinking. In addition, the EV/B copolymers could find direct materials applications stemming from the flame retardancy induced in bromine containing materials,[180] or more generally based on the modified physical properties and their influence on adhesion, wettability, and surface energy.[177]

Olefin metathesis offers distinct advantages over previously used methods for the synthesis of EV/B polymers. Acyclic diene metathesis polymerization (ADMET) is now widely accepted as a route to polyolefins having a precisely defined primary structure, for it entails mild chemistry, which does not lead to side reactions involving the reactive bromine functionality. Thus far we have produced a precise EV/B ADMET polymer with a bromine atom located on each and every 19th carbon along the polyethylene backbone.[168] We now extend this study to a larger family of EV/B polymers in order to examine the effect of bromine content and sequence distribution on the thermal and crystalline properties of this novel class of polymers.

4.2 Results and Discussion

Synthesis of the necessary brominated ADMET α–ω diene monomers is illustrated in Figure 4-1. The alcohol precursors (**4-6**) were prepared according to the methods previously described[181] and converted to the corresponding bromine monomers (**7-9**) by reaction with carbon tetrabromide and triphenylphosphine.[168] Bulk polymerization with Grubbs' first generation ruthenium catalyst, followed by exhaustive hydrogenation under mild conditions with Wilkinson's catalyst led to the precise EV/B polymers **PE9Br**, **PE15Br**, and **PE21Br** containing a bromine atom on each and every 9th, 15th, and 21st carbon along the PE backbone, respectively. The primary structure of the polymers was confirmed by ^{1}H NMR, ^{13}C NMR, and elemental analysis.

The primary structure of these polymers was confirmed further by thermogravimetric analysis (TGA) (Figure 4-2a) and infrared spectroscopy (Figure 4-2b). All three polymers exhibit a two-stage TGA weight loss where the first stage corresponds to the loss of HBr and the second stage marks the catastrophic decomposition of the polymer. Analogous to our previous work on ethylene vinyl halide polymers[168] and the reported decomposition of poly (vinyl bromide),[180,182] the mass loss in the first stage quantitatively reflects the halogen content of the polymer. The observed values for mass loss in the first stage are found to be in agreement with the calculated HBr content for each of the polymers at 39%, 28%, and 22% for **PE9Br**, **PE15Br**, and **PE21Br** respectively.

The IR spectra also display characteristic information regarding the primary structure of the polymers. The absence of a peak at 967 cm^{-1} for all three polymers indicates complete hydrogenation, based on the disappearance of the out-of plane olefin C-H wag, observed in the unhydrogenated polymers **UPE9Br**, **UPE15Br**, and **UPE21Br** (Figure 4-4). Characteristic peaks corresponding to C-Br stretching are found in the region from 700-450 cm^{-1} and in all cases the peaks at ~613 cm^{-1} and ~538 cm^{-1} can be assigned to secondary bromines in the gauche and trans configuration respectively.[183] From these data it becomes clear that with increasing bromine content, the ratio of gauche C-Br (~613 cm^{-1}) increases relative to trans C-Br (~538 cm^{-1}). Corresponding methylene peaks at 1368 cm^{-1} and 1308 cm^{-1} also indicate the presence of gauche and trans conformations, specifically the symmetric and antisymmetric wagging modes of gauche-trans-gauche triads.[101] Other characteristic methylene peaks are assigned for all polymers at ~1470 cm^{-1} and ~1432 cm^{-1} for methylene bending modes,[184,185] and at ~720 cm^{-1} for methylene rocking.[186] Importantly these spectra suggest, in accord with our previous work on

PE19Br, that these three precise E/VB polymers possess a triclinic rather than an orthorhombic crystal structure based on the absence of doublets at 1463-1472 cm^{-1} and 721-730 cm^{-1}.[168,184]

The proposed triclinic structure is also supported by differential scanning calorimetry (DSC) as well (Figure 4-3). Melting points (T_m) observed on the second cycle of heating and cooling are plotted relative to the bromine content of the polymers (Figure 4-3a). A linear decrease in T_m is evident with increasing bromine content. This linear trend has been observed for a series of precise *methyl* branched PE derivatives synthesized via ADMET[128] (Figure 4-5); and here, the correlation of the trends is accentuated by the *similarity in the size of the bromine atom and the methyl group*. The decrease in T_m can be explained using the same arguments proposed for PE19Br and similar halogenated ADMET polyolefins,[168] specifically, that increased bromine content in the crystal is the direct consequence of polymer composition and the larger incorporation of defects leads to a proportionally decreasing T_m. Bromine side groups were also found to enter the crystals of random EV/B polymers.[103] Figure 4-3b shows the relationship between the enthalpy of fusion (ΔH_f) and the bromine content. Here the ΔH_f (on a weight basis) shows a dramatic decrease as bromine content is increased at low mole fractions, while increases in bromine content at high mole fraction show markedly smaller changes in ΔH_f. The initial large decrease in ΔH_f for **PE21Br** relative to PE reflects a predicted change in the crystal structure from orthorhombic to triclinic as we previously observed with PE19Br.[168]

Owing to the participation of multiple repeating units in the crystalline unit cells of the brominated ADMET polyolefins, most useful will be the comparison of thermodynamic ΔH_f data, per mole of crystalline repeating unit, for the same triclinic crystal structures. Since these values are at the present time unknown, we use the observed heats of melting to infer trends with length of repeating unit. From the observed values, 17989 J/mol (**PE21Br**), 10140 J/mol

(**PE15Br**) and 4248 J/mol (**PE9Br**), ΔH_f scales proportionally to the number of CH_2 groups in the repeating unit. The value of **PE9Br** is nearly one fourth of ΔH_f of **PE21Br** denoting that as the crystals of the same structure incorporate more defects (bromine), the energy required to disorder the all trans packing of the backbone repeating unit is dramatically decreased. Concomitantly, the associated entropy of melting (in J/mol K) decreases from 52.5 J/mol K (**PE21Br**) to 16.4 J/mol K (**PE9Br**) following the expected impact of Br side groups in reducing the configurational entropy of the melt (Table 4-1).

Comparatively, the crystalline properties of this series of precision brominated polyethylenes follow the behavior of trans poly(alkenamers) for which the melting temperatures increase with the number of carbon atoms in the repeating unit for the same crystal structure. The enthalpy and entropy of fusion increase with the size of the repeating unit. However, the value of ΔS per single bond remains effectively constant.[187,188] It appears that this feature may also hold for the precision Br samples as the calculated average ΔS per bond in the series is 2.2 ± 0.3 J/ mol K.

4.3 Conclusion

The results presented here illustrate that metathesis chemistry is an efficient method for the synthesis of precisely defined EV/B polymers. The regular structure of these materials is reflected in the primary structure characterization and thermal analysis indicating strong correlations between properties and bromine content. Further work will serve to definitively establish the crystal and phase structure of these polymers utilizing WAXS and solid-state ^{13}C NMR techniques, and also to begin to define potential applications for such polymers.

4.4 Experimental

Chemicals. Chemicals were purchased from the Aldrich Chemical Company and used as received unless noted. Grubbs' first generation ruthenium catalyst, bis(tricyclohexylphosphine)-benzylidene ruthenium (IV)dichloride, was purchased from Strem Chemical and stored in an Argon filled dry box prior to use. Wilkinson's catalyst $RhCl(PPh_3)_3$ was purchased from Strem. Methylene chloride and *o*-xylene were distilled over CaH_2. The same ADMET PE sample published[145] by our group was used for comparison.

Instrumentation. Solution ^1H NMR (300 MHz) and ^{13}C NMR (75 MHz) spectra were recorded on a Varian Associates Gemini 300, VXR 300 or Mercury 300 spectrometer. All chemical shifts for ^1H and ^{13}C NMR spectra were referenced to residual signals from $CDCl_3$ (^1H = 7.27 ppm and ^{13}C = 77.23 ppm) with an internal reference TMS 0.03% v/v. High-resolution mass spectral (HRMS) data were obtained on a Finnegan 4500 gas chromatograph/mass spectrometer using the electron ionization (EI) mode. Elemental analyses were carried out by Atlantic Microlabs Inc., Norcross, GA. The GPC measurements for samples in THF were taken on a Waters GPCV 2K instrument. Samples were run with HPLC grade THF at 40 ºC on Waters Styrage1HR 5E columns relative to polystyrene standards. IR data was obtained using a Perkin-Elmer Spectrum One FTIR outfitted with a $LiTaO_3$ detector. Measurements were automatically corrected for water and carbon dioxide. Thermogravimetric analysis (TGA) data was obtained with a Perkin-Elmer 7 series thermal analysis system. The TGA samples (2-5 mg) were heated from 50 ºC to 700 ºC at 10 ºC/min. Melting and crystallizations were obtained at 10 °C/min in a differential scanning calorimeter TA Instrument DSC-Q1000 V9.6 Build 290 under nitrogen flow and calibrated with indium.

Synthesis: General procedure for Grignard reaction. 5-bromopent-1-ene (**1**), 8-bromooct-1-ene (**2**), 11-bromoundec-1-ene (**3**) were synthesized using a published procedure.[189] Bromine compounds **1**, **2**, **3** were then used as a reagents for Grignard reaction in the presence of Mg and formaldehyde in THF using the same methodology as reported in the literature[181] to yield precursor alcohol compounds undeca-1,10-dien-6-ol (**4**), heptadeca-1,16-dien-9-ol (**5**), and tricosa-1,22-dien-12-ol (**6**). The alcohol precursors were purified with column chromatography on silica gel eluted by a hexane:ether (5:1) mixture (yields 50-55%).

Undeca-1,10-dien-6-ol (4). ^{1}H NMR (300 MHz $CDCl_3$) δ 5.80 (m, 2H), 4.97 (m, 4H), 3.60 (br, 1H), 2.07 (q, 4H), 1.25-1.62 (br, 8 H).^{13}C NMR (75 MHz, $CDCl_3$) δ 138.88, 114.75, 71.79, 37.06, 33.89, 25.08. HRMS calcd. for $C_{11}H_{20}O$ $(M+H)^+$, 169.1600; found, 169.1607. Anal. Calcd. for $C_{11}H_{20}O$: C, 78.51; H, 11.98; Found: C, 78.58; H, 12.03.

Heptadeca-1,16-dien-9-ol (5). ^{1}H NMR (300 MHz $CDCl_3$) δ 5.81 (m, 2H), 4.97 (m, 4H), 3.58 (br, 1H), 2.06 (q, 4H), 1.22-1.53 (br, 20 H). ^{13}C NMR (75 MHz, $CDCl_3$) δ 139.33, 114.37, 72.18, 37.68, 33.98, 29.76, 29.31, 29.80, 25.82. HRMS calcd. for $C_{17}H_{33}O$ $(M+H)^+$, 253.2531; found, 253.2534. Anal. Calcd. for $C_{17}H_{33}O$: C, 80.88; H, 12.78; Br. Found: C, 80.92; H, 12.83.

Tricosa-1,22-dien-12-ol (6). ^{1}H NMR (300 MHz $CDCl_3$) δ 5.82 (m, 2H), 4.98 (m, 4H), 3.59 (m, 1H), 2.04 (q, 4H), 1.20-1.50 (br, 32H). ^{13}C NMR (75 MHz, $CDCl_3$) δ 139.44, 114.30, 72.22, 37.7, 34.03, 29.92, 29.83, 29.77, 29.70, 29.35, 29.15, 25.87. HRMS calcd. for $C_{23}H_{44}O$ $(M)^+$, 336.3314; found, 336.3306. Anal. Calcd. for $C_{23}H_{44}O$: C, 82.07; H, 13.18. Found: C, 82.15; H, 13.38.

General procedure for bromination reaction. The precursor alcohols **4**, **5**, and **6** were subjected to the same synthetic route which we reported earlier[168] to yield brominated ADMET monomers 6-bromoundeca-1,10-diene (**7**), 9-bromoheptadeca-1,16-diene (**8**), and 12-

bromotricosa-1,22-diene (**9**). The brominated ADMET monomers were purified with column chromatography on silica gel eluted by hexane (yield 85%).

6-bromoundeca-1,10-diene (7). ^{1}H NMR (300 MHz $CDCl_3$) δ 5.80 (m, 2H), 5.00 (m, 4H), 4.05 (p, 1H), 2.05 (m, 4H), 1.82 (m, 4H), 1.77-1.41 (br, 4H). ^{13}C NMR (75 MHz, $CDCl_3$) δ 138.48, 115.14, 58.39, 38.72, 33.28, 26.98. HRMS calcd. for $C_{11}H_{19}Br$ $(M+Br)^-$, 380.9848; found, 380.9856. Anal. Calcd. for $C_{11}H_{19}Br$: C, 57.15; H, 8.28; Br, 34.56. Found: C, 57.24; H, 8.26; Br, 34.72.

9-bromoheptadeca-1,16-diene (8). ^{1}H NMR (300 MHz $CDCl_3$) δ 5.81 (m, 2H), 4.97 (m, 4H), 4.05 (p, 1H), 2.05 (m, 4H), 1.80 (m, 4H), 1.61-1.30 (br, 16H). ^{13}C NMR (75 MHz, $CDCl_3$) δ 139.29, 114.45, 59.11, 39.37, 33.96, 29.17, 29.12, 29.04, 27.74. HRMS calcd. for $C_{17}H_{31}Br$ (M^+), 314.1609; found, 314.1595. Anal. Calcd. for $C_{17}H_{31}Br$: C, 64.75; H, 9.91; Br, 25.34. Found: C, 64.97; H, 9.92; Br, 25.16.

12-bromotricosa-1,22-diene (9). ^{1}H NMR (300 MHz $CDCl_3$) δ 5.81 (m, 2H), 4.97 (m, 4H), 4.05 (p, 1H), 2.05 (m, 4H), 1.81 (m, 4H), 1.61-1.00 (br, 28H). ^{13}C NMR (75 MHz, $CDCl_3$) δ 139.44, 114.33, 59.23, 39.40, 34.03, 29.72, 29.69, 29.67, 29.34, 29.28, 29.16, 27.80. HRMS calcd. for $C_{23}H_{43}Br$ $(M+Br)^-$, 417.1726; found, 417.1728. Anal. Calcd. for $C_{23}H_{43}Br$: C, 69.15; H, 10.85; Br, 20.00. Found: C, 69.16; H, 10.88; Br, 20.01.

General procedure for bulk polymerization. Monomer and Grubbs' first generation catalyst were combined in a ratio of 500:1 under argon atmosphere. The polymerization was conducted at 35-40 ºC under vacuum with stirring for 5 days. The reaction was then stopped and 5 mL of toluene was added to dissolve the polymer with stirring. The reaction was allowed to cool to room temperature. The polymers were then precipitated by dripping the toluene solution into cold acidic methanol. They were then isolated by filtration and dried.

Polymerization of 6-bromoundeca-1,10-diene (UPE9Br). ^{1}H NMR (300 MHz $CDCl_3$) δ 5.80 (b, 0.02H), 5.41 (m, 2H), 5.00 (b, 0.06 H), 4.03 (p, 1H), 2.00 (m, 4H), 1.80 (m, 4H), 1.75-1.4 (b, 4 H). ^{13}C NMR (75 MHz, $CDCl_3$) δ 130.47, 129.96, 58.70, 58.63, 38.91, 38.83, 32.13, 27.83, 27.68, 26.81. M_w (GPC vs. PS) = 18,400 g/mol. PDI = (M_w/M_n) = 1.99.

Polymerization of 9-bromoheptadeca-1,16-diene (UPE15Br). ^{1}H NMR (300 MHz $CDCl_3$) δ 5.81 (b, 0.02H), 5.39 (m, 2H), 4.97 (b, 0.04 H), 4.03 (p, 1H), 1.97 (m, 4H), 1.71 (m, 4H), 1.6-1.1 (b, 16 H). ^{13}C NMR (75 MHz, $CDCl_3$) δ 130.55, 130.07, 64.58, 38.76, 32.77, 29.88, 29.77, 29.38, 29.28, 29.24, 27.39, 26.71. M_w (GPC vs. PS) = 35,300 g/mol. PDI = (M_w/M_n) = 1.75.

Polymerization of 12-bromotricosa-1,22-diene (UPE21Br). ^{1}H NMR (300 MHz $CDCl_3$) δ 5.81 (b, 0.01H), 5.39 (m, 2H), 5.00 (b, 0.02 H), 4.03 (p, 1H), 1.97 (m, 4H), 1.80 (m, 4H), 1.65-1.0 (b, 28 H). ^{13}C NMR (75 MHz, $CDCl_3$) δ 130.58, 130.12, 59.26, 39.63, 32.84, 29.89, 29.78, 29.53, 29.40, 29.32, 27.83, 27.44. M_w (GPC vs. PS) = 75,800 g/mol. PDI = (M_w/M_n) = 2.19.

General Procedure for hydrogenation. The bromine containing polymers (**UPE9Br**), (**UPE15Br**), and (**UPE21Br**) were hydrogenated using a 150 mL Parr high-pressure reaction vessel equipped with a glass liner and Teflon stirbar. Unsaturated polymer (1.0g) and Wilkinson's catalyst (0.02g) were added to the glass liner under a nitrogen blanket. Finally, 20 mL of toluene were added. The vessel was sealed and attached to a grade 5 hydrogen tank and purged with hydrogen several times. The bomb was charged with 550 psi of H_2 and stirred for 5 days at room temperature ºC. The hydrogenated polymer was dissolved in toluene, and precipitated into methanol. The polymer was then filtered and dried under reduced pressure.

PE9Br. ^{1}H NMR (300 MHz $CDCl_3$) δ 4.03 (p, 1H), 1.81 (m, 4H), 1.65-1.2 (bm, 12H), 0.9 (t, 0.12H). ^{13}C NMR (75 MHz,$CDCl_3$) δ 59.23, 39.41, 29.62, 29.25, 27.80, 1.24. Anal. Calcd.: C,

52.70; H, 8.35; Br, 38.95. Found: C, 52.86; H, 8.36; Br, 38.72. M_w (GPC vs. PS) = 23,600 g/mol. PDI = (M_w/M_n) = 1.75.

PE15Br. ^{1}H NMR (300 MHz $CDCl_3$) δ 4.04 (p, 1H), 1.82 (m, 4H), 1.65-1.2 (bm, 24H) 0.9 (t, 0.20H). ^{13}C NMR (75 MHz,$CDCl_3$) δ 59.29, 39.42, 29.89, 29.87, 29.82, 29.74, 29.32, 27.83, 1.24. Anal. Calcd.: C, 62.28; H, 10.10; Br, 27.62. Found: C, 61.61; H, 10.09; Br, 27.26. M_w (GPC vs. PS) = 27,600 g/mol. PDI = (M_w/M_n) = 1.68.

PE21Br. ^{1}H NMR (300 MHz $CDCl_3$) δ 4.04 (p, 1H), 1.81 (m, 4H), 1.7-1.2 (bm, 36H), 0.9 (t, 0.11H). ^{13}C NMR (75 MHz,$CDCl_3$) δ 59.27, 39.42, 29.94, 29.88, 29.82, 29.74, 29.32, 27.82, 1.24. Anal. Calcd.: C, 67.54; H, 11.07; Br, 21.40. Found: C, 67.64; H, 11.06; Br, 21.39. M_w (GPC vs. PS) = 94,100 g/mol. PDI = (M_w/M_n) = 2.23.

Table 4-1. Summary of thermal properties measured via DSC for the family of ethylene/vinyl bromide polymers.

Sample	M_o(g/mol)	ΔH_f(J/g)[b]	ΔH_f(J/mol)[c]	Tm(^oC)	Tm(K)	ΔS_f(J\molK)[d]	ΔS_f\bond[e]
PE9Br	205.14	20.71	4248	-14.81	258.35	16.44	1.83
PE15Br	289.29	35.05	10140	48.84	322.00	31.49	2.10
PE19Br[a]	345.40	43.35	14973	63.89	337.05	44.42	2.34
PE21Br	373.45	48.17	17989	69.63	342.79	52.48	2.50

(a) ref [168] The Tm and ΔH values listed were obtained in a new specimen for baseline consistency within the series. (b), (c), (d), (e). From observed DSC values

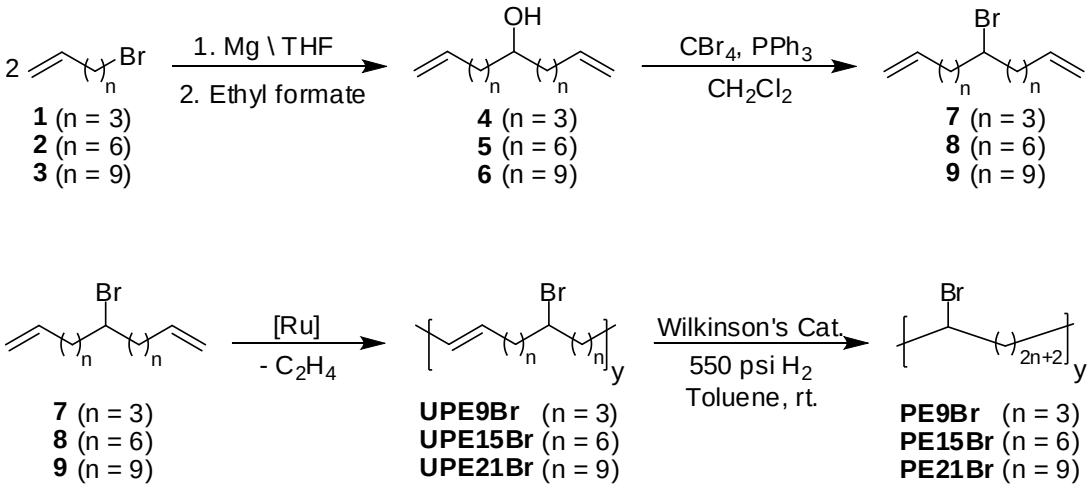

Figure 4-1. Synthesis of precision bromine polymers.

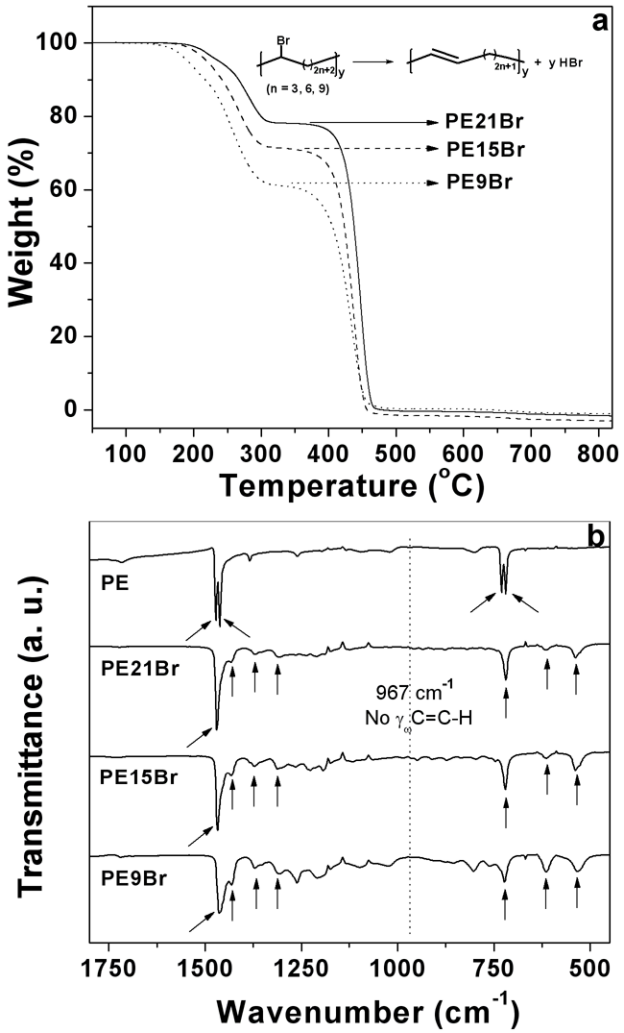

Figure 4-2. Thermogravimetric analysis and infrared spectra of PEXBr. (a) TGA for PE21Br (solid line), PE15Br (dashed line), and PE9Br (dotted line). (b) IR spectra for PE, PE21Br, PE15Br, and PE9Br.

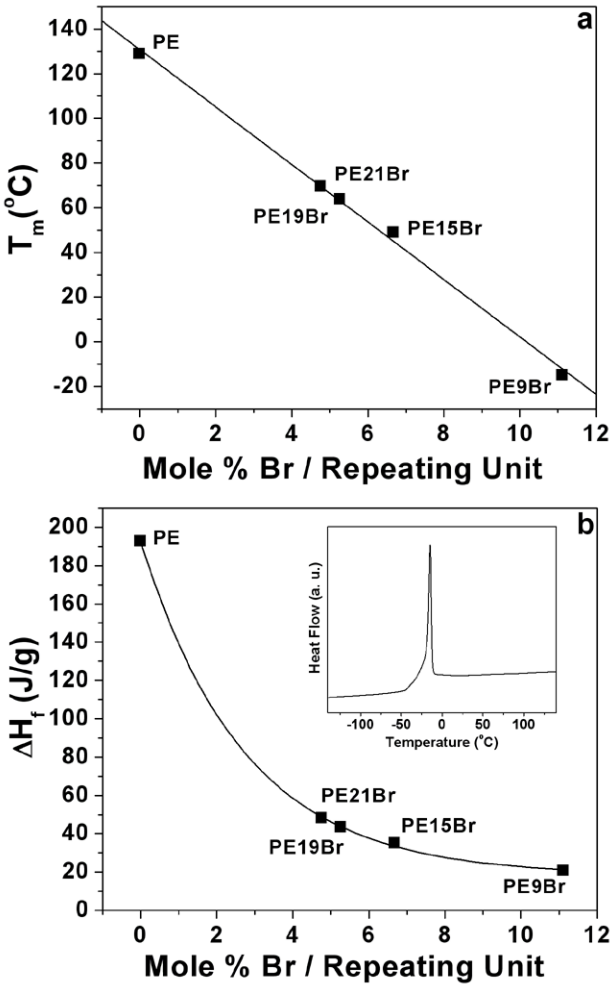

Figure 4-3. Melting and heat of fusion trends for PEXBr polymers. (a) Relationship of the melting point (T_m) with the mole percentage of bromine in the repeating unit for PE, PE21Br (4.8% bromine), PE19Br (5.3% bromine), PE15Br (6.7% bromine) and PE9Br (11.1% bromine). (b) Relationship of ΔH_f with the mole percentage of bromine in the repeating unit for PE, PE21Br (4.8% bromine), PE19Br (5.3% bromine), PE15Br (6.7% bromine) and PE9Br (11.1% bromine). The inset shows the second heating cycle for PE9Br.

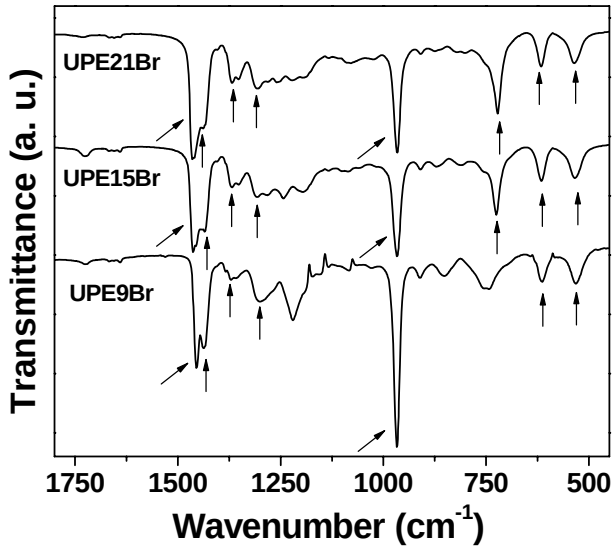

Figure 4-4. IR spectra of UPE9Br, UPE15Br, UPE21Br. Indicated peaks correspond to those in Figure 4-2b, with the exception of the intense peak found at 967 cm^{-1} corresponding to the out of plane olefin C-H wag in the unhydrogenated samples UP21Br, UP15Br, and UP9Br shown here.

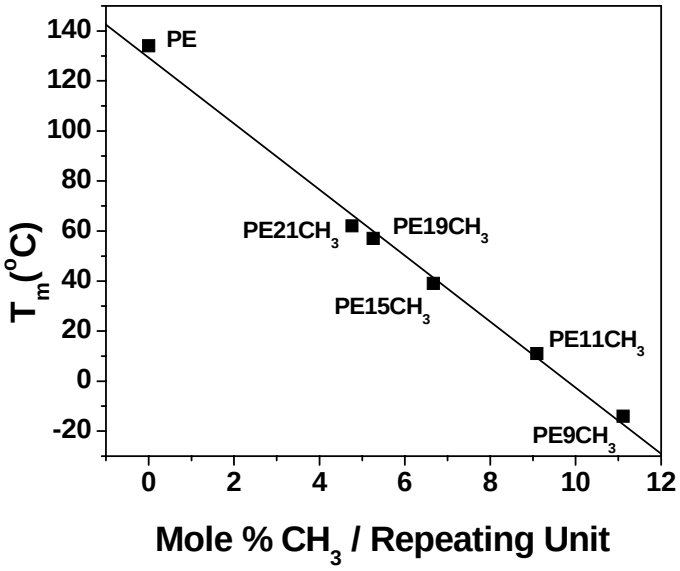

Figure 4-5. T_m vs number of moles of CH_3 in repeating unit for $PE9CH_3$, $PE11CH_3$, $PE15CH_3$, PE19CH3, $PE21CH_3$, and PE.

CHAPTER 5
WELL DEFINED PRECISION ETHYLENE/VINYL FLUORIDE POLYMERS VIA CONDENSATION POLYMERIZATION

5.1 Introduction

Fluoropolymers are industrially important materials that find application in areas where thermal and chemical resistance are critical to performance.[190] As the first and most well-known fluoropolymer, poly(tetrafluoroethylene) (PTFE or Teflon) finds numerous applications in household, industrial, and aerospace settings.[66] While PTFE is a fully fluorinated polyethylene (PE) analogue, numerous partially fluorinated analogues are also known and used commercially in a variety of applications. Among the most well known partially fluorinated polymers are poly(vinylfluoride) (PVF), poly(vinylidene fluoride) (PVDF), poly(ethylene tetrafluoroethylene) (PETFE), and random ethylene vinyl fluoride (EVF) polymers.[11,191] In all such polymers, a variation in properties is achieved via the tuning of the fluorine content as well as the distribution of hydrogens and fluorines in the backbone.[191]

In an attempt to correlate properties with polymer composition in these partially fluorinated polymers, the presence of defects within the polymer backbones must be taken into account. Common defects include head-to-head and tail-to-tail linkages and chain branching.[11] In order to fully correlate fluorine content with physical properties, a family of well-defined and defect free partially fluorinated polymers is required. Herein we present a family of precision EVF polymers with a fluorine atom on each and every 9^{th}, 15^{th}, and 21^{st} carbon, synthesized using acyclic diene metathesis (ADMET) polymerization followed by hydrogenation. In addition to providing the means of studying the properties of EVF polymers, characterization of this family of precision EVF polymers provides a comparison to the previously reported precision ethylene/vinyl chloride[192] (EVC) and precision ethylene vinyl/bromide[169] (EVB) polymers with

matched compositions. Therefore, a comparison based not only on halogen content, but based on halogen size is presented here.

5.2 Results and Discussion

5.2.1 Monomer and Polymer Synthesis

Synthesis of the necessary fluorinated α-ω diene monomers is illustrated in Figure 5-1. The alcohol precursors (4-6) were prepared as described earlier.[169] Conversion of the alcohols to the corresponding fluorine monomers (7-9) was realized by reaction with DAST ((Diethylamino)sulfur trifluoride). Polymerization was carried out in toluene at 45 °C with Grubbs' first generation ruthenium catalyst, followed directly by exhaustive hydrogenation by diimide reduction[144] to give the polymers PE9F, PE15F, and PE21F. The nomenclature acronym used herein is PEXF, which indicates a polyethylene backbone with a fluorine substituent on every X^{th} carbon, where X = 9, 15, 21. Polymer molecular weights are shown in Table 5-1 and vary between 7,600 and 10,400 g/mol.

5.2.2 Primary Structure Characterization

The primary structure of these precise EVF polymers was established using a combination of ^{1}H NMR, ^{13}C NMR, elemental analysis, IR spectroscopy, and TGA (thermogravimetric analysis). The precise structure of the polymers is supported by NMR and the composition is confirmed by elemental analysis. The IR spectra in Figure 5-2 also provide characteristic information regarding the primary structure of the polymers, where the absence of a peak at 967 cm^{-1} for all three EVF polymers indicates complete hydrogenation, based on the disappearance of the out-of plane olefin C-H wagging vibrational mode.[145] Characteristic peaks are found in several regions of the IR spectra. Vibrational modes associated with C-F stretching are observed at 1069 cm^{-1} for all three EVF polymers.[147] The strong peaks at 1091 cm^{-1} and 1019 cm^{-1} in PE9F are due to a combination of C-F and C-C stretching.[193] The accentuation of these additional C-F

related modes in PE9F is caused by the higher fluorine concentration relative to PE15F and PE21F. Doublets corresponding to methylene bending modes at ~1472-1463 cm^{-1} and methylene rocking modes at ~730-720 cm^{-1} are indicative of methylene sequences in PE analogues with an orthorhombic crystal structure.[194, 195] Notice also a shoulder in all of the EVF samples at ~1434, which can be attributed to bending modes for the methylene groups α to the C-F groups.[148]

5.2.3 Thermal and X-Ray Analysis

While NMR and IR support the proposed primary structure, TGA results directly support the precise composition of the polymers. Figure 5-3 displays the thermal decomposition curves of all three EVF polymers. In all cases, a two-stage decomposition is observed, where the first stage corresponds to the loss of HF and the second stage marks the catastrophic decomposition of the polymer. Analogous to our previous work on ethylene vinyl halide polymers, the mass loss in the first stage quantitatively reflects the halogen content of the polymer.[168] The observed values for mass loss in the first stage are found to be in agreement with the calculated HF content for each of the EVF polymers at 14%, 9%, and 6% for PE9F, PE15F, and PE21F respectively. Figure 5-3 also shows that the onset of decomposition for the first stage loss of HF increases with decreasing fluorine content (Table 5-1). Therefore, EVF samples become more stable with increasing content of ethylene units as the labile fluorine content decreases. For comparison, the onset of decomposition for the first stage HF loss in PVF is 455 °C.[196] The significantly higher value, relative to the EVF polymers reported here, can be attributed to the strong dipole-dipole interactions present in PVF, which results in the enhanced stability.

Figure 5-4 shows the second cycle of heating and cooling as measured by DSC for PE9F, PE15F, and PE21F. Several key pieces of information are readily apparent. First, the melting temperatures (T_m) and crystallization temperatures (T_c) of the three polymers are essentially

equivalent (Table 5-1). Importantly, both melting and crystallization are marked by sharp transitions, characteristic of the crystallization of homopolymers of similar molar mass, in which halogens are incorporated into the crystal at a composition equivalent to the overall composition of the polymer. This has been confirmed by XRD and SSNMR previously for the case of PE19F.[168] From the heat of melting and crystallization the degrees of crystallinity were estimated under the assumption that the heat of fusion per mole of pure crystalline unit is, for the three EVF samples, the same as for polyethylene. The values, listed in Table 5-1, decrease from 74 to 53% with increasing fluorine content.

WAXS patterns of precision EVF samples and a linear polyethylene fraction, shown in Figure 5-5, confirm that the orthorhombic packing of the un-substituted chain is maintained in the EVF series. Clearly, the linear polyethylene and molecules with precise substitution of fluorine atoms at distances even as close as nine methylenes, are isomorphous materials. Small shifts of the two main reflections to lower angles indicate some expansion of the unit cell axes due to the substitution of hydrogen for the larger fluorine atom. In addition, the tacticity can not be controlled in the ADMET synthesis, thus, the fluorine substitution imparts a defected nature to the precision molecules, that attests for the depression of the melting temperature from 133°C for the PE chain to 124 ± 1°C, for the EVF series. Nonetheless, the expansion is not as severe as that rendered by larger halogens (Cl, Br), which crystallize in a less symmetric triclinic packing.[168] Values of the unit cell dimensions, densities of the EVF orthorhombic lattices calculated assuming a uniform fluorine distribution and constant *c* axis, and degrees of crystallinity calculated from the WAXD patterns after peak deconvolution, are listed in Table 5-2. The decrease in crystallinity with fluorine parallels the estimated values from heat of fusion and reflects, in reference to polyethylene, the perturbation of the fluorine atom to the

development of crystallinity. The similarity between both crystallinities supports the assumption of minor differences in ΔH^o (energy to melt one mole of crystalline repeated backbone unit) in the EVF series.

The DSC results point to an interesting comparison of EVF with our previous work on precision EVC[192] and ethylene vinyl bromide EVB[169] polymers of analogous halogen content. Figure 5-6a illustrates the variation in polymer melting temperature relative to halogen size and content. It is observed that for a constant mole percentage of halogen per repeating unit, the T_m decreases as the size of the halogen increases. This is in accord with our previously reported comparison of PE19X polymers (where X = F, Cl, and Br)[168] and is attributed to the accommodation of the halogens into the crystal lattice, which serve as defects, lowering the T_m by an amount proportional to the atomic size of the halogen. Notice also in Figure 5-6a, that for a constant halogen substituent, the T_m decreases as halogen content increases for the case of Cl and Br, but not for F. It is clear that accommodation of greater contents of the larger Cl (van der Waals radius = 1.75 Å) and Br (van der Waals radius = 1.85 Å) atoms into the lattice serves as a defect, that changes the crystalline packing of the precision molecules with respect to the un-substituted chain, thus resulting in a concomitant proportional decrease in T_m. However, the compositionally invariant T_m for the fluorine containing polymers attests to the fact that the size of the fluorine atom (van der Waals radius = 1.47 Å) is sufficiently small relative to a hydrogen atom (van der Waals radius = 1.2 Å), such that lattice strains due to the inclusion of fluorine are minimal and the orthorhombic packing is maintained. Figure 5-6b illustrates the variation in ΔH_f relative to halogen size and content for all of the precision EVH polymers. The first observation based on these relationships is that for a constant halogen composition per repeat unit, the ΔH_f decreases with increasing halogen size. This result is indicative of the amount of strain that each

halogen induces upon incorporation into the crystal lattice as it relates to the amount of energy that must be added to the system to effect melting. The other observation is that, for the same halogen atom, as the content of halogen increases, the ΔH_f decreases. This has already been explained for the case of the precision EVC[192] and EVB[169] polymers where the incorporation of more halogen atoms into the crystals results in a decrease in crystallinity and in the amount of energy required to disorder the all trans backbone in the crystal lattice. Similarly, for the EVF polymers the percent crystallinity decreases with increasing fluorine content, as calculated from heat of fusion and WAXD.

5.3 Conclusions

Herein we have described the synthesis of a family of precision EVF polymers, which have a F atom on each and every 9^{th}, 15^{th}, and 21^{st} carbon. The precise primary structures and compositions are supported by NMR, IR, TGA, and elemental analysis. In a manner analogous to compositionally matched precision EVC and EVB polymers, DSC shows sharp melting and crystallization transitions characteristic of homopolymers. As opposed to these precision EVC and EVB polymers with analogous compositions, which show decreasing T_m values with increasing halogen content, the T_m values of the EVF polymers are compositionally invariant due to the small size of the F atom. Thus, while all precision EVH polymers show the characteristics of homopolymers, the size of the halogen has a significant effect on the specific thermal properties of the polymer.

5.4 Experimental

Chemicals. Chemicals were purchased from the Aldrich Chemical Company and used as received unless noted. Grubbs' first generation ruthenium catalyst, bis(tricyclohexylphosphine)-benzylidine ruthenium (IV)dichloride, was purchased from Strem Chemical and stored in an Argon filled dry box prior to use. Methylene chloride and *o*-xylene were distilled over CaH_2.

Instrumentation. Solution ^{1}H NMR (300 MHz) and ^{13}C NMR (75 MHz) spectra were recorded on Mercury 300 spectrometer. All chemical shifts for ^{1}H and ^{13}C NMR were referenced to residual signals from $CDCl_3$ (^{1}H = 7.27 ppm and ^{13}C = 77.23 ppm) and to residual signals from $C_6D_5CD_3$ (^{1}H = 2.09 ppm and ^{13}C = 137.86 ppm) with an internal reference TMS 0.03% v/v to internal TMS standard for 0. In all the NMR work the solvents were chloroform-*d* or toluene-*d*8 the temperature was 25 ºC or 80 ºC.

High-resolution mass spectral (HRMS) data were obtained on a Finnegan 4500 gas chromatograph/mass spectrometer using the electron ionization (EI) mode. Elemental analyses were carried out by Atlantic Microlabs Inc., Norcross, GA. The GPC measurements for samples were taken on a Waters Associates 150C high-temperature gel permeation chromatograph equipped with three Polymer Laboratories mixed bed Type B columns and an internal DRI detector. The mobile phase was BHT-inhibited 1,2,4-trichlorobenzene (135 °C, flow rate 1.0 mL/minute, typical sample concentration 2 mg/mL). IR data was obtained using a Perkin-Elmer Spectrum One FTIR outfitted with a $LiTaO_3$ detector. Measurements were automatically corrected for water and carbon dioxide. Thermogravimetric analysis (TGA) data was obtained with a Perkin-Elmer 7 series thermal analysis system. The TGA samples (2-5 mg) were heated from 50 ºC to 700 ºC at 10 ºC/min under nitrogen. Melting and crystallizations were obtained at 10 °C/min in a differential scanning calorimeter TA Instrument DSC-Q1000 V9.6 Build 290 under nitrogen flow and calibrated with indium.

WAXD diffractograms were collected at room temperature on samples crystallized from the melt at ~ 1 °C/min using a slit collimated Siemens D-500 diffractometer in a 2θ range between 5º and 40º with a step size of 0.02º. The instrument was calibrated for d spacing with a standard polished piece of polycrystalline quartz, and the film thickness was offset using shims.

Synthesis: General procedure for Grignard reaction. Synthesis of 5-bromopent-1-ene (1), 8-bromooct-1-ene (2), 11-bromoundec-1-ene (3) undeca-1,10-dien-6-ol (4), heptadeca-1,16-dien-9-ol (5), and tricosa-1,22-dien-12-ol (6) was describe previously.[169]

General procedure for fluorination reaction. A solution of diethylaminosulfur trifluoride (DAST) (2.0 equiv.) in CH_2Cl_2 was cooled to -78 °C and a solution of the precursor alcohol 4, 5, or 6 (1 equiv.) in CH_2Cl_2 and dry pyridine (2.5 mL) was added dropwise. The mixture was stirred at this temperature for 2 h and then warmed to room temperature and stirred overnight. At this time water was added and the organic phase was extracted with CH_2Cl_2 and then dried with Na_2SO_4 and then the solvent was removed to give the colorless oils 6-fluoundeca-1,10-diene (7) and 9-fluoroheptadeca-1,16-diene (8), and the white solid 12-fluorotricosa-1,22-diene (9) which were purified by chromatography using 97:3 hexanes:ethyl acetate to give (55-60%) of the product.

6-fluoroundeca-1,10-diene (7). ^{1}H NMR (300 MHz $CDCl_3$) δ 5.81 (m, 2H), 5.00 (m, 4H), 4.57-4,41 (dp, 1H), 2.09 (m, 4H), 1.78-1.40 (br, 8H). ^{13}C NMR (75 MHz, $CDCl_3$) δ 138.67, 114.99, 95.51, 93.30, 34.90, 34.63, 33.71, 24.61, 24.55. HRMS calcd. for $C_{11}H_{19}F$ $(M+H)^+$, 170.1478; found, 170.1474. Anal. Calcd. for $C_{11}H_{19}F$: C, 77.59; H, 11.25; F, 11.16. Found: C, 77.62; H, 11.50; F, 11.01.

9-fluoroheptadeca-1,16-diene (8). ^{1}H NMR (300 MHz $CDCl_3$) δ 5.81 (m, 2H), 4.99 (m, 4H), 4.56-4.40 (dp, 1H), 2.06 (m, 4H), 1.69-1.20 (br, 20H). ^{13}C NMR (75 MHz, $CDCl_3$) δ 139.32, 114.42, 95.85, 93.64, 35.51, 35.24, 33.98, 29.58, 29.22, 29.05, 25.34, 25.28. HRMS calcd. for $C_{17}H_{31}F$ (M^+), 254.2404; found, 254.2418. Anal. Calcd. for $C_{17}H_{31}F$: C, 80.25; H, 12.28; F, 7.47. Found: C, 80.15; H, 12.36; F, 7.41.

12-fluorotricosa-1,22-diene (9). ^{1}H NMR (300 MHz $CDCl_3$) δ 5.81 (m, 2H), 4.97 (m, 4H), 4.56-4.40 (dp, 1H), 2.06 (m, 4H), 1.78-1.20 (br, 32H). ^{13}C NMR (75 MHz, $CDCl_3$) δ 139.43, 114.32, 95.89, 93.68, 35.54, 35.27, 34.04, 29.74, 29.69, 29.35, 29.16, 25.39, 25.33. HRMS calcd. for $C_{23}H_{43}F$ (M^+), 338.3343; found, 338.3357. Anal. Calcd. for $C_{23}H_{43}F$: C, 81.59; H, 12.80; F, 5.61. Found: C, 81.59; H, 12.80; F, 5.43.

General procedure for solution polymerization and hydrogenation. Monomer and Grubbs' first generation catalyst (500:1 ratio) were dissolved in toluene under argon and stirred at 45 °C for 5 days. The same amount of catalyst (based on the above ratio) was added into the solution every 24 hours. After 5 days the reaction was then stopped and 50 mL of toluene was added to dissolve the polymer with stirring. The reaction was allowed to cool to room temperature. The polymers were then precipitated by dripping the toluene solution into cold acidic methanol. They were then isolated by filtration and dried.

The unsaturated fluorine containing polymers were then hydrogenated using a modified version of the method described by Hahn[144] by dissolving in dry *o*-xylene under argon and adding 3.3 equivalents of *p*-toluenesulfonyl hydrazide (TSH) and 4 equivalents of tri-*n*-propyl amine (TPA). The solutions were refluxed for 9 hours and then cooled to room temperature. The hydrogenated polymer was precipitated into ice-cold methanol and isolated by filtration. The dried polymer was then redissolved in toluene and re-precipitated by dripping into ice-cold acidic methanol. A white solid was collected by filtration and the polymers were isolated in quantitative yield.

PE9F. ^{1}H NMR (300 MHz toluene-*d*8) δ 4.44-4.28 (dp, 1H), 1.75-1.2 (bm, 16H). ^{13}C NMR (75 MHz, toluene-*d*8) δ 95.41, 93.16, 36.27, 35.98, 30.32, 30.25, 26.01, 25.95. Anal.

Calcd.: C, 75.89; H, 12.10; F, 12.00. Found: C, 66.36; H, 11.05; F, 10.77. M_w (GPC vs. PE) = 8,900 g/mol. PDI = (M_w/M_n) = 2.0.

PE15F. ^{1}H NMR (300 MHz toluene-*d*8) δ 4.44-4.28 (dp, 1H), 1.75-1.2 (bm, 28H). ^{13}C NMR (75 MHz, toluene-*d*8) δ 95.41, 93.17, 36.28, 36.00, 30.48, 30.41, 30.38, 30.00, 26.04, 25.97. Anal. Calcd.: C, 78.88; H, 12.80; F, 8.32. Found: C, 74.14; H, 12.37; F, 7.14. M_w (GPC vs. PE) = 10,400 g/mol. PDI = (M_w/M_n) = 2.2.

PE21F. ^{1}H NMR (300 MHz toluene-*d*8) δ 4.44-4.28 (dp, 1H), 1.75-1.2 (bm, 40H). ^{13}C NMR (75 MHz, toluene-*d*8) δ 95.41, 93.16, 36.28, 36.00, 30.53, 30.41, 30.38, 26.04, 25.97. Anal. Calcd.: C, 80.70; H, 13.22; F, 6.08. Found: C, 79.01; H, 13.17; F, 5.83. M_w (GPC vs. PE) = 7,600 g/mol. PDI = (M_w/M_n) = 1.8.

Table 5-1. Molar mass and thermal data of precision EVF

Sample	M_w x10^3	$M_w \backslash M_n$	T_m(ºC)	T_c(ºC)	ΔH_f(J/g)	$(X_c)^b$	First stage onset of decomposition[c] (ºC)	Second stage onset of decomposition[d](ºC)
PE21F	7.6[a]	1.8	124	113	205	74	294	418
PE15F	10.4[a]	2.2	124	114	174	64	257	410
PE9F	8.9[a]	2.0	123	114	137	53	210	408

a.) GPC vs. PE in DCB b.) % crystallinity (X_c) from heat of fusion in reference to the value of fully crystalline polyethylene, 293 J/g[197] corrected by fluorine content. c.) Recorded at first stage 5% total mass loss under nitrogen gas, 10 °C/min. d.) Recorded at second stage 10% total mass loss under nitrogen gas, 10 °C/min.

Table 5-2. Orthorhombic lattice parameters and crystallinity from WAXD patterns

Sample	$2\theta_{(110)}$	$2\theta_{(200)}$	*a*(Å)	*b*(Å)	*c*(Å)	V(Å)^3	density (g/cm^3)	$Xc_{(x\text{-ray})}$ [(a)]
PE	21.44	23.78	7.484	4.978	2.547	94.894	0.9798	0.88
PE21F	21.38	23.68	7.515	4.989	2.547	95.495	1.0332	0.87
PE15F	21.32	23.62	7.534	5.003	2.547	96.013	1.0514	0.75
PE9F	21.22	23.50	7.572	5.026	2.547	96.929	1.0962	0.62

[(a)] Degree of crystallinity

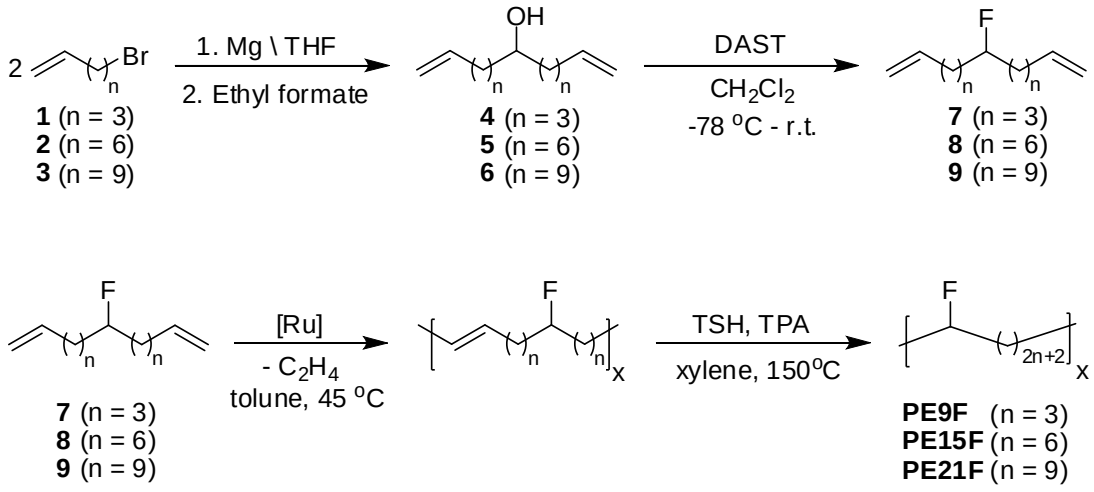

Figure 5-1. Synthesis of precision EVF polymers.

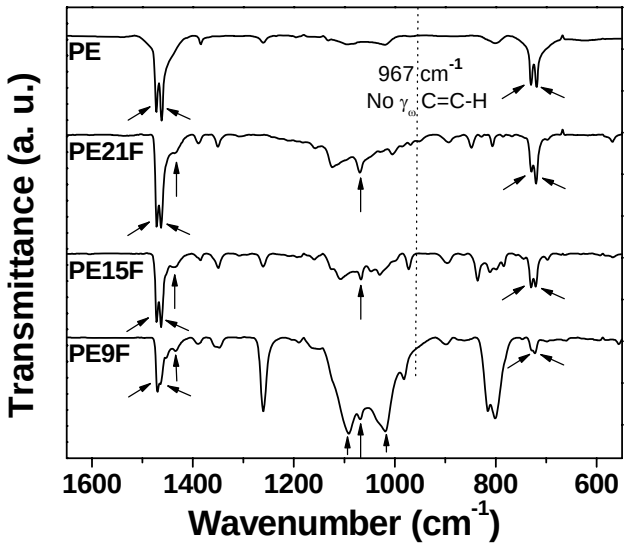

Figure 5-2. Infrared spectra of PE, PE21F, PE15F, PE9F.

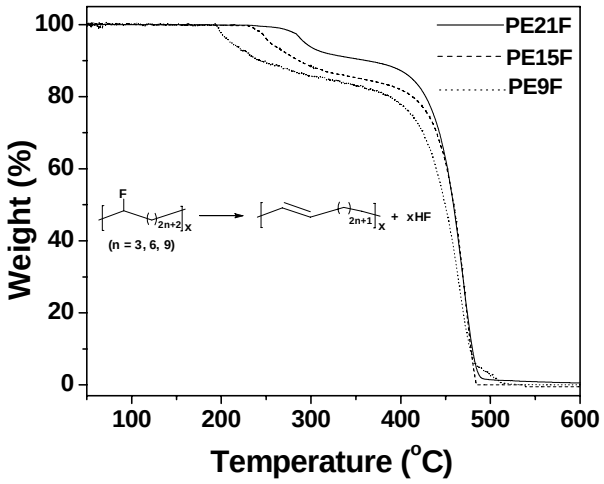

Figure 5-3. Thermogravimetric analysis results for PE21F, PE15F, and PE9F.

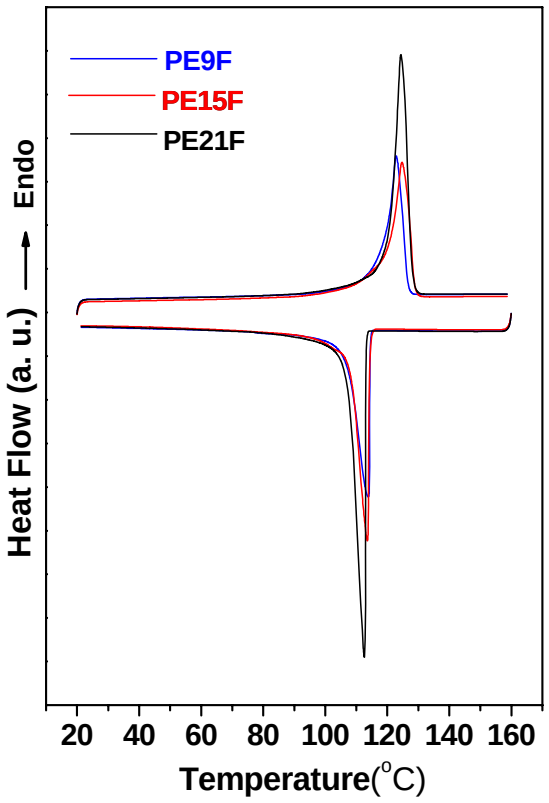

Figure 5-4. Differential scanning calorimetry exotherms and endotherms for PE9Cl, PE15Cl, PE21Cl.

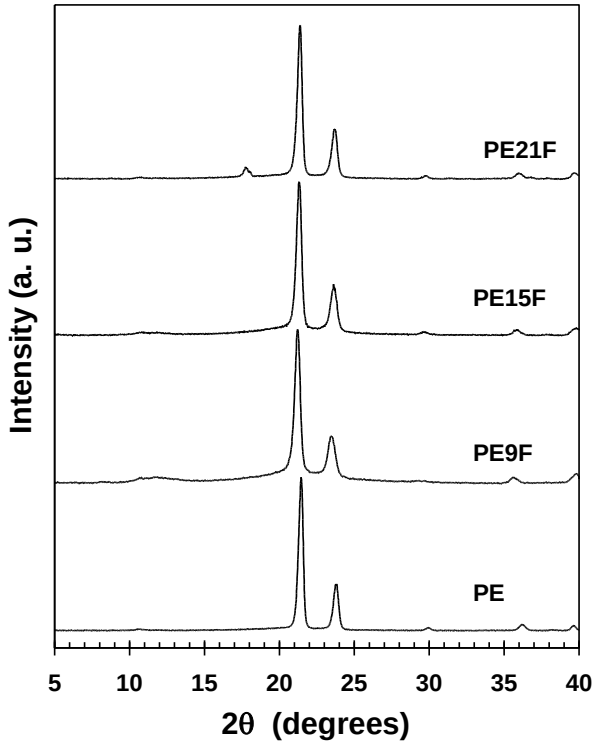

Figure 5-5. Wide angle X-ray diffractograms of a linear polyethylene fraction (M_w = 16,500; M_w/M_n = 1.26) and ADMET precision EVF samples slowly cooled from the melt at ~ 1 °C/min. The peak at 2θ = 17.9° in PE21F belongs to some impurity.

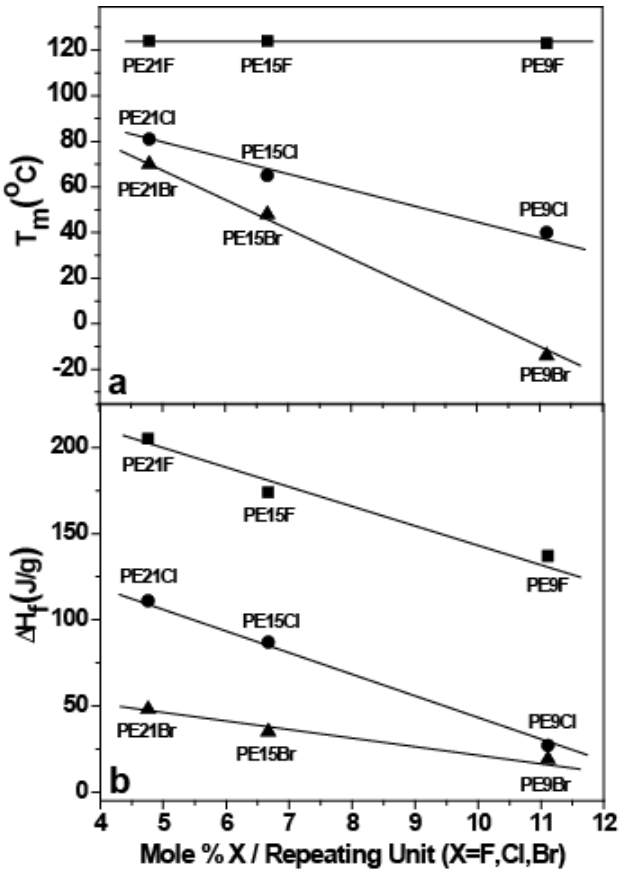

Figure 5-6. Trends for the variation in T_m (a) and ΔH_f (b) vs. mole % halogen per repeating unit.

CHAPTER 6
STATISTICALLY RANDOM, DEFECT FREE ETHYLENE / VINYL HALIDE MODEL COPOLYMERS VIA CONDENSATION POLYMERIZATION

6.1 Introduction

Polyolefins represent the largest class of industrially produced polymers and their importance is manifested in diverse applications ranging from packaging to biomaterials and electronics.[1] Even though polyethylene (PE) itself possesses a broad and dynamic property set, additional application specific variations can be introduced through copolymerization with other vinyl monomers.[118,119] Specifically, copolymerization with polar vinyl monomers can be used to vary the mechanical and physical properties of the polymer.[75, 198] However, direct copolymerization via common free-radical methods often leads to poorly defined polymers with limited compositional ranges based on reactivity differences between ethylene and polar monomers as well as the numerous defects (e.g. branching) introduced through free-radical techniques.[198, 199] Therefore, a variety of other polymerization methods have been employed in an effort to model the properties of such copolymers.[129,145] Olefin metathesis has emerged as an attractive method for modeling ethylene copolymers containing polar groups, based on the functional group tolerance of the employed late-transition metal catalysts and the fidelity of the reaction, which provides perfectly linear polymers, free of structural defects.[76]

Using Acyclic Diene Metathesis (ADMET) we have pursued halogen containing ethylene polymers, and we have capitalized on the ability of ADMET to produce precision polymers in which fluorine, chlorine, and bromine atoms are separated by a constant methylene sequence.[168,169,192,200] In such systems, we have observed unique crystallization and thermal behavior attributed to the homopolymer-like behavior of these precise ethylene / vinyl halide (EVH) polymers. Here we extend these EVH polymers for use as effective models for industrial polymers via copolymerization of halogen-containing $\alpha-\omega$ dienes with 1,9-decadiene to yield

statistically random and defect free EVH polymers. Such polymers are more relevant as model systems for chain-addition EVH polymers produced by free radical techniques based on the ability to attain continuous methylene sequences of significant length and broad distributions of length. Variation in halogen size and content allows us to more accurately derive structure-property relationships in such polymers. The defect-free nature of the polymer backbone allows the use of NMR analysis to prove the random nature of the polymers, while thermal analysis via differential scanning calorimetry (DSC) provides insight into the compositional dependence of the thermal properties in these random polymers relative to their precise analogues.

6.2 Results and Discussion

6.2.1 Polymer Synthesis

The synthesis of the statistically random copolymers is shown in Figure 6-1. Copolymerization was carried out using a halogen-containing monomer (abbreviated [X]) and 1,9-decadiene (abbreviated [H]). Synthesis of the fluorine,[200] chlorine,[192] and bromine[169] containing monomers has been previously reported. Copolymerization was carried out using Grubb's first generation ruthenium catalyst, to yield the unsaturated ADMET polymers **RUPE15X** and **RUPE21X**. Following ADMET polymerization, the fluorine and chlorine containing copolymers were exhaustively hydrogenated via diimide reduction,[144] while Wilkinson's catalyst[169] was used for hydrogenation of the bromine containing polymers to yield the fully saturated copolymers **RPE15X** and **RPE21X**. In the acronyms, R indicates random, U indicates unsaturation, and PE15X and PE21X indicate random polyethylene backbones with halogen contents equivalent to the precise analogues with a halogen on each and every 15th or 21st carbon. Molecular weight data are given for all six of the random copolymers in Table 6-1.

6.2.2 Primary Structure Characterization

The primary structure of these random copolymers RUPE15X, RUPE21X, RPE15X, and RPE21X was established using a combination of ^{1}H NMR, ^{13}C NMR, elemental analysis, IR spectroscopy, and TGA (thermogravimetric analysis). In-depth analysis by ^{1}H and ^{13}C NMR described below, definitively establishes the statistically random nature of the copolymers presented.

The assignment of signals in the ^{1}H and ^{13}C NMR spectra is presented for the Cl random copolymers, **RUPE15Cl** and **RUPE21Cl** as an example. The numbering of the positions is given in Figure 6-2: plain numbers for the 6-chloroundeca-1,10-diene moiety (Cl-moiety) and prime numbers for the 1,9-decadiene moiety (H-moiety). We add a *t* or a *c* after this number to mark the *trans* or *cis* configuration of the closest double bond. If this double bond connects to a 1,9-decadiene moiety *t* becomes *t'* and *c* becomes *c'*.

The proton spectra in Figure 6-3 for **RUPE15Cl** (top) and **RUPE21Cl** (bottom) can be easily assigned based on the chemical shifts of the homopolymers **PE9Cl** and **PE15Cl**.[192] For the case of **RUPE15Cl** (top), seven regions can be integrated separately: 5.50-5.30 (3.25H, *1+1'*), 3.95-3.80 (1H, *5*), 2.10-1.90 (6.60H, *2+2'*), 1.80-1.65 (4.02H, *4*), 1.65-1.55 (2.16H, *3a*), 1.55-1.40 (2.02H, *3b*) and 1.40-1.20 (5.57H, *3'+4'*). The above integrals were used to calculate the H moiety : Cl moiety ratio ([H]:[Cl]) for **RUPE15Cl** to be 0.64:1. The ratios derived from ^{1}H NMR integration are given for all random polymers (X = Cl, F, and Br moieties) in Table 6-2.

The alkene region of the ^{13}C NMR spectra for **RUPE15Cl** and **RUPE21Cl** (Figure 6-4 top and bottom, respectively) shows four major signals and four minor ones. The most intense carbon at 130.24 corresponds to a symmetric *trans* double bond joining two Cl-moieties, in our nomenclature, *1t*. Indeed, in the GHMBC spectrum for **RUPE15Cl** (Figure 6-5) this carbon couples with the proton at 5.39 both over one and over two bonds. The next two most intense

carbons, at 131.06 and 129.51, carry the protons at 5.41 and 5.37 correspondingly, and each of these carbons displays a cross-peak with the protons of the other, meaning that they belong to the asymmetric *trans* double bond joining an H- and a Cl-moiety. Of these two carbons, 129.51 couples with 1.46 and 1.59 (as does 130.24, Figure 6-6) therefore it is the one from the Cl-moiety, *1t*'. The fourth major carbon at 130.32 displays in the GHMBC spectrum cross-peaks over one and two bonds with 5.38, therefore it is from a *trans* double bond joining two H-moieties, *1't'*.

The signals of *1t*, *1't* + *1t'* and *1't'* correspond to the XX, HX and HH diads respectively, therefore the integrals of these signals can be used to determine the degree of randomness (DR) in the copolymers. Due to the signal overlap, three integrals can be measured reliably, corresponding to *1't*, *1t* + *1't'* and *1t'*. Therefore we define DR = 2(XX+HH)/HX/(r + 1/r), where XX+HH is the integral for *1t*+*1't'*, HX is the sum of the integrals for *1't* and *1t'* and r is the ratio of the H and X monomers. For a random copolymer DR = 1, for an alternating polymer DR = 0, for a block copolymer DR = ∞. The values of DR given in Table 6-2 indicate a random distribution for all of these copolymers.

Each of the alkene signals in Figure 6-4 is accompanied by a minor signal, *ca*. 20-30% of the major, about 0.5 ppm upfield. These signals belong to the corresponding *cis* double bond, as demonstrated by their cross-peak with 2.05 (*H2c*) and 2.01 (*H2'c*) (Figure 6-7). *C1't*' and *C1'c'* display a pattern of three lines, while all the other lines for *C1* and *C1'* display a pattern of four lines (visible for **RUPE21Cl**, Figure 6-4). Based on their intensities, the lines can be assigned to the tetrads. For instance, of the four lines of *C1't* the most intense corresponds to the tetrad Cl-H-Cl-Cl, the least intense to H-H-Cl-H, and the two of equal intensities to Cl-H-Cl-H and H-H-Cl-Cl. The intensities of the lines for *C1t* suggest that the center, most intense line corresponds to

Cl-Cl-Cl-Cl + H-Cl-Cl-H, while the outer lines of equal intensities correspond to the two different carbons in the H-Cl-Cl-Cl tetrad.

The *C5* signal at 64.0 displays a pattern of three lines, corresponding to the triads Cl-Cl-Cl, HCl-Cl and H-Cl-H (visible for **RUPE21Cl**, Figure 6-8). *H5* couples with the *C4* carbons at 38.05, 37.96 (Figure 6-9) and the *C3* carbons 26.56, 26.52, 26.43, 26.38 shown in Figure 6-10 (Figure 6-11). Based on the relative intensity and chemical shifts difference, these signals were assigned as 4c+4c', 4t+4t', 3c', 3c, 3t' and 3t, correspondingly. The signals of *C4* were used to determine the *trans* : *cis* ratios given in Table 6-2.

The signals for positions *2* and *2'* were identified by their coupling with the alkene protons (Figure 6-12). Based on their chemical shifts and relative intensities, the signals at 32.61, 32.58, 32.05, 32.03, 27.26, 27.22, 26.69 and 26.65 have been assigned to *2't'*, *2't*, *2t'*, *2t*, *2'c*, *2'c'*, *2c* and *2c'*, correspondingly.

The remaining eight signals, all in the region 29.0 - 29.8 ppm (Figure 6-10), correspond to *3'* and *4'*. The signals at 29.75, 29.70, 29.64 and 29.57 couple with the alkene protons, therefore they correspond to *3'*. Based on their pattern of relative intensities, they have been assigned as *3'c'*, *3'c*, *3't'* and *3't,* correspondingly. The signals for position *4'*, 29.22, 29.19, 29.09 and 29.05, display a different intensities pattern, respectively 1 : 3.3 : 3.3 : 13.1, consistent with their chemical shifts sensing the configuration of the two double bonds in the H-moiety only, and not the nature, H- or Cl-, of the neighboring moieties. The differences in chemical shifts are also consistent with $\Delta\delta_{trans\text{-}cis}$ over 3 and 4 bonds seen in homopolymers **UPE15Cl** and **UPE21Cl**. These signals have been assigned respectively to *4'cc+4'cc'+4'c'c+4'c'c'*, *4'ct+4'ct'+4'c't+4'c't'*, *4'tc+4't'c+4'tc'+4't'c'* and *4'tt+4'tt'+4't't+4't't'*, where the first

letter denotes the configuration of the closest double bond, and the second letter denotes the configuration of the other double bond originating from the same monomer unit.

The analysis of the F and Br random copolymers was done in a similar way. The ^{13}C chemical shifts are given in Table 6-3. In the F copolymer, the carbons in positions *3*, *4* and *5* displayed couplings with fluorine. Values for the coupling constants are also given in Table 6-3.

Table 6-4 presents the differences in ^{13}C chemical shifts for the same position in the three copolymers. These data indicate that the halogen makes no difference in the chemical shifts in positions 2', *3'*, and *4'*. For position *1'*, the difference exists only when across the double bond there is an X monomer unit, *i.e.* for *1't* and *1'c*. The larger the halogen, the more deshielded this position becomes. Differences in positions *2-5* are the same for *t, t', c, c'*, indicating the additivity of the effects of the halogen and all the other effects on ^{13}C chemical shifts. ^{13}C chemical shifts in position *1* reflect whether past the double bonds there is a H or an X unit.

Table 6-5 presents the $\Delta\delta_{trans\text{-}cis}$ values in positions 1,2,1'-4' do not depend on the halogen and are characteristic for an unsubstituted alkyl chain,[192] while values in positions 3 and 4 reflect the presence of the halogen.

Differences *t-t', c-c'*, (Table 6-6) indicate that an X unit past a trans double bond produces a deshielding of 0.65, 0.73 and 0.79 ppm for F, Cl, Br, respectively, for both positions 1 and 1'. The differences for *cis* bonds are 0.03 ppm lower. Smaller differences *t-t', c-c'* can be seen for positions *2,3*, and *2',3'*, and the differences in positions *2* and *2'* are the same, as it is true for the differences in positions *3* and *3'*.

Data in Tables 6-4 – 6-6 indicate that the ^{13}C chemical shifts in polymers of the type (=CH-CH2-CH2-CH2-CHX-CH2-CH2-CH2=)n(=CH-CH2-CH2-CH2-CH2-CH2-CH2=)m can be calculated with a precision of +/- 0.02 ppm by adding the effect of the halogen and the effect

of the configuration of the double bond. The corresponding increments are given in Table 6-7. As an example, the chemical shift for *C3c* in the Cl copolymers is 29.64-3.21-0.07+0.15=26.51 *vs*. 26.52. For *C1't* in the Br copolymers, the chemical shift is 130.34+0.80=131.14 *vs.* 131.12.

The IR spectra in Figure 6-13 also provide characteristic information regarding the primary structure of the polymers. Here the **RPE15X** polymers are shown as representative examples. In each case, characteristic peaks support the presence of the expected halogens. For **RPE15F**, a peak at 1068 cm^{-1} corresponds to C-F stretching vibrations.[147] For **RPE15Cl**, the peaks at 612 and 664 cm^{-1} correspond to C-Cl stretching vibrations.[148] Finally, peaks at 537 and 615 cm^{-1} for **RPE15Br** correspond to C-Br stretching vibrations.[183] Characteristic peaks at ~720 cm^{-1} and ~1470 cm^{-1}, which correspond to vibrational modes of methylene sequences in PE analogues are also observed for each of the samples. For **RPE15F**, the doublets observed at 729-721 cm^{-1} and 1472-1463 cm^{-1} are the same as observed in orthorhombic crystalline PE.[194,195] Singlets observed at 722, 1467 cm^{-1} and 722, 1466 cm^{-1} for **RPE15Cl** and **RPE21Cl**, respectively, indicate a change in crystal packing when compared to **RPE15F**.

6.2.3 Thermal Analysis – TGA

Figure 6-14 shows the TGA data for all six random polymers. It can be observed that all six polymers undergo two-step degradation processes, marked by the initial loss of HX (X = F, Cl, Br) and followed by catastrophic decomposition.[168] The first stage loss of HX is a good measure of primary structure composition. In all cases the mass loss corresponding to HX conforms closely to the theoretically calculated value based on the monomer feed ratios in each polymer. For **RPE21Br** and **RPE15Br**, the first stage mass loss gave approximately 22 and 28% mass loss, respectively, in agreement with the calculated HBr loss. For **RPE21Cl** and **RPE15Cl**, the first stage mass loss gave approximately 11 and 15% mass loss, respectively, in accord with

the calculated HCl loss. For **RPE21F** and **RPE15F**, the first stage mass loss gave approximately 6 and 9% mass loss, respectively, in accord with the calculated HF loss.

6.2.4 DSC

The thermal properties of these random copolymers have been further investigated by DSC. Here the most interesting results are observed when compared to their precise analogues as illustrated in Figure 6-15. A tabular summary of the data is also given in Table 6-1. Figure 6-15a shows the melting transitions for **RPE21Cl**, **PE21Cl**, **RPE15Cl**, and **PE15Cl**. Several observations can be made in the comparison of the melting behavior of the direct analogues. First, it can be seen, as previously reported,[192] that **PE21Cl** has a T_m 18 °C higher than **PE15Cl**, due to lower incorporation of Cl into the crystalline lattice of the **PE21Cl**. Accordingly, these precise polymers behave as homopolymers and display sharp melting transitions. Notice with the random copolymers, that much broader melt transitions are observed. When comparing direct analogues (either **RPE21Cl** and **PE21Cl** or **RPE15Cl** and **PE15Cl**) it can be seen that the random copolymer displays a higher T_m than the precise polymer, despite the same overall composition. This feature was also observed for methyl branched precise vs. random analogues[145] and provides additional evidence in support of very different crystallization mechanisms for these two types of polymers. Polymers with precisely placed halogens crystallize as homopolymers, as evidenced in our earlier work.[168] However, despite the feasibility of halogen participation in the crystal lattice, the crystallization of random copolymers is led by an early selection of sequences with the least constraints to form ordered arrays. Primarily methylene sequences are selected first, followed by sequences with higher halogen contents. This sequence selection leads to a broader melt, due to the variable composition of the crystalline phase with crystallites defined by a range of Cl contents. This broad melt is a reflection of the changing composition of the melt phase, which is originally rich in Cl, but

becomes progressively closer to the composition of the overall copolymer. The peak melting temperature of the random copolymers is higher than that of the precise polymers due to the presence of lower defect content crystallites generated via sequence selection. The final melting transition comparison to make is between **RPE15Cl** and **RPE21Cl**, where a T_m 17 °C higher is observed for the latter. This is expected due to the higher concentration of Cl in **RPE15Cl** leading to more defected crystals and a melt richer in Cl.

A more dramatic example of the differences in crystallization between precise and random analogues is given by the melting traces after isothermal crystallization shown in Figure 6-16 for increasing crystallization times. Single sharp melting peaks along the kinetic process of PE21Cl crystallized at 73 °C are characteristic of homopolymers. The double melting of isothermally crystallized **RPE21Cl** is a general feature of random ethylene copolymers with comonomers that are totally or partially excluded from the crystalline regions.[201,202] It is explained as a result of partitioning of crystallizable sequences.[201] Long crystalline sequences, primarily methylene-based, are selected first and form the early crystalline structure that further melts at the highest temperatures in Figure 6-16b. The remaining crystallizable sequences form a second population of crystallites with slower kinetics, richer in Cl and morphologically different from the first. The lower melting endotherms of Figure 6-16b are associated with this second population of crystallites. They are formed to a large extent from sequences pinned to the initially formed crystallites. Note that while the area under the high melting peak is basically constant with time, the lower melting endotherm increases continuously, reflecting large differences in kinetics. At the isothermal crystallization temperature of 76 °C, the initial selection of primarily long methylene sequences is very fast. However, pinning of the remaining sequences to the first population of crystallites imposes constraints in the melt topology for gathering additional

sequences richer in Cl with a concomitant decrease in kinetics as reflected in the melting behaviour.

The Br containing polymers behave similarly (Figure 6-15b). It is observed that while the precise polymers show sharp, well-defined melt transitions, the random analogues show broad double-melting transitions. As discussed for Cl copolymers, this is evidence of a different mechanism for crystallization between the precise polymers and the random copolymers. The lack of a well-defined T_m in **RPE21Br** and **RPE15Br** is evidence that the homopolymer-like crystallization of their precise analogues is no longer operative as is expected to be replaced by a mechanism based on selection of long most crystallizable sequences as described above for the Cl polymers.

In the case of the fluorine containing polymers, large differences in melting behavior are not expected, based on the small size of the fluorine atom, which does not introduce a large strain on incorporation into the crystal lattice.[200] In Figure 6-15c, results are shown for **RPE21F**, **PE21F**, **RPE15F**, and **PE15F**. Several observations can be made in this case. First, it is clear that all fluorine containing random copolymers and precise polymers display sharp, well-defined melt transitions. Secondly, the peak melting temperatures of all four polymers are very close (in the range of 120-127 °C). Looking more closely, for a comparison of **RPE21F** and **PE21F**, it is observed that the random copolymer melts 3 °C higher than its precise analogue (127 °C vs. 124 °C). It is expected that the random polymer will display a higher T_m than its precise analogue, which has been shown to display homopolymer-like crystallization due to a mechanism of selection of long crystallizable sequences, which is expected to operate in such random polymers. The two T_m values are suspected to be so close based on the small size of the F atom and its ability to enter into the crystalline lattice with a minimum of disruption. Note that despite

the low strain exerted to the lattice by the F atom, the T_m of RPE15F is 7 °C lower than the value of RPE21F in agreement to the sequence selection-based crystallization behaviour of a random copolymer. The early formed crystallites of RPE15F are in equilibrium with a melt with a composition in F richer than comparable crystallites from RPE21F. Thus, RPE15F crystals melt at lower T_m.

6.3 Conclusion and Outlook

Here we have shown that ADMET copolymerization of a halogen containing α-ω diene and 1,9-decadiene is a useful method for the synthesis of industrially relevant model PE copolymers. As evidenced by NMR studies on the unsaturated precursor polymers, a statistically random distribution of comonomers is achieved in a defect-free perfectly un-branched polymer backbone. Thermal analysis via DSC confirms the distinct difference between precise and random EVH polymers produced via ADMET. In the case of precise polymers, sharp and well-defined melt transitions show a homopolymer-like crystallization in which all halogens are equally partitioned between crystalline and non-crystalline regions, while the random copolymers show broad melting transitions that conform to a mechanism of crystallization based on the selection of long crystallizable sequences. Future work will focus on elucidating the crystal structures of the random polymers via x-ray diffraction and developing a quantitative measure of the distribution of halogens between the crystalline and amorphous phases via solid state NMR.

6.4 Experimental

Chemicals. Chemicals were purchased from the Aldrich Chemical company and used as received unless noted. Grubbs' first generation ruthenium catalyst, bis(tricyclohexylphosphine)-benzylidene ruthenium (IV)dichloride, was purchased from Strem Chemical and stored in an

Argon filled dry box prior to use. Wilkinson's catalyst $RhCl(PPh_3)_3$ was purchased from Strem. Methylene chloride and *o*-xylene were distilled over CaH_2.

Instrumentation. Unsaturated samples' NMR spectra were acquired on a Varian Inova Spectrometer, operating at 500 MHz for H1 and 125 MHz for C13, equipped with a 5 mm indirect detection probe, and with *z*-axis gradients. The temperature was 25 ºC and the solvent chloroform-*d*. H1 and C13 chemical shifts were carefully referenced to internal TMS. H1 spectra were collected in one transient, with a relaxation delay of 10 s and an acquisition time of 5 s. Baseline correction was applied prior to integration. C13 spectra were collected in 60,000 transients, with zero relaxation delay and an acquisition time of 3 seconds, which produced a digital resolution of approximately 1 ppb/point. GHMBC spectra were collected with 4096 points over a spectral window of 2600 Hz in *f2*, and 4096 increments over a spectral window of 15000 Hz in *f1*, with 16 transients per increment. The relaxation delay was 1 s. The experiment was optimized for a long range H1-C13 coupling of 8 Hz. Saturated polymer samples' solution ^1H NMR (300 MHz) and ^{13}C NMR (75 MHz) spectra were recorded on Mercury 300 spectrometer. All chemical shifts for ^1H and ^{13}C NMR were referenced to residual signals from $CDCl_3$ (^1H = 7.27 ppm and ^{13}C = 77.23 ppm) and to residual signals from $C_6D_5CD_3$ (^1H = 2.09 ppm and ^{13}C = 137.86 ppm) with an internal reference TMS 0.03% v/v to internal TMS standard for 0. In all the NMR work the solvents were chloroform-*d* or toluene-*d*8 the temperatures were 25 ºC or 80 ºC.

Elemental analyses were carried out by Atlantic Microlabs Inc., Norcross, GA.

The GPC measurements for samples in THF were taken on a Waters GPCV 2K instrument. Samples were run with HPLC grade THF at 40 ºC on Water Styragel HR 5E columns relative to polystyrene standards. Polymer molecular weights reported versus polyethylene standards were

measured using a Waters Associates 150C high temperature gel permeation chromatograph equipped with three Polymer Laboratories mixed bed Type B columns and an internal DRI detector. The mobile phase was BHT-inhibited 1,2,4-trichlorobenzene (135 °C, flow rate 1.0 mL / minute, typical sample concentration 2 mg / mL).

IR data was obtained using a Perkin-Elmer Spectrum One FTIR outfitted with a $LiTaO_3$ detector. Measurements were automatically corrected for water and carbon dioxide. Thermogravimetric analysis (TGA) data was obtained with a Perkin-Elmer 7 series thermal analysis system. The TGA samples (2-5 mg) were heated from 50 ºC to 800 ºC at 10 ºC/min.

Melting and crystallizations were obtained at 10 °C/min in a differential scanning calorimeter TA Instrument DSC-Q1000 V9.6 Build 290 under nitrogen flow and calibrated with indium.

General procedure for bulk polymerization. Monomers and Grubbs' first generation catalyst were combined in a ratio of 500:1 under argon atmosphere for chlorine and bromine containing polymers. The polymerization was conducted at 35-40 °C under vacuum with stirring for 5 days. The reaction was then stopped and 50 mL of toluene was added to dissolve the polymer with stirring. The reaction was allowed to cool to room temperature. The polymers were then precipitated by dripping the toluene solution into cold acidic methanol. They were then isolated by filtration and dried.

General procedure for solution polymerization. Monomers and Grubbs' first generation catalyst (500:1 ratio) were dissolved in toluene for fluorine containing polymers under argon and stirred at 45 °C for 5 days. The same amount of catalyst was added into the solution every 24 hours. The same procedure as described above was used to isolate the polymer.

RUPE15F. Synthesized by the solution method as above using 0.624 g ($3.66x10^{-3}$ mol) 6-fluoroundeca-1,10-diene,[200] 0.376 g ($2.72x10^{-3}$ mol) 1,9 decadiene, and $1.05x10^{-2}$ g ($1.28x10^{-5}$ mol) of Grubbs' first generation catalyst. Analytical yield. For ^{1}H NMR and ^{13}C NMR data see Table 6-2.

RUPE21F. Synthesized by the solution method as above using 0.454 g ($2.67x10^{-3}$ mol) 6-fluoroundeca-1,10-diene,[200] 0.546 g ($3.95x10^{-3}$ mol) 1,9 decadiene, and $1.09x10^{-2}$ g ($1.32x10^{-5}$ mol) of Grubbs' first generation catalyst. Analytical yield. For ^{1}H NMR and ^{13}C NMR data see Table 6-2.

RUPE15Cl. Synthesized by the bulk method as above using 0.964 g ($5.16x10^{-3}$ mol) 6-chloroundeca-1,10-diene,[192] 0.536 g ($3.87x10^{-3}$ mol) 1,9 decadiene, and $1.48x10^{-2}$ g ($1.81x10^{-5}$ mol) of Grubbs' first generation catalyst. Analytical yield. For ^{1}H NMR and ^{13}C NMR data see Table 6-2.

RUPE21Cl. Synthesized by the bulk method as above using 0.711 g ($3.81x10^{-3}$ mol) 6-chloroundeca-1,10-diene,[192] 0.789 g ($5.71x10^{-3}$ mol) 1,9 decadiene, and $1.56x10^{-2}$ g ($1.90x10^{-5}$ mol) of Grubbs' first generation catalyst. Analytical yield. For ^{1}H NMR and ^{13}C NMR data see Table 6-2.

RUPE15Br. Synthesized by the bulk method as above using 1.035 g ($4.48x10^{-3}$ mol) 6-bromoundeca-1,10-diene,[169] 0.465 g ($3.36x10^{-3}$ mol) 1,9 decadiene, and $1.29x10^{-2}$ g ($1.57x10^{-5}$ mol) of Grubbs' first generation catalyst. Analytical yield. For ^{1}H NMR and ^{13}C NMR data see Table 6-2.

RUPE21Br. Synthesized by the bulk method as above using 0.791 g ($3.42x10^{-3}$ mol) 6-bromoundeca-1,10-diene,[169] 0.709 g ($5.13x10^{-3}$ mol) 1,9 decadiene, and $1.40x10^{-2}$ g ($1.71x10^{-5}$

mol) of Grubbs' first generation catalyst. Analytical yield. For ^{1}H NMR and ^{13}C NMR data see Table 6-2.

General Procedure for hydrogenation. The polymers containing F or Cl halogens were then hydrogenated using a modified version of the method described by Hahn[144] by dissolving in dry *o*-xylene under argon and adding 3.3 equivalents of *p*-toluenesulfonyl hydrazide (TSH) and 4 equivalents of tri-*n*-propyl amine (TPA). The solutions were refluxed for 9 hours and then cooled to room temperature. The hydrogenated polymer was precipitated into ice-cold methanol and isolated by filtration. The dried polymer was then redissolved in toluene and re-precipitated by dipping into ice-cold acidic methanol. A white solid was collected by filtration and the polymers were isolated in quantitative yield.

The polymers containing Br halogen were hydrogenated using a 150 mL Parr high-pressure reaction vessel equipped with a glass liner and Teflon stirbar. Unsaturated polymer (1.0g) and Wilkinson's catalyst (0.02g) were added to the glass liner under nitrogen blanket.[169] Finally, 20 mL of toluene were added. The vessel was sealed and attached to a grade 5 hydrogen tank and purged with hydrogen several times. The bomb was charged with 500 psi of H_2 and stirred for 5 days at room temperature. The hydrogenated polymer was dissolved in toluene, and precipitated into methanol. The polymer was then filtered and dried under reduced pressure.

RPE15F. Hydrogenation was performed as above. ^{1}H NMR (300 MHz toluene-*d*8) δ 4.53-4.37 (dp, 1H), 1.8-1.23 (bm, 28H). ^{13}C NMR (75 MHz, toluene-*d*8) δ 95.40, 93.16, 36.27, 35.99, 30.53, 30.41, 30.38, 30.32, 30.26, 26.01, 25.95. Anal. Calcd.: C, 78.88; H, 12.80; F, 8.32. Found: C, 71.38; H, 12.16; F, 6.97. M_w (GPC vs. PE) = 7,900 g/mol. PDI = (M_w/M_n) = 2.5.

RPE21F. Hydrogenation was performed as above. ^{1}H NMR (300 MHz toluene-*d*8) δ 4.45-4.28 (dp, 1H), 1.8-1.23 (bm, 40H). ^{13}C NMR (75 MHz, toluene-*d*8) δ 95.41, 93.16, 36.28, 36.00,

30.53, 30.38, 25.97. Anal. Calcd.: C, 80.70; H, 13.22; F, 6.08. Found: C, 72.63; H, 12.51; F, 5.35. M_w (GPC vs. PE) = 21,600 g/mol. PDI = (M_w/M_n) = 1.6.

RPE15Cl. Hydrogenation was performed as above. ^{1}H NMR (300 MHz, $CDCl_3$) δ 3.89 (p, 1H), 1.69 (m, 4H), 1.60-1.20 (b, 24H). ^{13}C NMR (75 MHz, $CDCl_3$) δ 64.61, 38.76, 29.94, 29.82, 29.76, 29.65, 29.43, 29.38, 26.72. Anal. Calcd.: C, 73.58; H, 11.94; Cl, 14.48. Found: C, 69.75; H, 11.74; Cl, 13.52. M_w (GPC vs. PS) = 73,600 g/mol. PDI = (M_w/M_n) = 2.1.

RPE21Cl. Hydrogenation was performed as above. ^{1}H NMR (300 MHz, $CDCl_3$) δ 3.90 (p, 1H), 1.70 (m, 4H), 1.60-1.17 (b, 36H). ^{13}C NMR (75 MHz, $CDCl_3$) δ 64.61, 38.76, 29.95, 29.83, 29.77, 29.65, 29.44, 29.39, 26.75. Anal. Calcd.: C, 76.66; H, 12.56; Cl, 10.78. Found: C, 75.04; H, 12.55; Cl, 10.84. M_w (GPC vs. PS) = 118,500 g/mol. PDI = (M_w/M_n) = 2.2.

RPE15Br. Hydrogenation was performed as above. ^{1}H NMR (300 MHz $CDCl_3$) δ 4.03 (p, 1H), 1.81 (m, 4H), 1.70-1.00 (bm, 24H). ^{13}C NMR (75 MHz,$CDCl_3$) δ 59.24, 39.40, 29.93, 29.82, 29.73, 29.61, 29.31, 29.25, 27.79. Anal. Calcd.: C, 62.28; H, 10.10; Br, 27.62. Found: C, 60.34; H, 9.85; Br, 29.71. M_w (GPC vs. PS) = 72,100 g/mol. PDI = (M_w/M_n) = 1.8.

RPE21Br. Hydrogenation was performed as above. ^{1}H NMR (300 MHz $CDCl_3$) δ 4.03 (p, 1H), 1.81 (m, 4H), 1.65-1.15 (bm, 36H). ^{13}C NMR (75 MHz,$CDCl_3$) δ 59.23, 39.41, 29.94, 29.82, 29.74, 29.62, 29.31, 29.25, 27.82. Anal. Calcd.: C, 67.54; H, 11.07; Br, 21.40. Found: C, 65.68; H, 10.92; Br, 23.65. M_w (GPC vs. PS) = 55,500 g/mol. PDI = (M_w/M_n) = 1.7.

Table 6-1. Polymer properties of precise and random ADMET samples.

Sample	M_w x10^3	$M_w \backslash M_n$	T_m(ºC)	T_c(ºC)	ΔH_f(J/g)	ΔH_c(J/g)
RPE21F	21.6	1.6	127	119	157	170
RPE15F	7.9	2.5	120	107	151	163
RPE21Cl	118.5	2.2	88	73	78	86
RPE15Cl	73.6	2.1	71	56	68	76
RPE21Br	55.5	1.7	-	-	56	71
RPE15Br	72.1	1.8	-	-	36	45

Table 6-2. Monomer ratio, degree of randomness (DR) and *trans*:*cis* ratio in copolymers.

copolymer	F	Cl	Br
Ratio H:X in RUPE15X	0.70	0.64	0.43
Ratio H:X in RUPE21X	1.40	1.28	1.04
(X+HH)/HX in RUPE15X	1.01	1.19	1.08
(X+HH)/HX in RUPE21X	1.08	0.99	1.06
DR in RUPE15X	0.95	1.08	0.78
DR in RUPE21X	1.02	0.96	1.06
Ratio trans:cis in RUPE15X	3.34	3.68	3.72
Ratio trans:cis in RUPE21X	3.29	3.46	2.82

Table 6-3. C13 chemical shifts in random copolymers.

	1	2	3	4	5	1'	2'	3'	4'
F ($^1J_{C-F}$)			*4.0*	*20.9*	*167.6*				
t	130.30	32.34	25.05	34.63	94.29	131.00	32.59	29.59	29.05
t'	129.65	32.36	25.08	34.63	94.29	130.34	32.61	29.64	29.05
c	129.78	26.99	25.20	34.74	94.29	130.49	27.25	29.71	29.19
c'	129.17	26.96	25.23	34.74	94.29	129.88	27.22	29.75	29.19
Cl									
t	130.24	32.03	26.38	37.96	63.92	131.06	32.58	29.57	29.05
t'	129.51	32.05	26.43	37.96	63.92	130.32	32.61	29.64	29.05
c	129.72	26.69	26.52	38.05	63.92	130.56	27.26	29.70	29.19
c'	129.02	26.65	26.56	38.05	63.92	129.86	27.22	29.75	29.19
Br									
t	130.25	31.90	27.44	38.60	58.42	131.12	32.57	29.56	29.04
t'	129.46	31.92	27.50	38.60	58.42	130.32	32.60	29.63	29.04
c	129.72	26.57	27.60	38.68	58.42	130.61	27.26	29.69	29.18
c'	128.96	26.53	27.63	38.68	58.42	129.86	27.22	29.74	29.18

Table 6-4. Differences in C13 chemical shifts between the Cl, Br, and F copolymers.

	1	2	3	4	5	1'	2'	3'	4'
Cl									
t	-0.06	-0.31	1.33	3.33	-30.37	0.06	-0.01	-0.02	0.00
t'	-0.14	-0.31	1.35	3.33	-30.37	-0.02	0.00	0.00	0.00
c	-0.06	-0.30	1.32	3.31	-30.37	0.07	0.01	-0.01	0.00
c'	-0.15	-0.31	1.33	3.31	-30.37	-0.02	0.00	0.00	0.00
Br									
t	-0.05	-0.44	2.39	3.97	-35.87	0.12	-0.02	-0.03	-0.01
t'	-0.19	-0.44	2.42	3.97	-35.87	-0.02	-0.01	-0.01	-0.01
c	-0.06	-0.42	2.40	3.94	-35.87	0.12	0.01	-0.02	-0.01
c'	-0.21	-0.43	2.40	3.94	-35.87	-0.02	0.00	-0.01	-0.01

Table 6-5. Differences in C13 chemical shifts between the *trans* and *cis* configuration of the double bond in copolymers.

	1	2	3	4	5	1'	2'	3'	4'
F									
t-c	0.52	5.35	-0.15	-0.11	0.00	0.51	5.34	-0.12	-0.14
t'-c'	0.48	5.40	-0.15	-0.11	0.00	0.46	5.39	-0.11	-0.14
Cl									
t-c	0.52	5.34	-0.14	-0.09	0.00	0.50	5.32	-0.13	-0.14
t'-c'	0.49	5.40	-0.13	-0.09	0.00	0.46	5.39	-0.11	-0.14
Br									
t-c	0.53	5.33	-0.16	-0.08	0.00	0.51	5.31	-0.13	-0.14
t'-c'	0.50	5.39	-0.13	-0.08	0.00	0.46	5.38	-0.11	-0.14

Table 6-6. Differences in C13 chemical shifts *t-t'* and *c-c'* in copolymers.

	1	2	3	4	5	1'	2'	3'	4'
F									
t-t'	0.65	-0.02	-0.03	0.00	0.00	0.66	-0.02	-0.05	0.00
c-c'	0.61	0.03	-0.03	0.00	0.00	0.61	0.03	-0.04	0.00
Cl									
t-t'	0.73	-0.02	-0.05	0.00	0.00	0.74	-0.03	-0.07	0.00
c-c'	0.70	0.04	-0.04	0.00	0.00	0.70	0.04	-0.05	0.00
Br									
t-t'	0.79	-0.02	-0.06	0.00	0.00	0.80	-0.03	-0.07	0.00
c-c'	0.76	0.04	-0.03	0.00	0.00	0.75	0.04	-0.05	0.00

Table 6-7. Increments for the calculus of the C13 chemical shifts in copolymers.

	1	2	3	4	5	1'	2'	3'	4'
base	130.34	32.61	29.64	29.05	29.49	130.34	32.61	29.64	29.05
increment F	-0.69	-0.25	-4.56	5.58	64.80	0.66	-0.02	-0.05	0.00
increment Cl	-0.83	-0.56	-3.21	8.91	34.43	0.74	-0.03	-0.07	0.00
increment Br	-0.88	-0.69	-2.14	9.55	28.93	0.80	-0.03	-0.07	0.00
increment *cis*	-0.52	-5.34	0.15	0.09	0.00	-0.51	-5.32	0.13	0.14

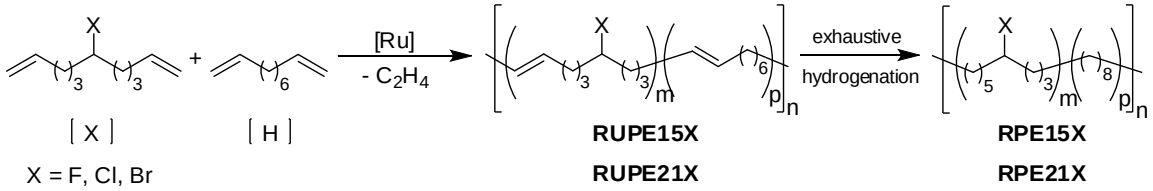

Figure 6-1. Synthesis of random copolymers via ADMET.

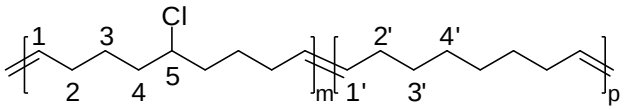

Figure 6-2. Repeat unit structure for RPEXCl polymers.

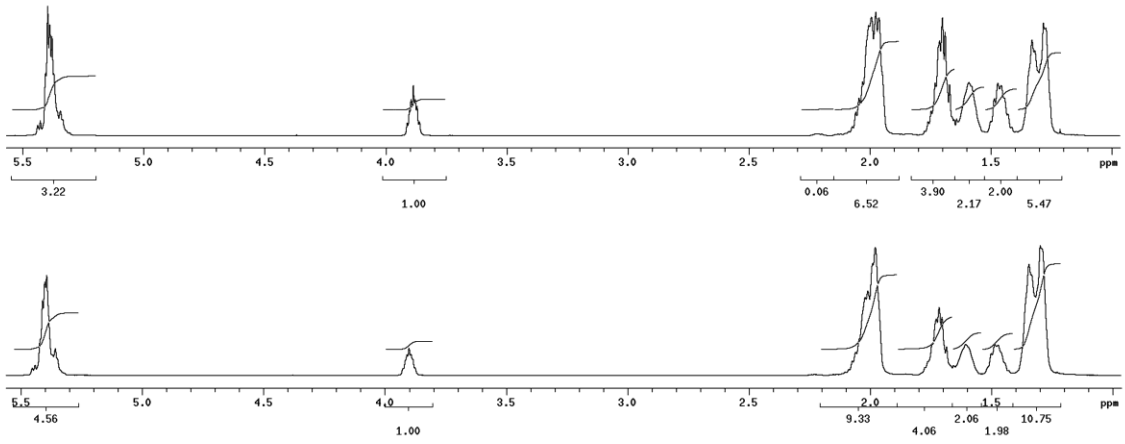

Figure 6-3. ^{1}H NMR spectra for RUPE15Cl (top) and RUPE21Cl (bottom).

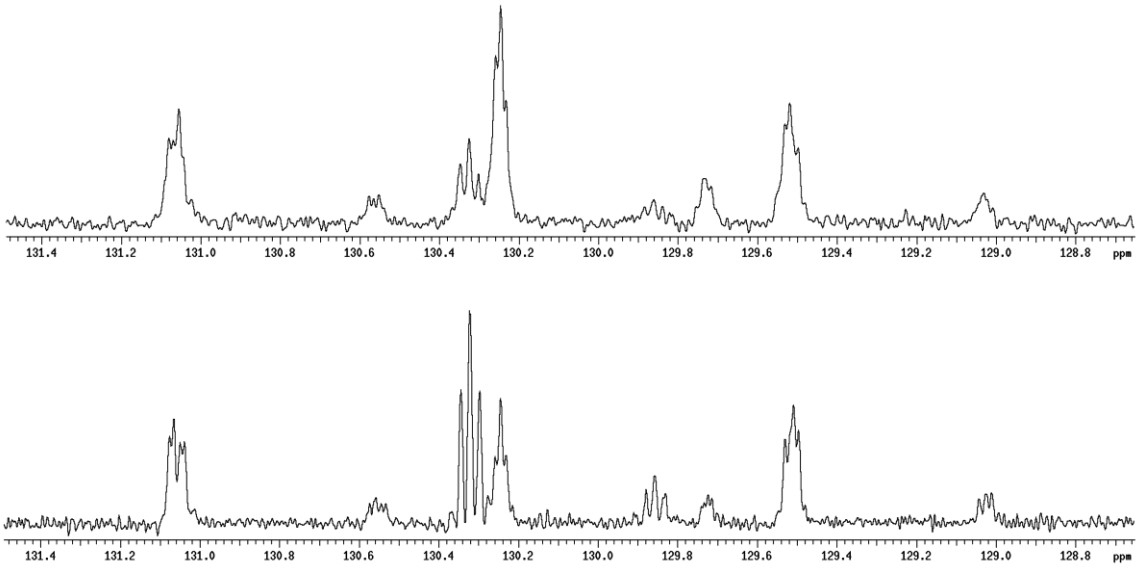

Figure 6-4. ^{13}C NMR for RUPE15Cl (top) and RUPE21Cl (bottom).

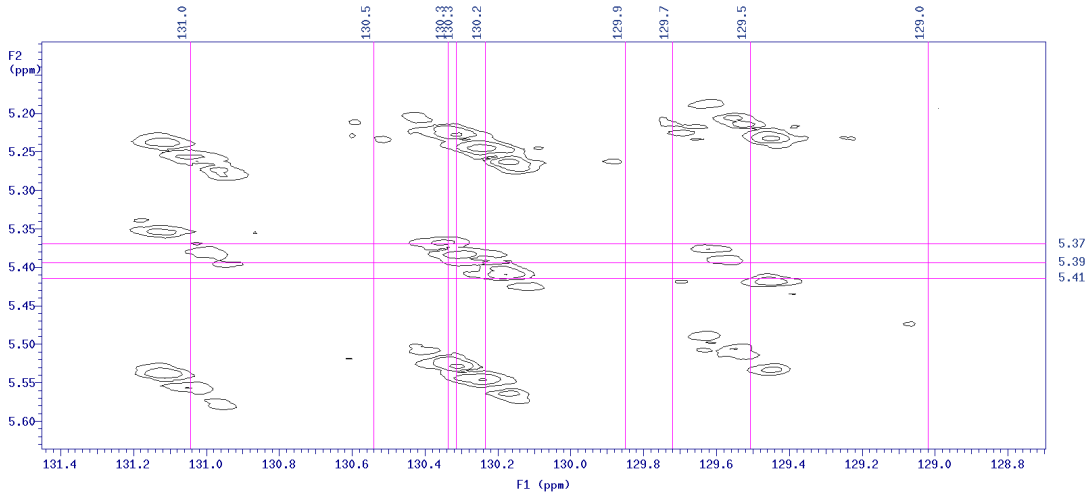

Figure 6-5. Expansion (1) of the GHMBC spectrum of RUPE15Cl.

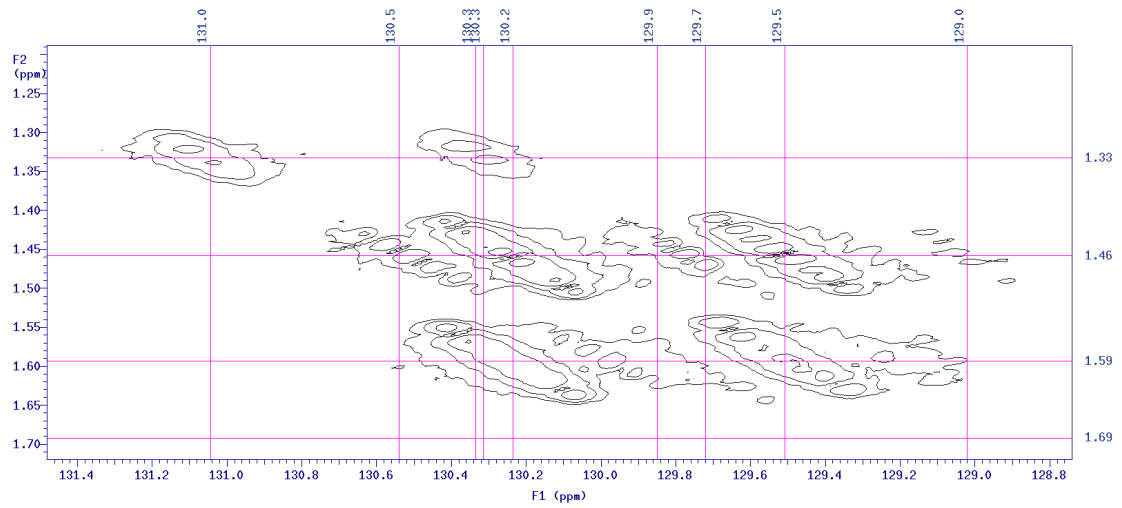

Figure 6-6. Expansion (2) of the GHMBC spectrum of RUPE15Cl.

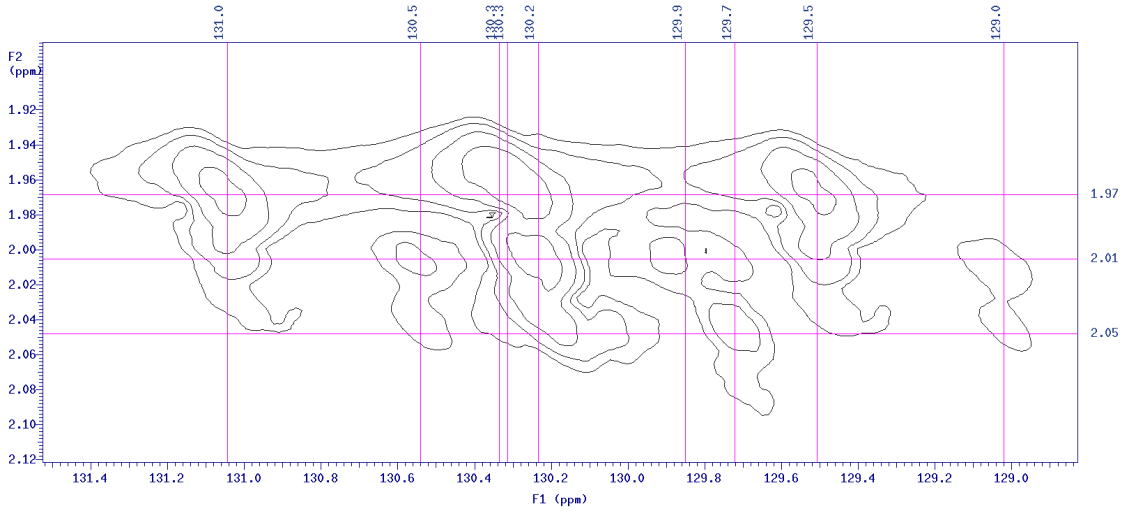

Figure 6-7. Expansion (3) of the GHMBC spectrum of RUPE15Cl.

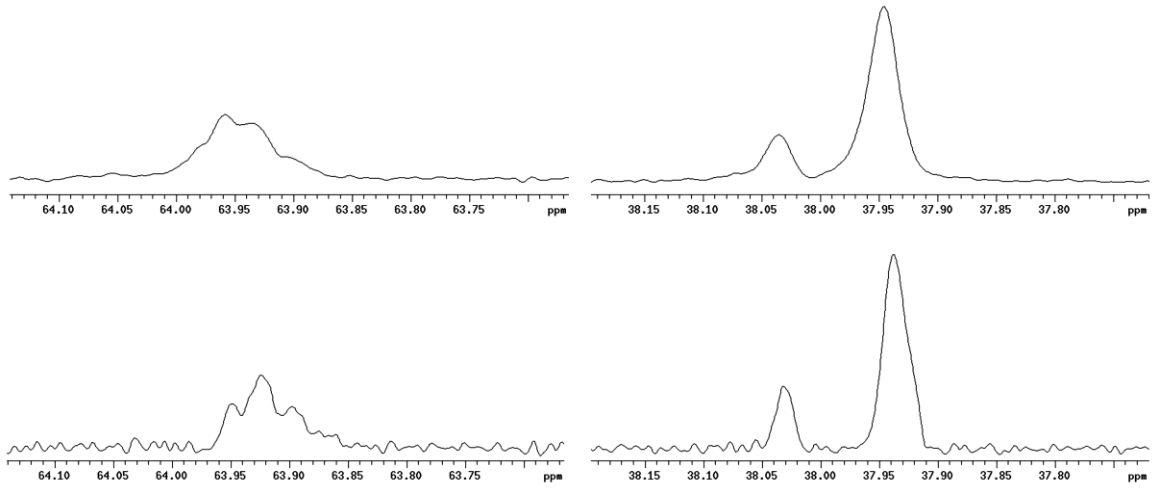

Figure 6-8. ^{13}C NMR for RUPE15Cl (top) and RUPE21Cl (bottom).

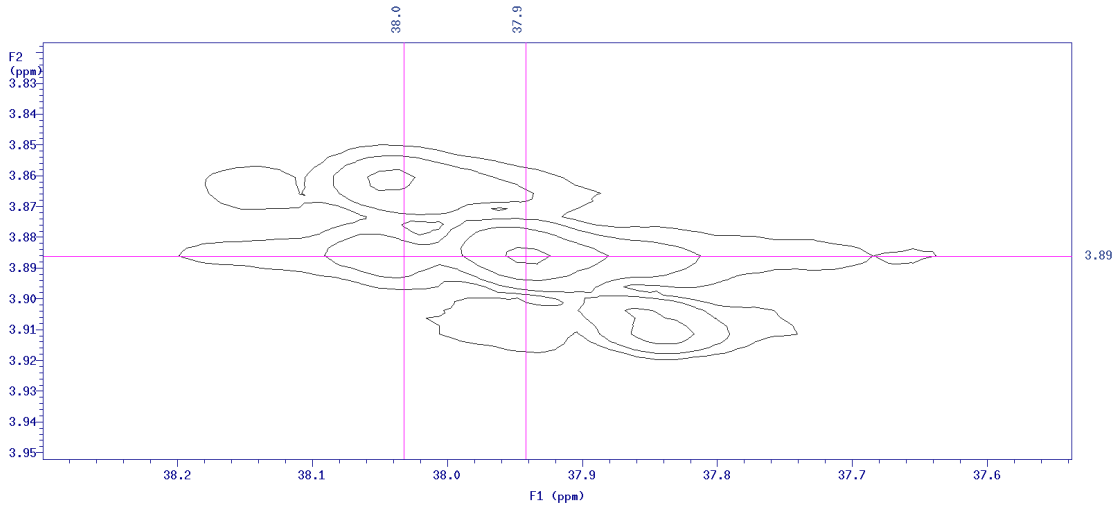

Figure 6-9. Expansion (4) of the GHMBC spectrum of RUPE15Cl.

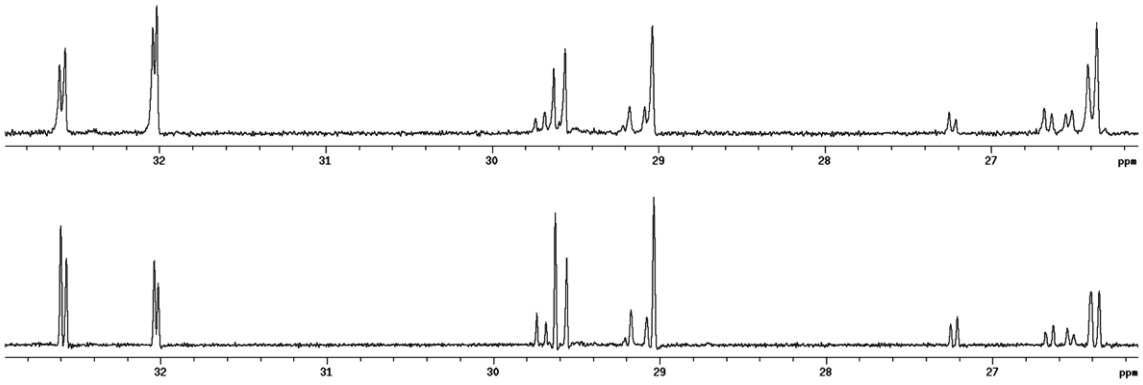

Figure 6-10. ^{13}C NMR for RUPE15Cl (top) and RUPE21Cl (bottom).

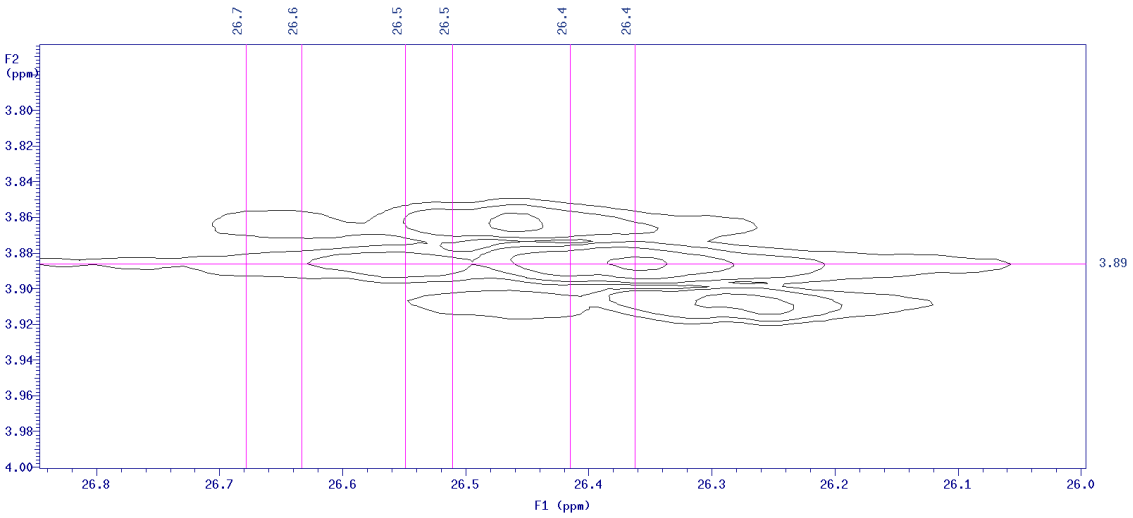

Figure 6-11. Expansion (5) of the GHMBC spectrum of RUPE15Cl.

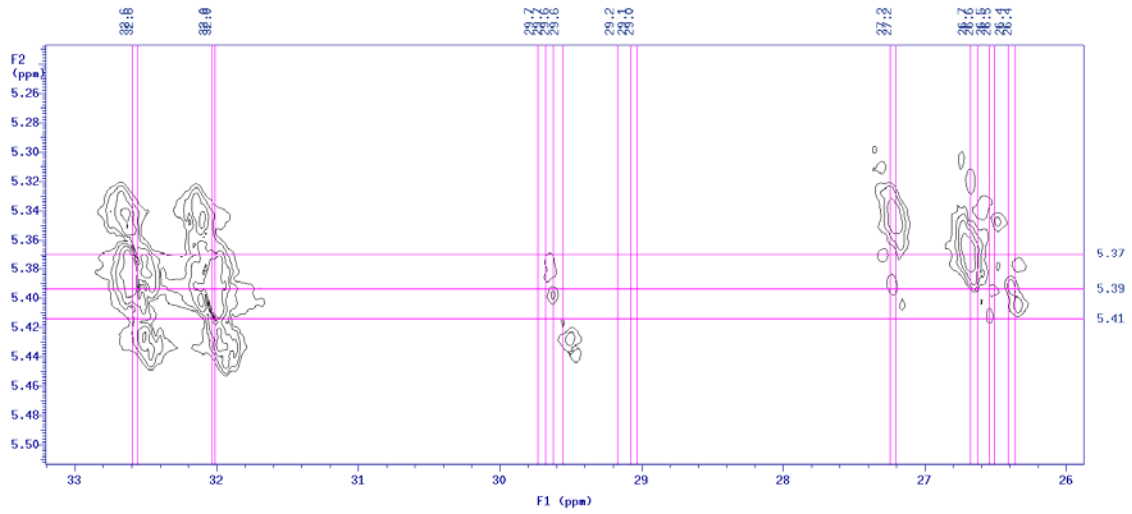

Figure 6-12. Expansion (6) of the GHMBC spectrum of RUPE15Cl.

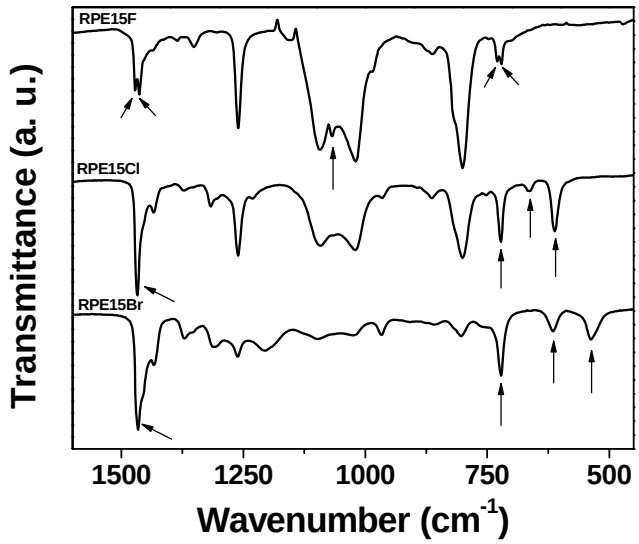

Figure 6-13. IR spectra for RPE15F (top), RPE15Cl (middle), and RPE15Br (bottom).

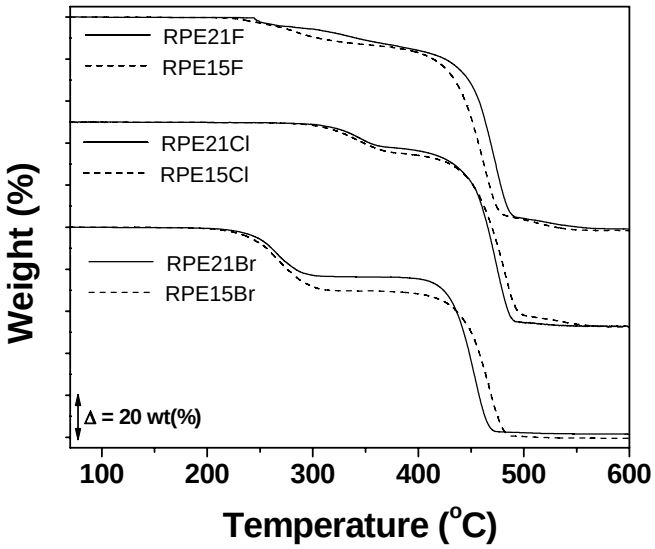

Figure 6-14. TGA results for all six random polymers, RPE21X (solid lines) and RPE15X (dashed lines), where X = F (top), Cl (middle), and Br (bottom).

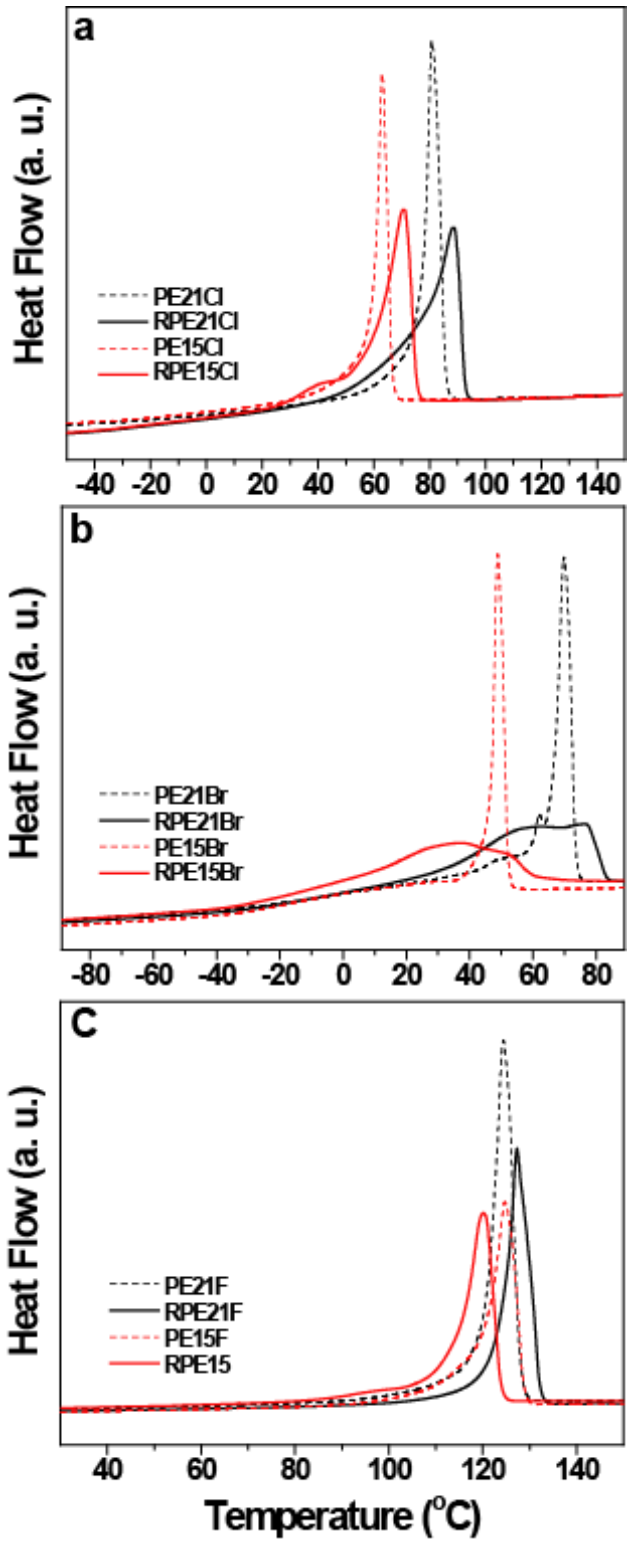

Figure 6-15. DSC comparison of random copolymers and precise analogues. (a) RPE21Cl, RPE15Cl, PE21Cl, PE15Cl. (a) RPE21Br, RPE15Br, PE21Br, PE15Br. (a) RPE21F, RPE15F, PE21F, PE15F.

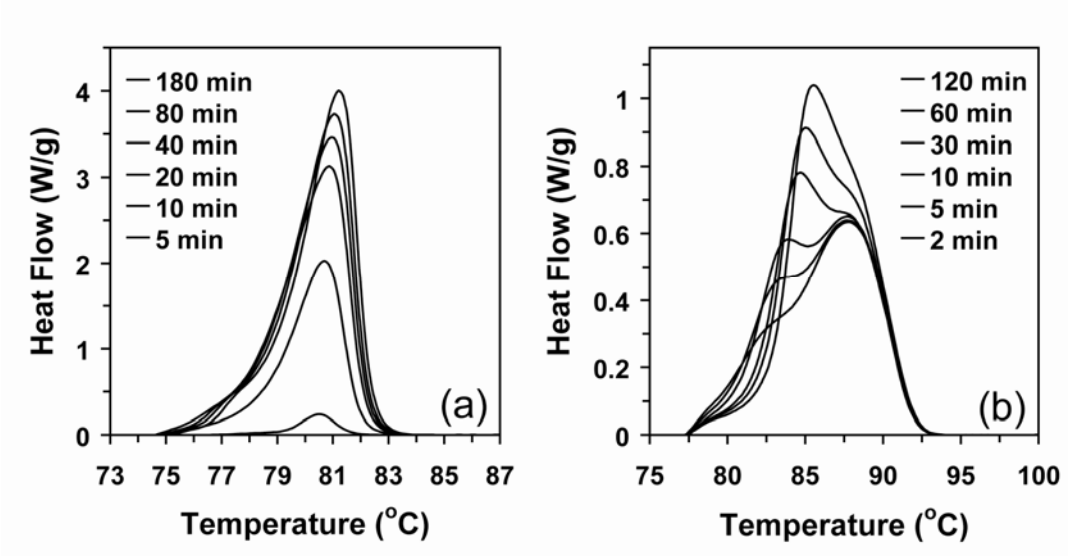

Figure 6-16. Melting thermograms of precise PE21Cl (a) and random copolymer analogue RPE21Cl (b), isothermally crystallized at 76 °C and 73 °C respectively for the times indicated.

LIST OF REFERENCES

1. Mathot, V.B.F.; Reynaers, H. In *Handbook of Thermal Analysis and Calorimetry*, 1st ed.; Cheng, S.Z.D., Ed.; Elsevier: New York, 2002; Vol. 3, p 197.

2. Kattas, L.; Gastrock, F.; Levin, I.; Cacciatore, A. In *Modern Plastics Handbook*, Harper, C. A., Ed.; McGraw-Hill: New York, 2000; p 4.1.

3. Peacock, A, J. *Handbook of Polyethylene: Structures, Properties, and Applications*, Marcel Dekker: New York, 2000; p 375.

4. Miller, E. *Introduction to Plastics and Composites: Mechanical Properties and Engineering Applications*, Marcel Dekker: New York, 1996; p 81.

5. Iwamichi, H.; Adachi, Y. Jpn. Patent 74,027,108, 1974.

6. Frielink, J. G. Brit. Patent 1,161,958, 1969.

7. Ebnesajjad, S. In *Encyclopedia of Polymer Science and Technology*, Kroschwitz, J. I., Ed.; Wiley-Interscience: New Jersey, 2003; Vol. 4, p 438.

8. Ebnesajjad, S. In *Encyclopedia of Polymer Science and Technology*, Kroschwitz, J. I., Ed.; Wiley-Interscience: New Jersey, 2003; Vol. 4, p 445.

9. Scientific Polymer Products Inc., Ontario, NY.

10. Goerlitz, M.; Minke, R.; Trautvetter, W.; Weisgerber, G. *Angew. Makromol. Chem.* **1973**, *29-30*, 137-162.

11. Cais, R.E.; Kometani, J. M. *Polymer* **1988**, *29*, 168-172.

12. Zerbi, G.; Cortili, G. *Spectrochim. Acta* **1970**, *26*, 733-739.

13. Boyer, R. F. *J. Polym. Sci., Part C* **1975**, *50*, 189-242.

14. Boyer, R. F.; Miller, R. L. *Macromolecules*, **1977**, *10*, 1167-1169.

15. Natta, G.; Bassi, I. W.; Allegro, G. *Atti Accad. Nazi. Lincei, Rend., Classe Sci. Fis., Mat. Nat.* **1961**, 31, 850-856.

16. Lando, J. B.; Olf, H. G.; Peterlin, A. *J. Polym. Sci. Polym. Chem. Ed.* **1966**, *4*, 941-951.

17. Bank, M. I.; Krimm, S. *J. Appl. Phys.* **1968**, *39*, 4951-4958.

18. Kavesh, S.; Schultz, J. M. *J. Polym. Sci., Polym. Phys. Ed.* **1970**, *8*, 243-276.

19. Kitamaru, R.; Mandelkern, L. J. *Polym. Sci., Polym. Phys. Ed.* **1970**, *8*, 2079-2087.

20. Rosenberg, Y.; Siegmann, A.; Narkis, M.; Shkolnik, S. *J. Appl. Polym. Sci.* **1992**, *45*, 783-795.

21. Jennings, T. C., Starnes, W. H., Jr. In *PVC Handbook* 1st ed.; Wilkes, C. E., Summers, J. W., Daniels, C. A., Eds.; Hanser: Munich, 2005; p 95.

22. Witenhafer, D. E.; Poledna, D. J. In *PVC Handbook* 1st ed.; Wilkes, C. E., Summers, J. W., Daniels, C. A., Eds.; Hanser: Munich, 2005; p 57.

23. Carman, C. J. *Macromolecules* **1973**, *6*, 725-728.

24. Matthews, G. *PVC: Production, Properties, and Uses*, The Institute of Materials: London, 1996; p 41.

25. Summers, J. W. *J. Vinyl Technol.* **1981**, *3*, 107-110.

26. Natta, G.; Corradini, P. *J. Polym. Sci.* **1956**, *20*, 251-266.

27. Witenhafer, D. E. *J. Macromol. Sci. Phys.* **1970**, *4*, 915-929.

28. Aubin, M.; Prud'homme, R. E. *Macromolecules* **1988**, *21*, 2945-2949.

29. Starnes, W. H. *Prog. Polym. Sci.* **2002**, *27*, 2133-2170.

30. Allsopp, M. W.; Vianello, G. In *Encyclopedia of Polymer Science and Technology*, Kroschwitz, J. I., Ed.; Wiley-Interscience: New Jersey, 2003; Vol. 8, p 437.

31. Ramey, K. C.; Lini, D. C. In *Encyclopedia of Polymer Science and Technology*, Mark, H. F.; Gaylord, N. G.; Bikales, N. M.O. Menges, G.; Kroschwitz J. I., Eds.; Wiley-Interscience: New York, 1971; Vol. 14, p 273.

32. Frata, M.; Vidotto, G.; Talamini, G. *Chimica e l'Industria* **1966**, *48*, 42-44.

33. Riande E. S. E.; Delgado, M. P.; Barrales-Rienda, J. M. *Macromolecules* **1982**, *15*, 1152-1157.

34. O'Shea, M. L.; Low, M. J. D.; Morterra, C. *Mater. Chem. Phys.* **1989**, *23*, 499-516.

35. Burnett, D. M.; Ross, F. L.; Hay, J. N. *Polym. Lett.* **1967**, *5*, 271-276.

36. Miller, R. L. In *Polymer Handbook*, 4th ed.; Brandrup, J.; Immergut, E. H.; Grulke, E. A. Eds.; Wiley-Interscience: New York, 1999; Chapter 6.

37. Herman, J. A.; Roberge, P. C. *Trans. Farad. Soc.* **1966**, *62*, 3183-3188.

38. Herman, J. A.; Roberge, P. C. *Trans. Farad. Soc.* **1969**, *65*, 1315-1324.

39. Dietrich, B.; Eckart, S. *Kolloid-Z.* **1965**, *201*, 111-115.

40. Herman, J. A.; Roberge, P. C. *J. Polym. Sci.* **1962**, *62*, S116-S118.

41. Jungnickel, B. J. In *Polymeric Materials Encyclopedia*, Salamone, J. C. Ed.; CRC Press: Boca Raton, 1996; Vol. 9, p 7115.

42. Russo, S.; Behari, K.; Chengji, S.; Pianca, M.; Barchiesi, E.; Moggi, G. *Polymer* **1993**, *34*, 4777-4781.

43. Tashiro, K. In *Ferroelectric Polymers: Chemistry, Physics, and Applications*, Nalwa, H., Ed.; Marcel Dekker: New York, 1995; p 97.

44. Maccone, P.; Brinati, G.; Arcella, V. *Polym. Eng. Sci.* **2000**, *40*, 761-767.

45. Hasegawa, R.; Kobayashi, M.; Tadokoro, H. *Polym. J.* **1972**, *3*, 591-599.

46. Humphrey, J. S.; Amin-Sanayei, R. In *Encyclopedia of Polymer Science and Technology*, Kroschwitz, J. I., Ed.; Wiley-Interscience: New Jersey, 2003; Vol. 4, p 510.

47. Bachmann, M. A.; Lando, J. B. *Macromolecules* **1981**, *14*, 40-46.

48. Lovinger, A. J. *Macromolecules* **1981**, *14*, 322-325.

49. Prest, W. M.; Luca, D. J. *J. Appl.Phys.* **1978**, *49*, 5042-5047.

50. Gregorio, R., Jr.; Cestari, M.; Chaves, N.; Nociti, P. S.; de Mendonca, J. A.; de Almeida Lucas, A. In *Polymeric Materials Encyclopedia*, Salamone, J. C. Ed.; CRC Press: Boca Raton, 1996; Vol. 9, p 7128.

51. Liu, Z.; Marechal, P.; Jerome, R. *Polymer* **1997**, *38*, 4925-4929.

52. Lee, S.; Knaebel, K. S. *J. Appl. Polym. Sci.* **1997**, *64*, 455-492.

53. Kusanagi, H. *Chem. Lett.* **1997**, *7*, 683-684.

54. Wessling, R. A.; Gibbs, D. S.; Obi, B. E.; Beyer, D. E.; Delassus, P. T.; Howell, B. A. In *Encyclopedia of Polymer Science and Technology*, Kroschwitz, J. I., Ed.; Wiley-Interscience: New Jersey, 2003; Vol. 4, p 458.

55. Kinsinger, J. B.; Fischer, T. M.; Wilson, C. W. III. *J. Polym. Sci. Polym. Lett. Ed.* **1967**, *5*, 285-294.

56. Matsuo, K.; Stockmayer, W. H. *Macromolecules* **1975**, *8*, 660-663.

57. Boyer, R. F.; Spencer, R. S. *J. App. Phys.* **1944**, *15*, 398-405.

58. Illers, K. H. *Kolloid-Z.* **1963**, *190*, 16-34.

59. Landes, B. G.; De Lassus, P. T.; Harrison, I. R. *J. Macromol. Sci. Phys.* **1983**, *B22*, 735-745.

60. Landes, B. G.; Raich, W. J.; De Lassus, P. T.; Harrison, I. R. *J. Macromol. Sci. Phys.* **1983**, *B22*, 747-762.

61. Okuda, K *J Polym. Sci., Part A:* **1964**, *2*, 1749-1764.

62. Howell, B. A.; Delassus, P. T. *J. Polym. Sci., Part A: Polym. Chem.* **1987**, *25*, 1697-1708.

63. Narita, S.; Ichinohe, S.; Enomoto, S. *J. Polym. Sci.* **1959**, *37*, 251-261.

64. Day, M.; Suprunchuk, T.; Cooney, J. D.; Wiles, D. M. *J. Appl. Polym. Sci.* **1987**, *33*, 2041-2052.

65. Narita, S.; Okuda, K. *J. Polym. Sci.* **1959**, *38*, 270-272.

66. Kerbow, D. L. In *Polymeric Materials Encyclopedia*, Salamone, J. C. Ed.; CRC Press: Boca Raton, 1996; Vol. 9, p 6884.

67. Gangal, S. V. In *Encyclopedia of Polymer Science and Technology*, Kroschwitz, J. I., Ed.; Wiley-Interscience: New Jersey, 2003; Vol. 3, p 378.

68. Chanzy, H. D.; Smith, P.; Revol, J. F. *J. Polym. Sci., Part C: Polym. Lett.* **1986**, *24*, 557-563.

69. Bunn, C. W.; Howells, E. R. *J. Polym. Sci.* **1955**, *18*, 307-310.

70. Bunn, C. W. *J. Polym. Sci.* **1955**, *16*, 323-343.

71. Khanna, Y. P.; Chomyn, G.; Kumar, R.; Murthy, N. S.; O'Brien, K. P.; Reimschuessel, A. C. *Macromolecules* **1990**, *23*, 2488-2494.

72. Scheerer, K.; Wilke, W. *Colloid. Polym. Sci.* **1987**, *265*, 206-209.

73. Ebnesajjad, S.; Khaladkar, P. R. In *Fluoropolymers Applications in Chemical Processing Industries*, Ebnesajjad, S., Ed.; William Andrew: Norwich, 2005; p 15.

74. Bowmer, T. N.; Tonelli, A. E. *Polymer* **1985**, *26*, 1195-1201.

75. Boffa, L. S.; Novak, B. M. *Chem. Rev.* **2000**, *100*, 1479-1493.

76. Lehman S. E., Jr.; Wagener K. B.; Baugh, L. S.; Rucker, S. P.; Schulz, D. N.; Varma-Nair, M.; Berluche, E. *Macromolecules* **2007**, *40*, 2643-2656.

77. Boone, H. W.; Athey, P. S.; Mullins, M. J.; Philipp, D.; Muller, R.; Goddard, W. A. *J. Am. Chem. Soc.* **2002**, *124*, 8790-8791.

78. Stoeva, S.; Vlaev, L. *Macromol. Chem. Phys.* **2002**, *203*, 346-353.

79. Chang, B. H.; Zeigler, R.; Hiltner, A. *Polym. Eng. Sci.* **1988**, *28*, 1167-1172.

80. Era, V. A. *Die Makromol. Chem.* **1974**, *175*, 2191-2198.

81. Friese, K.; Hobelbarth, B.; Reinhardt, J.; Newe, R. *Die Angew. Makromol. Chem.* **1996**, *234*, 119-132.

82. du Toit, F. J.; Sanderson, R. D.; Engelbrecht, W. J.; Wagener, J. B. *J. Fluorine Chem.* **1995**, *74*, 43-48.

83. Schonhorn, H.; Gallagher, P. K.; Luongo, J. P.; Padden, F. J., Jr. *Macromolecules* **1970**, *3*, 800-801.

84. Ferraria, A. M.; da Silva, J. D. L.; do Rego, A. M. B. *Polymer* **2003**, *44*, 7241-7249.

85. Ferraria, A. M.; da Silva, J. D. L.; do Rego, A. M. B. *J. Fluorine Chem.* **2004**, *125*, 1087-1094.

86. Cruz-Barba, L. E.; Manolache, S.; Denes, F. *Langmuir* **2002**, *18*, 9393-9400.

87. Kharitonova, A. P.; Taege, R.; Ferrier, G.; Teplyakov, V.V.; Syrtsova, D.A.; Koops, G. H. *J. Fluorine Chem* **2005**, *126*, 251–263.

88. Stoeva, S.; Tsocheva, D.; Terlemezyan, L. *J. Therm. Anal. Calorim.* **2006**, *85*, 439-447.

89. Sobottka, J. *Acta Polymerica* **1983**, *34*, 647-650.

90. Zhikuan, C.; Lianghe, S.; Sheppard, R. N. *Polymer* **1984**, *25*, 369-374.

91. Saito, T.; Matsumura, Y.; Hayashi, S. *Polym. J.* **1970**, *1*, 639-655.

92. Hosselbarth, B. *Die Angew. Makromol. Chem.* **1995**, *231*, 161-169.

93. Chang, B. H.; Dai, J. W.; Siegmann, A.; Hiltner, A. *Polym. Eng. Sci.* **1988**, *28*, 1173-1181.

94. Era, V. A.; Lindberg, J. J. *J. Polym. Sci., Part:A2* **1972**, *10*, 937-944.

95. Blundell, D. J.; Keller, A. *J. Macromol. Sci., Part:B2* **1968**, *2*, 337-359.

96. Grimm, H. J.; Thomas, E. L. *Polymer* **1985**, *26*, 38-44.

97. Keller, A.; Matreyek, W.; Winslow, F. H. *J. Polym. Sci.* **1962**, *62*, 291-300.

98. Stoeva, S.; Popov, A.; Rodriguez, R. *Polymer*, **2004**, *45*, 6341-6348.

99. Cross, E. M.; McCarthy, T. J. *Macromolecules* **1992**, *25*, 2603-2607.

100. Nakagawa, T.; Yamada, S. *J. Appl. Polym. Sci.* **1972**, *16*, 1997-2012.

101. Harrison, I. R.; Baer, E. *J. Polym. Sci.: Part A-2* **1971**, *9*, 1305-1324.

102. Arroyo, N. A.; Hiltner, A. *J. Appl. Polym. Sci.* **1979**, *23*, 1473-1485.

103. Landes, B. G.; Harrison, I. R. *Polymer* **1987**, *28*, 911-917.

104. Jameison, F. A.; Schilling, F. C.; Tonelli, A. E. *Macromolecules* **1986**, *19*, 2168-2173.

105. Braun, D.; Mao, W.; Bohringer, B.; Garbella, R. W. *Die Angew. Makromol. Chem.* **1986**, *141*, 113-129.

106. Pourahmady, N.; Bak, P. I.; Kinsey, R. A. *J. Macromol. Sci. Pure Appl. Chem.* **1992**, *29*, 959-974.

107. Cais, R. E.; Kometani, J. M. *Macromolecules* **1982**, *15*, 954-960.

108. Gomez, M. A.; Tonelli, A. E.; Lovinger, A. J.; Schilling, F. C.; Cozine, M. H.; Davis, D. D. *Macromolecules*, **1989**, *22*, 4441-4451.

109. Stephens, C. H.; Yang, H.; Islam, M.; Chum, S. P.; Rowan, S. J.; Hiltner, A.; Baer, E. *J. Polym. Sci.Part B: Polym. Phys.* **2003**, *41*, 2062-2070.

110. Gutzler, F.; Wegner, G. *Colloid and Polym. Sci.* **1980**, *258*, 776-786.

111. Hanna, R. J.; Fields, J. W. *J. Vinyl Tech.* **1982**, *4*, 57-61.

112. Lopez, D.; Reinecke, H.; Hidalgo, M.; Mijangos, C. *Polym. Int.* **1997**, *44*, 1-10.

113. Baughman, T. W.; Wagener, K. B. *Adv. Polym. Sci.* **2005**, *176*, 1-42.

114. Watson, M. D.; Wagener, K. B. *Macromolecules* **2000**, *33*, 8963-8970.

115. Jama, C.; Quensierre, J.-D.; Gengembre, L.; Moineau, V.; Grimblot, J.; Dessaux, O.; Goudmand, P. *Surf. Interface Anal.* **1999**, *27*, 653-658.

116. Peacock, A, J. *Handbook of Polyethylene: Structures, Properties, and Applications*, Marcel Dekker: New York, 2000; p 459.

117. Anton, D. *Adv. Mater.***1998**, *10*, 1197-1205.

118. Feldman, D.; Barbalata, A. *Synthetic Polymers*; Chapman and Hall: London, 1996; Chapter 2.

119. Gottesman, R. T.; Goodman, D. In *Applied Polymer Science*, 2nd ed.; Tess, R. W.; Poehlein, G. W., Eds.; ACS: Washington, D. C., 1985; p 383.

120. Mathews, G. *PVC: Production, Properties, and Uses;* The Institute of Materials: London, 1996; p 280.

121. Yang, H.; Islam, M.; Budde, C.; Rowan, S. J. *J. Polym. Sci., Part A: Polym. Chem.* **2003**, *41*, 2107-2116.

122. Walsby, N.; Sundholm, F.; Kallio, T.; Sundholm, G. *J. Polym. Sci., Part A: Polym. Chem.* **2001**, *39*, 3008-3017.

123. Tonelli, A. E. *Macromolecules* **1982**, *15*, 290-293.

124. Endo, K.; Saitoh, M. *Polym. Bull.* **2003**, *49*, 411-416.

125. Schilling, F. C.; Tonelli, A. E.; Valenciano, M. *Macromolecules* **1985**, *19*, 356-360.

126. Stoeva, S. *J. Appl. Polym. Sci.* **2004**, *94*, 189-196.

127. Younkin, T. R.; Cornor, E. F.; Henderson, J. I.; Friedrich, S. K.; Grubbs, R. H.; Bansleben, D. A. *Science* **2000**, *287*, 460-462.

128. Smith, J. A.; Brzezinska, K. R.; Valenti, D. J.; Wagener, K. B. *Macromolecules* **2000**, *33*, 3781-3794.

129. Sworen, J. C.; Smith, J. A.; Berg, J. M.; Wagener, K. B. *J. Am. Chem. Soc.* **2004**, *126*, 11238-11246.

130. Alamo, R.; Domszy, R.; Mandelkern, L. *J. Phys. Chem.* **1984**, *88*, 6587-6595.

131. Alamo, R.G., Mandelkern L. *Thermochimica Acta*, **1994**, *238*, 155-201.

132. L. Mandelkern, *Crystallization of Polymers*, 2nd ed.; Cambridge University Press: 2002; Vol. 1.

133. Isasi, J.R., Haigh, J.A., Graham, J.T., Mandelkern, L., Alamo. R.G. *Polymer*, **2000**, *41*, 8813-8823.

134. Flory, P.J.; *Trans. Faraday Soc.* **1955**, *51*, 848-857.

135. Crist, B.; Howard, P.R. *Macromolecules*, **1999**, *32*, 3057-3067

136. Chen, H.Y.; Chum, S.P.; Hiltner, A., Baer, E. *J. Polym. Sci., Polym. Phys. Ed.* **2001**, *39*, 1578-1593.

137. Ver Strate, G.; Wilchinsky, Z.W.; *J. Polym. Sci., Part A-2*, **1971**, *9*, 127-142.

138. (a) Wild, L.; Blatz, C. In *New Advances in Polyolefins*, Young, T.C., Ed.; Lenum Press: New York, 1993. (b) Anantawaraskul, S.; Soares, J.B.P.; Wood-Adams, P.M.; Monrabal, B. *Polymer* **2003**, *44*, 2393-2401.

139. Wang, W-J.; Zhu, S. *Macromolecules* **2000**, *33*, 1157-1162.

140. Hu, W.; Sirota, E.B. *Macromolecules* **2003**, *36*, 5144-5149.

141. Ruiz de Ballesteros, O.; Auriemma, F.; Guerra, G.; Corradini, P. *Macromolecules*, **1996**, *29*, 7141-7148.

142. Hopkins, T. E.; Wagener, K. B. *Macromolecules* **2003**, *36*, 2206-2214.

143. Watson, M. D.; Wagener, K. B. *Macromolecules* **2000**, *33*, 5411-5417.

144. Hahn, S. F. *J. Polym. Sci.: Part A: Polym. Chem.* **1992**, *30*, 397-408.

145. Sworen, J. C.; Smith, J. A.; Wagener, K. B.; Baugh, L. S.; Rucker, S. P. *J. Am. Chem. Soc.* **2003**, *125*, 2228-2240.

146. Baughman, T. W.; van der AA, E.; Lehman, S. E.; Wagener, K. B. *Macromolecules* **2005**, *38*, 2550-2551.

147. du Toit, F. J.; Sanderson, R. D. *J. Fluorine Chem.* **1999**, *98*, 107-114.

148. Bowmer, T. N.; Tonelli, A. E.,*J. Polym. Sci.: Part B: Polym. Phys.* **1986**, *24*, 1631-1650.

149. Hagemann, H.; Snyder, R.G.; Peacock, A.J.; Mandelkern, L. *Macromolecules.* **1989**, *22*, 3600-3606.

150. Gunter, L.; Wegner, G.; Smith, J. A.; Wagener K. B. *Colloid. Polym. Sci.* **2004**, *282*, 773-781.

151. Callister, W.D. Jr. *Materials Science and Engineering. An Introduction*, Wiley: New York, 2003.

152. Contrasting with the dimension of the "c" axis of orthorhombic crystals, 2.54 Å, the "c" axis of the triclinic cell corresponds to two full repeating units (>40 Å).

153. Simanke, A.G.; Alamo, R.G.; Galland, G. B.; Mauler, R. S. *Macromolecules*, **2001**, *34*, 6959-6971.

154. VanderHart, D.L. *J. Magnetic Reson.* **1981**, *44*,117-125.

155. VanderHart, D.L., Perez, E. *Macromolecules*, **1986**, *19*, 1902-1909.

156. Alamo, R.G.; VanderHart, D.L.; Nyden, M.R.; Mandelkern, L. *Macromolecules*, **2000**, *33*, 6094-6105.

157. Zhang, X.; Li, Z,; Yang, H.; Sun, C. *Macromolecules*, **2004**, *37*, 7393-7400.

158. Hosoda, S.; Nomura, H.; Gotoh, Y.; Kihara, H. *Polymer* **1990**, *31*, 1999-2005.

159. Holdsworth, Cutler D.J.; Hendra, P.J.; Cudby, M.E.A,; Willis, H.A. *Polymer* **1977**, *18*, 1005-1008.

160. Roe, R-J.; Gieniewski, C. *J. Crystal Growth* **1980**, *48*, 295-302.

161. Watson, M. D.; Wagener, K. B. *Macromolecules* **2000**, *33*, 3196-3201.

162. Braun, D. *J. Vinyl Addit. Technol.* **2001**, *7*, 168-176.

163. Smalley, D. In *PVC Handbook*, Wilkes, C. E.; Summers, J. W.; Daniels, C. A., Eds.; Hanser: Munich, 2005; p679.

164. Kline, M. W.; Skiest, E. N. In *Encyclopedia of PVC*, Nass, L. I., Ed.; Marcel Dekker: New York, 1976; p 109.

165. Kline, M. W.; Skiest, E. N. In *Encyclopedia of PVC*, Nass, L. I., Ed.; Marcel Dekker: New York, 1976; p 138.

166. Wilkes, C. E.; Westfahl, J. C.; Backderf, R. H. *J. Polym. Sci: Part A-1* **1969**, *7*, 23-33.

167. Hagiwara, M.; Miura, T.; Kagiya, T. *J. Polym. Sci: Part A-1* **1969**, *7*, 513-523.

168. Boz, E.; Wagener, K. B.; Ghosal, A.; Fu, R.; Alamo, R. G. *Macromolecules* **2006**, *39*, 4437-4447.

169. Boz, E.; Nemeth, A. J.; Alamo, R. G.; Wagener, K. B. *Adv. Synth. Catal.* **2007**, *349*, 137-141.

170. Wu, T. K. *Macromolecules* **1973**, *6*, 737-741.

171. Vogl, O.; Qin, M. F.; Zilkha, A. *Prog. Polym. Sci.* **1999**, *24*, 1481-1525.

172. Stehling, F.C.; Mandelkern, L. *Macromolecules*, **1970**, *3*, 242-252.

173. Maynard, H. D.; Grubbs, R. H. *Tetrahedron Lett.* **1999**, *40*, 4137-4140.

174. Brandrup, J.; Immergut, E. H.; Grulke, E. A. *Polymer Handbook*, 4th ed., Wiley-Interscience: New York, 1984.

175. G. Mathews, *PVC: Production, Properties, and Uses*, The Institute of Materials: London, 1996; p 13.

176. Lukac, I.; Pilichowski, J. F.; Lacoste, J. *Polym. Degrad. and Stab.* **1998**, *61*, 79-85.

177. Chanunpanich, N.; Ulman, A.; Strzhemechny, Y. M.; Schwarz, S. A.; Janke, A.; Braun, H. G.; Kraztmuller, T. *Langmuir* **1999**, *15*, 2089-2094

178. Lukac, I.; Pilichowski, J. F.; Lacoste, J. *Polym. Degrad. and Stab.* **1998**, *61*, 343-347.

179. Fréchet, J. M. J. *J. Macromol. Sci.-Chem.* **1981**, *A15*, 877-890.

180. Janovic, Z. *Polym. Degrad. and Stab.* **1999**, *64*, 479-487.

181. Hopkins, T. E.; Wagener, K. B. *Macromolecules* **2004**, *37*, 1180-1189.

182. Mehl, M.; Marongiu, A.; Faravelli, T.; Bozzano, G.; Dente, M.; Ranzi, E. *J. Anal. Appl. Pyrolysis* **2004**, *72*, 253-272.

183. Eguiluz, M.; Ishida, H.; Hiltner, A. *J. Polym. Sci. Polym. Phys.* **1979**, *17*, 893-897.

184. Snyder, R. G. *J Mol. Spectrosc.* **1961**, *7*, 116-144.

185. Narita, S.; Ichinohe, S.; Enomoto, S. *J. Polym. Sci.* **1959**, *37*, 273-280.

186. Chanunpanich, N.; Ulman, A.; Malagon, A.; Strzhemechny, Y. M.; Schwarz, S. A.; Janke, A.; Kraztmuller, T.; Braun, H. G. *Langmuir* **2000**, *16*, 3557-3560.

187. Natta, G.; Dall'Asta, G.; Bassi, I. W.; Carella, G. *Makromol. Chem.* **1966**, *91*, 87-106.

188. Gianotti, G.; Capizzi, A. *Eur. Polym. J.* **1970**, *6*, 743-752.

189. Baughman, T. W.; Sworen, J. C.; Wagener, K. B. *Tetrahedron* **2004**, *60*, 10943-10948.

190. Scheirs, J. In *Modern Fluoropolymers*, Scheirs, J., Ed.; Wiley: Chichester, 1997; p 1.

191. Ameduri, B.; Boutevin, B.*Well-Architectured Fluoropolymers: Synthesis, Properties and Applications*, Elsevier: Amsterdam, 2004; p 187.

192. Boz, E.; Nemeth, A. J.; Ghiviriga, I.; Jeon, K.; Alamo, R. G.; Wagener, K. B. *Macromolecules* accepted.

193. Hong, J. W.; Lando, J. B.; Koenig, J. L.; Chough, S. H.; Krimm, S. *Vibrational Spectroscopy*, **1992**, *3*, 55-66.

194. Tashiro, K.; Sasaki, S.; Kobayashi, M. *Macromolecules* **1996**, *29*, 7460-7469.

195. Ungar, G.; Zeng, X.-B. *Chem. Rev.* **2001**, *101*, 4157-4188.

196. Impallomeni, G.; Montaudo, G.; Puglisi, C.; Scamporrino, E.; Vitalini, D. *J. Appl. Polym. Sci.* **1986**, *31*, 1269-1274.

197. Wunderlich, B. *Macromolecular Physics: Crystal Structure, Morphology, Defects*, Academic Press: New York, 1973; Vol. 1, p 401.

198. Doak, K. W. In *Encyclopedia of Polymer Science & Engineering*, 2nd ed.; Mark, H. F.; Bikales, N. M.; Overberger, C. G.; Menges, G.; Kroschwitz, J. I.; Eds.; Wiley: New York, 1986; Vol. 6, p 386.

199. Klimesch, R.; Littmann, D.; Ma¨hling, F. O. In *Encyclopedia of Materials: Science and Technology*, Buschow, K. H. J.; Cahn, R. W.; Flemings, M. C.; Ilschner, B.; Kramer, E. J.; Mahajan, S., Eds.; Elsevier Science: New York, 2004; p 7181.

200. Boz, E.; Nemeth, A. J.; Jeon, K.; Alamo, R. G.; Wagener, K. B. *Macromolecules* submitted.

201. Crist, B.; Claudio, E.S. *Macromolecules* **1999**, *32*, 8945-9851.

202. Rabiej, S.; Goderis, B.; Janicki, J.; Mathot, V.B.F.; Koch, M.H.J.; Groeninckx, G.; Reynaers, H.; Gelan, J. Wlochowicz, A. *Polymer* **2004**, *45*, 8761-8778.

BIOGRAPHICAL SKETCH

Emine Boz was born in Antalya, Turkey in 1978. She received her B.S. in Chemistry from Hacettepe University in Ankara, Turkey in 2001. She then went on to complete her M.Sc. in Inorganic Chemistry in 2003 at Hacettepe University. Emine then joined the research group of Prof. Kenneth B. Wagener at the University of Florida in 2003, where she qualified in the organic division and conducted studies on the synthesis and crystallization of halogen containing polyolefins.